

THESIS

3

MICHIGAN STATE UNIVERSITY LIBRARIES



3 1293 01565 4407

This is to certify that the

thesis entitled

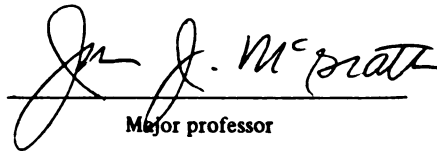
Measurement of Thermal Conductivity of Boron
Doped CVD Diamond Films as a Function
of Electrical Resistivity

presented by

Andrew Sayers

has been accepted towards fulfillment
of the requirements for

Master of Science degree in Mechanical Engineering


Major professor

Date 11/21/96

LIBRARY
Michigan State
University

PLACE IN RETURN BOX to remove this checkout from your record.
TO AVOID FINES return on or before date due.

DATE DUE	DATE DUE	DATE DUE
APR 2 2003 APR 2 2003	_____	_____
APR 2 2003	_____	_____
_____	_____	_____
_____	_____	_____
_____	_____	_____
_____	_____	_____
_____	_____	_____

**MEASUREMENT OF THERMAL CONDUCTIVITY OF BORON
DOPED CVD DIAMOND FILMS AS A FUNCTION
OF ELECTRICAL RESISTIVITY**

By

Andrew Sayers

A THESIS

Submitted to
Michigan State University
in partial fulfillment of requirements
for the degree of

MASTER OF SCIENCE

Department of Mechanical Engineering

1996

ABSTRACT

MEASUREMENT OF THERMAL CONDUCTIVITY OF BORON DOPED DIAMOND FILMS AS A FUNCTION OF ELECTRICAL RESISTIVITY

By

Andrew Sayers

A novel experimental technique has been used to determine thermal conductivity of boron doped diamond films. The method allows for electrical resistance heating for a range of resistivities, therefore possessing the capability to estimate thermal conductivities for different doping levels. Boron doped diamond films were deposited using the hot filament technique. Boron powder precisely placed during the diamond deposition process contributed to diamond growth with varying resistivities from sample to sample (and within each sample). The resistance of each sample was measured using the four probe method. Samples were chemically etched to obtain a 3mm diameter of free standing diamond film. The samples were then prepared, energized, and monitored using an infrared imaging system. Temperature distribution across the 3mm diamond window was extracted and used to estimate the film's thermal conductivity. Results show that thermal conductivity decrease as doping level increase. The thermal conductivity values range from 205 to 975 W/m K, while the uncertainty range from ± 10 to ± 65 . The samples' resistivities, which were used to quantify the level of doping, were measured in the region where temperatures were acquired and varied from 1.63 Ω cm to 68.4 Ω cm.

ACKNOWLEDGEMENTS

I would personally like to thank the three people who made this whole experience possible, Dr. Beck, Dr. Mcgrath, and Dr. Somerton. Each of these individuals has given me a great deal of guidance and support at Michigan State University. The time spent working with each of them has not only enhance me intellectually, but also personally.

Many thanks go to Dr. James Beck for all his support. I consider Dr. Beck a wonderful individual as well as a great scholar. His patience and support has always been there whenever it was needed. The time spent in his classroom and laboratory was very rewarding.

I would also like to extend my gratitude to Dr. John Mcgrath for his expertise in performing the experiments and overall guidance throughout. Dr. Mcgrath brilliance and experience was crucial in every phase of the project, and his critical reviews made the final version possible.

I also thank Dr. Craig Somerton for making all this possible. Dr. Somerton efforts in recruiting and retaining my services cannot go unnoticed or unappreciated. The experience gained while working under his supervision was highly rewarding.

Throughout this project there were many people who contributed their time and effort in helping. While most of their names are mentioned in the text, one individual went beyond what was necessary. I extend my thanks to Gwo-shi Yang for his effort in depositing the films.

Last, but not least, was my family. This would not be possible without their continued support. Although they are a few hundred miles away, I could not survive without their assistance. To my mom Gloria, my dad Julian, brothers Greg and Tom, and sister Debbie thank you very much.

TABLE OF CONTENTS

LIST OF TABLES	viii
LIST OF FIGURES	ix
LIST OF SYMBOLS	xi
1 Introduction	1
2 Background/Literature Review	4
2.1 Atomic structure of diamond	5
2.2 Mechanism of diamond growth	7
2.3 Diamond as a semiconductor	10
2.4 Determination of thermal conductivity	13
3 Mathematical Model	23
3.1 Heat conduction model	23
3.2 Radial heat flow model	25
3.3 Simplified model	27
3.3.1 Radiation consideration	27
3.3.2 Convection consideration	28

4	Sample Design	31
4.1	Wafer preparation	31
4.2	Mask	32
4.3	Diamond deposition	33
4.4	Etching	39
4.5	Sample preparation	42
4.6	Gold deposition	44
5	Experimental Method/Technique	48
5.1	Experimental setup	48
5.2	Infrared thermography	51
5.3	Determination of emissivity	55
5.4	Measurement of resistivity	64
5.5	Measurement of film thickness	67
5.6	Temperature acquisition	86
5.7	Data processing and parameter estimation of thermal Conductivity	90
6	Results and Discussion	93
6.1	Thermal conductivity as a function of electrical resistivity	93
6.2	Uncertainty analysis	111

7	Summary and Conclusions	123
8	Recommendation for Future Work	126
	Appendix	128
	Bibliography	183

LIST OF TABLES

Table 2.1	Round Robin Testing	4
Table 2.2	Yang's Resistance Measurements	12
Table 5.1	Emissivity of Black Paint	60
Table 5.2	Emissivity of Diamond (Test #1)	61
Table 5.3	Emissivity of Diamond (Test #2)	62
Table 5.4	Emissivity of Diamond (Test #3)	62
Table 5.5	Emissivity of Diamond (Test #4)	63
Table 5.6	Resistivity of Samples	66
Table 5.7	Global Resistivity using DMM	67
Table 5.8	Thickness Measurements using RST-Plus	71
Table 5.9	Thickness Measurements using ESEM	82
Table 5.10	Thickness Measurement using Sloan Dektak IIA	85
Table 5.11	Summary of Thickness Measurements	85
Table 5.12	Uncertainty and Standard Deviation of Each Instrument	86
Table 6.1	Estimated Doping Level for all Samples	100
Table 6.2	Average Resistivity and Standard Deviation	103
Table 6.3	Estimates of Thermal Conductivity with Average and Standard Deviation	103
Table 6.4	Uncertainty in Thermal Conductivity	114
Table 6.5	Parameter Contribution to Uncertainty in Thermal Conductivity	118
Table 6.6	Middle Resistivity, Uncertainty, and Percent Uncertainty	119
Table 6.7	Average Resistivity, Uncertainty, and Percent Uncertainty	120
Table 6.8	Parameter Contribution to Uncertainty in Resistivity	120

LIST OF FIGURES

Figure 2.1	Cubic Structure of Diamond	6
Figure 2.2	CVD Growth Environment	8
Figure 2.3	Dynamic Balance Model	9
Figure 2.4	Yang's Experimental Setup	12
Figure 2.5	Thermal Conductivity as a Function of Temperature	15
Figure 2.6	Thermal Conductivity as a Function of Methane to Hydrogen Ratio	17
Figure 2.7	Thermal Conductivity as a Function of Methane Concentration	19
Figure 2.8	Local Thermal Conductivity Parallel to the Surface as a Function of Temperature	21
Figure 3.1	Radial Heat Flow Model	26
Figure 4.1	Schematic of HFCVD System	34
Figure 4.2	Photograph of HFCVD System	35
Figure 4.3	Silicon Wafer with Mask	37
Figure 4.4	Side view of the Etched Diamond Sample	41
Figure 4.5	Top view of the Etched Diamond Sample	41
Figure 4.6	Conducting Strip	42
Figure 4.7	Sample Setup	43
Figure 4.8	Photograph of Sample Viewed from the Diamond Side	43
Figure 4.9	Photograph of the Sample Viewed from the Silicon Side	44
Figure 4.10	Photograph of the Emscope SC 500 Sputter Coater	46
Figure 5.1	Schematic Diagram of the Experimental Setup	49
Figure 5.2	Photograph of the Data Acquisition System	50
Figure 5.3	Photograph Model 600L (Scanner and Control Unit)	52
Figure 5.4	Optical Path of the Scanner	53
Figure 5.5	Photograph of Lens	55
Figure 5.6	Black Plate with Heater Attached	56
Figure 5.7	Black Plate at Room Temperature	58
Figure 5.8	Temperature Distribution of Heated Black Plate	58
Figure 5.9	Black Plate with Attached Sample	59
Figure 5.10	The Four Probe Method	64
Figure 5.11	Photograph of the Four Probe Instrument	65
Figure 5.12	Sloan Dektak IIA	68
Figure 5.13	Step Height using RST-Plus (Sample #17)	70
Figure 5.14	Step Height using RST-Plus (Sample #3)	70
Figure 5.15	Corner Profile of Thickness (Sample #17)	72

Figure 5.16	Corner Profile of Thickness (Sample #3)	72
Figure 5.17	Bullseye at the Center for Spherical Shape (Sample #3)	73
Figure 5.18	Focal Plane of LSM	74
Figure 5.19	Thickness Measurement on the left edge of Sample #3 using LSM	75
Figure 5.20	Thickness Measurement on the right edge of Sample #3 using LSM	76
Figure 5.21	Thickness Measurement Sample #4 using Newview 100	78
Figure 5.22	Thickness Measurement Sample #5 using Newview 100	78
Figure 5.23	Oblique Plot of Surface for Sample #5	79
Figure 5.24	Oblique Plot of Surface for Sample #4	79
Figure 5.25	Surface Profile of Sample #4	80
Figure 5.26	Surface Profile of Sample #5	80
Figure 5.27	Thickness Measurement (Test #3)	83
Figure 5.28	Thickness Measurement (Test #7)	84
Figure 5.29	Thickness Measurement (Test #9)	84
Figure 5.30	Adjustable Clamp with Sample	87
Figure 6.1	Measured versus Calculated Temperature (Sample #17)	94
Figure 6.2	Residuals (Sample #17)	95
Figure 6.3	Sequential Estimation of Thermal Conductivity (Sample #17)	96
Figure 6.4	Thermal Conductivity as a function of Average Resistivity	97
Figure 6.5	Irvin Curve for Diamond	99
Figure 6.6	Thermal Conductivity as a function of Middle Resistivity	101
Figure 6.7	Combine Plot of Measured Thermal Conductivity	102
Figure 6.8	Graebner et al. results showing effects of each type of defect	106
Figure 6.9	Curve Fit of Thermal Conductivity as a Function of Middle Resistivity	109
Figure 6.10	Curve Fit of Thermal Conductivity as a Function of Average Resistivity	110
Figure 6.11	Comparison between Calculated Uncertainty and Measured Uncertainty	115
Figure 6.12	Measured Uncertainty Relative to Mean Thermal Conductivity Estimates	116
Figure 6.13	Sensitivity of Thermal Conductivity to Thickness of Diamond	117
Figure 6.14	Experimental Results plotted as a Function of Average Resistivity with Error Bars	121
Figure 6.15	Experimental Results plotted as a Function of Middle Resistivity with Error Bars	121

LIST OF SYMBOLS

K, k	Thermal Conductivity
P	Power
L	Length
A	Area
k_B, σ	Boltzmann Constant
h	Planck Constant
T	Temperature
θ	Temperature difference, Debye Temperature
λ	Thermal Conductivity
δ, d	Thickness
ε	Emissivity
T_s	Surrounding Temperature
T_m	Minimum Temperature
T_{AC}	Temperature Amplitude
q	Quantity of Heat
f	Heating Frequency
C_p	Specific Heat
q_x, q_y, q_z	Heat Flow in the x, y, z Direction
ρ	Resistivity, Density
g	Internal Heat Generation
h	Convection Coefficient
r	Radial Position
m_f	Convective Fin Term
I_0	Modified Bessel Function of the First Kind of Order Zero
K_0	Modified Bessel Function of the Second Kind of Order Zero
q_{rad}	Heat Flow due to Radiation
b	Radius
R_D	Sheet Resistivity
V	Voltage
I	Current
T_i	Measured Temperature
Y_i	Calculated Temperature
δ_d	Thickness of Diamond
δ_g	Thickness of Gold
R	Resistance

T_b	Boundary Temperature
S	Least Square Function
ω	Phonon Frequency
v	Phonon velocity
a,b	Constants
Δ	Uncertainty

CHAPTER 1

INTRODUCTION

Thin films have been known to mankind for hundreds and possibly thousands of years. Examples would include the layers of paint used by prehistoric man to decorate his caves, and more recently some of the decorative glazes that were applied to primitive pottery. However, in the space of a few years, thin films have been elevated in status from relative obscurity to a firmly established technology which plays an important role in many industrial processes. Thin films as a specialized technology have come to refer to layers deposited by some type of atom by atom process rather than to layers produced by laying down relatively large particles to form a truly continuous layer. The type of thin films discussed here will be restricted to those deposited in some type of vacuum or low pressure environment. These techniques have been known for some time, and are centered around three major methods: vacuum evaporation, sputtering, and chemical vapor deposition (Maissel, 1973). In the following work, two of these techniques (chemical vapor deposition and sputtering) are utilized in an experimental technique for the determination of the thermal conductivity of thin diamond films.

Diamond is a material which has captivated the imagination of scientists and engineers for centuries, not only for its rare jewel status, but also because of its hardness, chemical composition (inert) and high thermal conductivity. Because of diamond's

unique physical properties, it has been proposed for application as a heat sink, wear resistant coating, cutting tool, and protective coating for infrared optics in harsh environments (May 1995). The use of diamond in such applications was hindered due to its limited abundance in nature and unsuccessful attempts by scientist and engineers to synthesize it in the laboratory. Diamond synthesis has attracted attention after it was discovered in 1797 that diamond is a crystalline form of carbon. Initially, synthesizing was attempted at high pressure since that diamond is a very dense form of carbon. In 1955, Bundy and coworkers at General Electric succeeded in the synthesis of diamond (Nassau, 1993). Their success was achieved at very high pressure and temperature, therefore limiting widespread production. However, recent developments in Chemical Vapor Deposition (CVD) methods has transformed diamond from a rare gem to an engineering material which can be produced easily and used rather extensively.

As mentioned above, one of the most attractive properties of diamond is its high thermal conductivity. Type IIa single crystal diamond has exhibited thermal conductivity values as high as 2200 W/m K, more than five times that of copper (400 W/m K). However, the degree to which CVD diamond film compares to single crystal diamond depends significantly on the preparation conditions. The conditions for synthesizing CVD diamonds films and its relationship to thermal conductivity has yet to be understood fully. Preliminary results of thermal conductivity have shown variation by a factor of 3 to 5 (Graebner, 1994).

One preparation condition of major importance is boron doping of diamond during synthesis. Boron allows the diamond crystals to become charge carriers, and the added impurities can greatly affect the thermal properties. Therefore, the thermal conductivity of diamond films must be determined as a function of the doping level of each film. Before this can be accomplished, a method to measure the doping level of each film must be determined. The boron used during synthesis causes the diamond crystals to become charge carriers, therefore allowing for electrical conductance. The doping level can be measured by relating it to the electrical resistance or resistivity of the film.

CHAPTER 2

BACKGROUND/LITERATURE REVIEW

One of the most attractive properties of diamond is its very high thermal conductivity, which in single crystals can be as high as 2200 W/m K (Graebner,1992). Polycrystalline diamond created by Chemical Vapor Deposition (CVD) has also shown high thermal conductivity. However it is not as large as that of its single crystal counterpart. Early reports for thermal conductivity of CVD diamond films indicate variation by factors of 3 to 5 from sample to sample (Graebner, 1994). While different experimental techniques has been used to determine thermal conductivity, it is presumed that this variation is due to the conditions under which the diamond films were fabricated rather than the technique used. However, measurements of a single sample by different researchers has also shown variation. Table 2.1 shows results of tests performed on one sample by different researcher.

Sample	Sinku-Riko (W/m K)	Norton (W/m K)	Wurzburg (W/m K)	GE (W/m K)	AT&T (W/m K)
LD-X	15.5	14.1		25.6	
LD-E	2.6-4.4	3.6		6.6	
SQ-E			2.6-4.0	4.7	5.1
SQ-T			5.2	8.0	14.0
SQ-F			5.9	9.2	12.3
SQ-FB			4.1	6.6	6.7
SQ-X			8.0	10.3	18.0

Table 2.1 Round robin testing

The results in Table 2.1 shows that measurements which should be comparable can actually differ by a factor of two (or more). In this chapter, a basic understanding of the atomic structure responsible for diamond's high thermal conductivity is presented, along with the mechanism necessary for diamond growth and the various techniques (and preparation conditions) used to experimentally determine the thermal properties. The principles and background presented in this chapter are essential to understand the doping process, and its affect on the thermal conductivity of diamond films.

2.1 ATOMIC STRUCTURE OF DIAMOND

As in any crystalline solid, the atoms in diamond are linked together in a simple and regular way. Diamond is exclusively a face-centered cubic structure with atoms bonded together in strong sigma type covalent bonds. The cubic structure is shown in Figure 2.1.

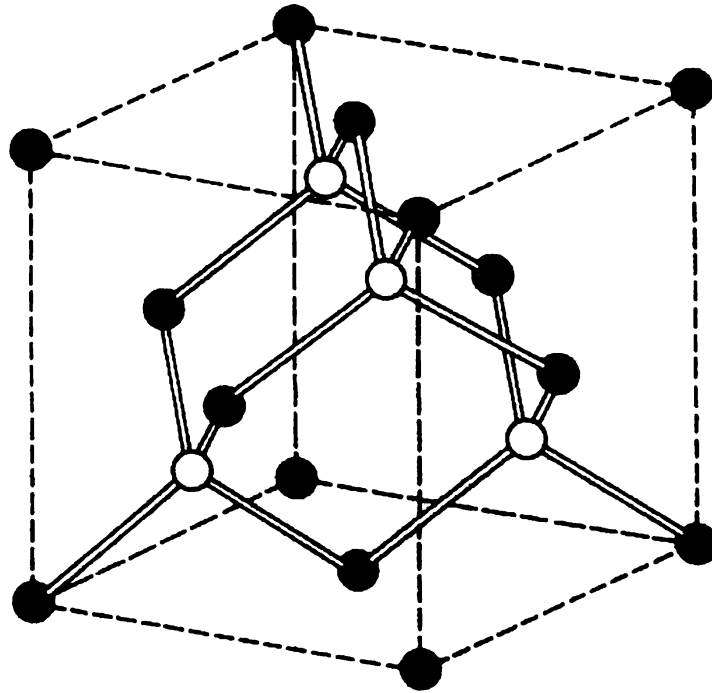


Figure 2.1 Cubic structure of diamond (Wilks, 1991)

As shown in Figure 2.1, the structure consists of eight corner atoms, six face-center, and four other atoms. Each carbon atom is tetrahedrally coordinated to four carbon atoms via sigma bonds emanating from Sp^3 hybrid atomic orbitals (Wilks, 1991). Within the cube are four atoms shown as open circles each of which is linked by four bonds to one of the black atoms around it. This arrangement repeats itself through the diamond. The atoms shown as open circles also lie on the points of another face-centered cubic lattice similar and parallel, but somewhat displaced from the first lattice. Therefore, the complete diamond lattice may be described as consisting of two interpenetrating face centered cubic lattices (Wilks, 1991). It is this structure and strong molecular bonding which gives diamond its extreme hardness and high thermal conductivity.

In polycrystalline diamond films made by CVD, various preparation conditions can contribute to impurities and geometric defects in the atomic structure. These anomalies can have a significant affect on the physical properties (including thermal conductivity). Therefore, in order to characterize CVD diamond film properties, the influence of impurities and geometric defects on the thermal conductivity must be understood for different preparation conditions.

2.2 MECHANISM OF DIAMOND GROWTH

The growth of diamond from the vapor phase in a reactor begins with nucleation, the initial formation of a crystal, followed by epitaxial growth, the deposition of additional carbon on the surface to increase bulk dimensions. While there are many CVD techniques which have successfully produced diamond, the basic principles necessary for an operative system are given below.

The CVD growth environment can be quite complex and varied, as shown in Figure 2.2.

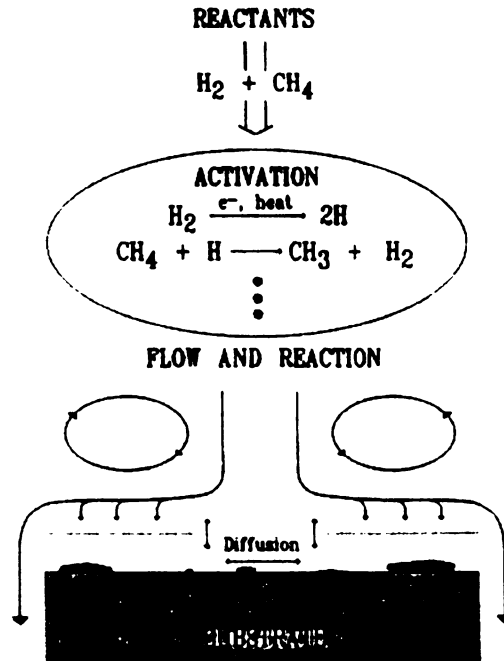


Figure 2.2 CVD Growth environment (Pehrsson, 1993)

The reactants, methane and hydrogen, enter a high temperature or energetic region in which the gas is activated by a plasma, hot filament, or a combustion flame front. The species participating in this reaction are transported by forced flow, diffusion, and convection throughout the reactor, eventually reaching the substrate (Pehrsson, 1993).

In order for nucleation to proceed, an incipient nucleus must form and be stable long enough for lattice growth to occur. The development of a critical nucleus (one large enough to survive and grow rather than decay) depends on the system free energy changes accompanying particle formation under growth conditions. The change in the system free energy must be negative for the process to occur, where the system includes the substrate, growing particles, and the gas-phase reservoir of species contributing to

lattice growth (Pehrsson, 1993). Therefore, the substrate and its pretreatment prior to growth have a large influence on nucleation and the initial stages of growth.

Epitaxial growth of diamond can be explained using various macroscopic models. One such model which is simple to explain is the dynamic balance model. In this model, the growth environment is viewed as a dynamic balance or kinetic competition between carbon deposition and etching processes for other forms of carbon, Figure 2.3 (Pehrsson, 1993).

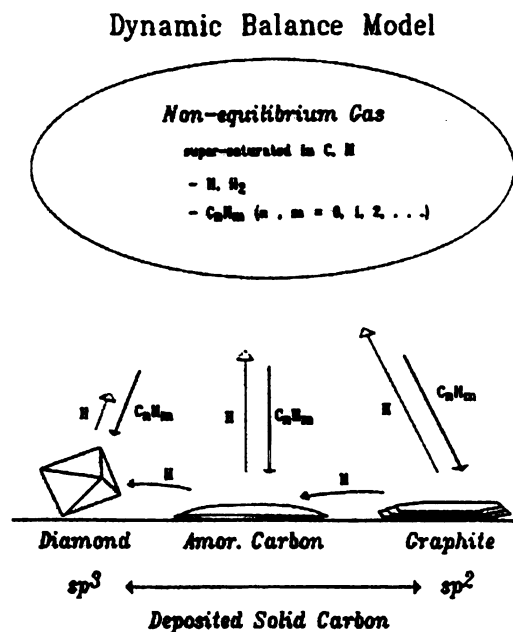


Figure 2.3 Dynamic balance model (Pehrsson, 1993)

Carbon supersaturation provides the driving force for the condensation of various forms of solid carbon including diamond, while atomic hydrogen provides a reactive

environment for the removal or suppression of the non-diamond carbon by etching of solid carbons and /or converting surface Sp^2 bonded sites into Sp^3 bonds. While this model does not identify the detailed gaseous or surface mechanism leading to diamond growth, it explains general results common to many growth environments (Pehrsson, 1993).

2.3 DIAMOND AS A SEMICONDUCTOR

In order for diamond to become a semiconductor, it must be doped with a material such as boron during synthesis. Boron allows the diamond crystals to become charge carriers, therefore allowing electrical conductivity in an otherwise insulating material (Herr, 1993). Boron was chosen as a suitable dopant because from a geometric and energetic standpoint, boron is probably the only element that substitutionally dopes diamond without significantly distorting its lattice structure. It can easily be incorporated into polycrystalline films during chemical vapor deposition from either a gas, powder, or solid source (Das, 1993). The ease with which boron allows for the semiconducting characteristic to be introduced into diamond makes doping an emerging technology.

The process which explains how the presence of boron leads to an electrical conductivity in diamond must be investigated on an atomic level. Consider a diamond in which a small number of carbon atoms have been replaced substitutionally by atoms of boron. Boron lies next to carbon in the periodic table of the elements so that the atoms

are of quite similar size but have only three electrons to share with the four surrounding carbon atoms. There is the possibility of electrons from the full valence band moving to the boron sites to bond with adjacent carbon atoms left unbounded. The boron therefore acts as an acceptor site, the energy of the extra electron being somewhat higher than the energy of the top of the valence band. Once electrons have moved up to the acceptor level, the valence band is no longer completely full. Therefore the electrons in the band can be accelerated without leaving the band, and carry a current which is proportional to the number of missing electrons or holes. Note that the diamond will only conduct if electrons in the valence band have enough energy to move up to the higher levels associated with boron atoms (Wilks, 1991).

While it is fairly easy to dope diamond using boron, it is rather difficult to control the level of doping. One method presently used to determine the level of doping is the electrical resistance of the diamond film. Since highly doped films will conduct electricity better (lower resistance), measurement of the electrical resistance for a film is a simple and an effective way to determine the amount of boron or level of doping present in each film. While the electrical resistance is easy to measure, it has been shown that boron doped diamond possesses a great deal of variability of resistance over relatively small area. In work conducted by Yang (1996) at Michigan State University, the resistance was investigated over a small area (approximately 2 cm) and the measured values are shown in Table 2.2. The local regions are

	R1	R3	R4	R6	R9	R10
Thickness (microns)	1.23	1.19	1.23	1.19	1.19	1.18
Width (microns)	267	260	272	253	261	256
Length (microns)	225	235	235	250	240	235
Resistance (Kilo ohms)	85.5	88.9	319.2	440.7	532.5	509.5

Table 2.2 Yang's resistance measurements (Yang, 1996)

represented by R1, R2, etc., and the dimensions corresponding to each region is shown. The data shows that the resistance increases as distance from R1 increase, except for the resistance at R9, which is greater than R10. This is evidence that boron doping using the method describe here varies randomly. The lengths, widths, and thicknesses are for the local area which was considered in each case. A diagram showing the setup and region investigated is also presented (Figure 2.4).

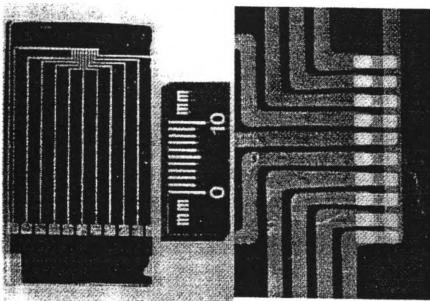


Figure 2.4 Yang's experimental setup (Yang, 1996)

The above information shows that boron doped diamond films can have resistances which vary by factors of 5 over a distance of approximately 2 cm. While the resistances in the films used in the present work have less variability (factor of 2 over 1.5 cm), it should be noted that the spatial distribution of resistance is not uniform in the boron doped diamond films used here.

2.4 DETERMINATION OF THERMAL CONDUCTIVITY

Because of diamond's fast thermal response, preparation conditions, and microstructural size, experimental determination of thermal properties is often difficult. For this reason, most techniques presently being used to determine thermal conductivity involve either special sample design or complicated and expensive equipment setup. Although complicated, many researchers have successfully studied diamond films, and preliminary results for the thermal conductivity has ranged from about 50 to 2200 W/m K. This enormous range of values is primarily due to the preparation conditions which contributed to diamond growth. Many researchers have shown that preparation conditions greatly affect the quality of diamond produced. Therefore, in order for diamond to be properly used in many industrial applications, the preparation conditions and their relationship to thermal properties must be thoroughly understood. The two most common methods to grow diamond, the hot filament chemical vapor deposition (HFCVD) method and the microwave plasma chemical vapor deposition (MPCVD) method, have proven to exert little influence on the thermal properties (Graebner, 1994).

However, the preparation conditions (doping, temperature, pressure, gas mixture content, etc.) can influence the properties of the diamond significantly. The diamond's quality ultimately dictates the magnitude of the thermal conductivity. In this section, a discussion of the various conditions used to grow diamond, and what affect each condition has on the measured thermal conductivity is presented.

Morelli, Beetz, and Perry (1988) investigated the thermal conductivity of diamond films as a function of temperature. In their work, two diamond films with dimension 10mm by 5mm were grown using the hot filament chemical vapor deposition (HFCVD) method with chamber pressure of approximately 9 Torr and methane concentration of about 0.18%. The thermal conductivity was measured using a steady state probe technique. The setup consisted of thermally anchoring one end of the sample to a copper clamp which was then exposed to a cold reservoir (closed cycle helium refrigerator). A lightweight strain gage heater was then attached to the other end using conductive silver paint. This heater was used to generate a temperature difference, ΔT , across the film. For a heater power, P , the thermal conductivity, K , of the film is given by

$$K = \left(\frac{P}{\Delta T}\right)\left(\frac{L}{A}\right) \quad (2.1)$$

where A is the cross sectional area of the film and L is the distance across the film where ΔT is generated. Morelli et al. attached a type E thermocouple (chromel-constantan) to the surface of the film. The thermal conductivity was measured over a temperature range from 10 to 300 K. The measured values for thermal conductivity over the temperature

range studied were smaller in magnitude relative to “bulk” single crystal diamond. In order to understand the behavior of their samples, Morelli et al. attempted to fit their data to a standard Debye-type expression for the thermal conductivity of a crystal given by

$$K = \frac{k}{2\pi^2 v} \left(\frac{k}{\hbar}\right)^3 T^3 \int_0^{\frac{\theta}{T}} \tau(x) \frac{x^4 e^x}{(e^x - 1)} dx \quad (2.2)$$

Using this model, it was concluded that the lower values for thermal conductivity were due to scattering processes acting in the films. These processes acting on the phonons were subsequently quantified to determine the role of each process on the value of thermal conductivity. Figure 2.5 shows their results along with comparison data from Berman et al.

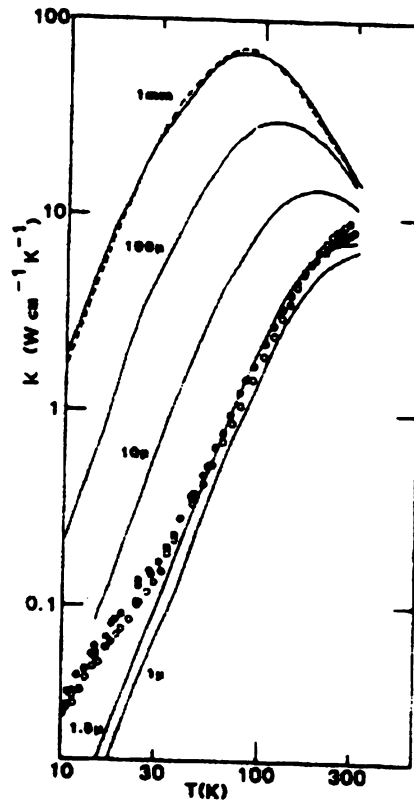


Figure 2.5 Thermal conductivity as a function of temperature (Morelli et al., 1988)

For diamond, the processes considered included scattering by crystal boundaries, other phonons via umklapp processes, and point defects such as isotopes and impurities in the lattice.

One work which specifically addresses thermal conductivity as a function of the preparation condition was that by Ono, Baba, and Funamoto (1986). In their investigation, the thermal conductivity was measured for different methane concentrations during synthesis. In the experimental setup, a thin sample was held by heated supports at both ends in a vacuum. The front and rear surfaces of the sample were coated with black paint so the temperature distribution along the length can be measured by a thermography system through an optical window. Since the sample was in a vacuum, heat transfer by convection was eliminated. Therefore, conduction and radiation were the primary modes of heat transfer. For steady state, the governing differential equation is

$$\lambda d \left(\frac{\partial^2 T}{\partial x^2} \right) = 2 \varepsilon_{h,r} \sigma (T^4 - T_s^4) \quad (2.3)$$

where λ = thermal conductivity, d = thickness, ε = emissivity, and σ = Boltzmann constant. After a few simplifying assumptions, the solution is given by

$$T = \frac{(T_m^4 - T_s^4)}{4T_m^3} (\cosh(kx - 1)) + T_m \quad (2.4)$$

where T_m is the minimum temperature of the sample at $x=0$ and the constant

$k = (8\epsilon_{h,r}\sigma T_m^3 / \lambda d)^2$, therefore thermal conductivity is given by

$$\lambda = \frac{8\epsilon_{h,r}\sigma T_m^3 x^2}{d \{ \cosh^{-1} [4T_m^3 (T - T_m) / (T_m^4 - T_s^4) - 1] \}^2} \quad (2.5)$$

The experiment was conducted on free standing polycrystalline diamond films $7\mu\text{m}$ to $30\mu\text{m}$ thick deposited by microwave CVD under a pressure of 4 kPa and a methane concentration ranging from 0.1% to 3.0% volume ratio of methane to hydrogen. The results showing thermal conductivity as a function of methane to hydrogen concentration ratios are shown in Figure 2.6

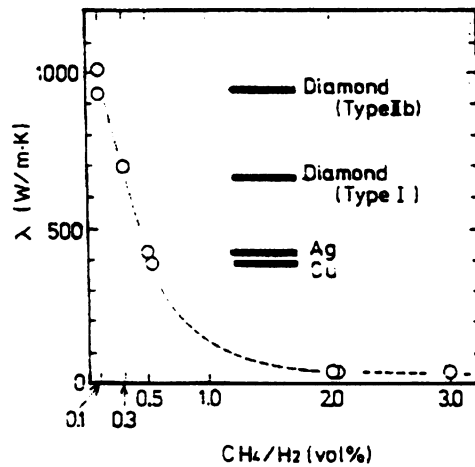


Figure 2.6 Thermal conductivity as a function of methane to hydrogen ratio (Ono et al., 1986)

In looking at the results, it should be noted that the effect of varying the thickness on the thermal conductivity was not addressed. Previous reports have shown that thermal conductivity varies with sample thickness. Therefore, the results presented by Ono et al.

possess uncertainty with respect to the variation of both thickness and methane to hydrogen concentration ratios.

Similar work based on methane concentration was performed by Baba, Aikawa, and Shahata (1991). In their work, diamond films were prepared by the hot filament CVD technique with varied CH₄/H₂ ratio, and thermal conductivity was subsequently estimated as a function of CH₄ concentration. The AC Calorimetric method was used to measure the thermal diffusivity, which estimated the thermal conductivity using published values of density and specific heat. In the AC Calorimetric method, one end of the sample is periodically heated by a halogen lamp and the temperature amplitude (AC temperature) at a point a distance X from the heating area is monitored with a thermocouple attached directly to the sample surface. The relation between AC temperature and distance x is given by

$$\ln|T_{AC}| = \ln\left(\frac{q}{4\Pi f C d}\right) - \left(\frac{\Pi f}{D}\right)x \quad (2.6)$$

where q is the quantity of heat absorbed by the sample, f is the heating frequency, and C, d, and D are specific heat, thickness, and thermal diffusivity of the sample, respectively.

For methane concentration which varies from 1% to 5%, the thermal conductivity varied from 200 to 1200 W/m K. A graph showing the results is given in Figure 2.7.

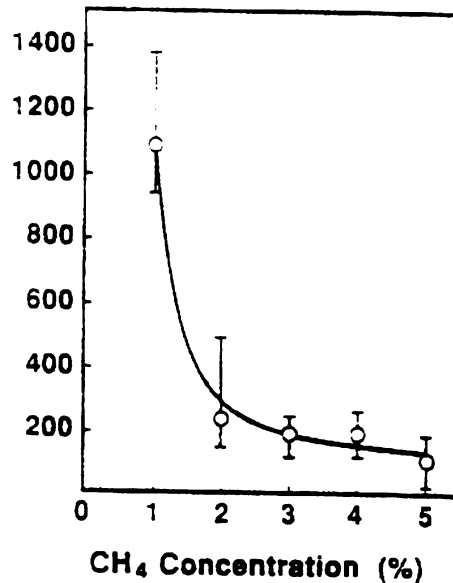


Figure 2.7 Thermal conductivity as a function of methane concentration (Baba et al., 1991)

The results agreed with those of Ono et al. except for the value of thermal conductivity (plotted on the y axis) at 1%. The authors suggested that the difference may be due to the difference in the deposition technique and the film qualities, such as grain size, impurities, defects, etc.

In order to quantify the values measured for the thermal conductivity of CVD diamond films, Graebner et al. (1994) compared isotropically enriched polycrystalline diamond to that of “gem quality single crystal” diamond. Studies of the thermal conductivity in enriched synthetic single crystal diamond have shown an increase in thermal conductivity as the ¹³C concentration is reduced from its natural abundance of

1.1% to 0.07%. The presence of ^{13}C causes point defects which increases phonon-phonon scattering, thereby adversely affecting the thermal conductivity. To understand this effect more thoroughly, the authors prepared thick films (650 μm) using ^{12}C enhanced methane.

The thermal conductivity was measured using a DC technique, and it was discovered that the enriched films have thermal conductivities of about 2180 W/m K parallel to the surface and 2600 W/m K perpendicular to the surface. The value of 2600 W/m K exceeds the highest reported data for natural abundance gem quality diamond (2400-2500 W/m K). Their results proved that enriched CVD films can ultimately reduce point defect scattering of phonons to less than those present in natural abundance diamond.

In another work by Graebner, Jin, Herb, and Gardinier (1992), the thermal conductivity of CVD diamond samples of various thicknesses were measured over a temperature range from 5-400K. It was discovered that thermal conductivity is anisotropic as well as having a gradient with respect to height above the substrate. In order to investigate thermal conductivity as a function of thickness, five samples were created under similar conditions with the exception of deposition time (and therefore thickness). The microwave enhanced CVD method was used with pressures of 100 Torr and temperatures between 800 and 900 C. The thermal conductivity was measured using a DC technique. This technique uses thin-film heaters deposited on the diamond surface

and fine-wire thermocouples attached with silver epoxy in the standard heated bar configuration. A second heater near thermal ground permits the detection of and correction for any heat loss by radiation.

The measurement technique used averages thermal conductivity over the thickness of the sample. A local conductivity is obtained by subtracting the conductance of any sample of thickness, Z , from the conductance of the next thicker sample and divides by the difference in thickness to obtain a conductivity average over only the upper part of the thicker sample. The local values of thermal conductivity at height, Z , above the substrate is given in Figure 2.8.

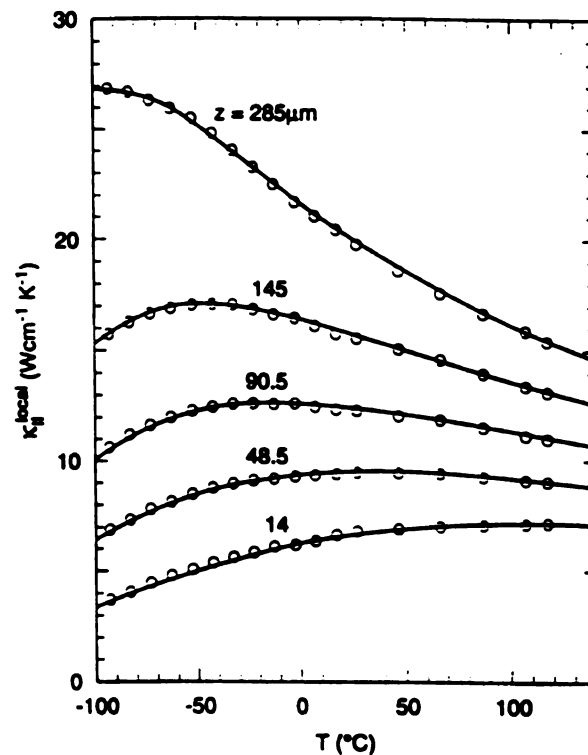


Figure 2.8 Local thermal conductivity parallel to sample surface as a function of temperature (Graebner et al., 1992)

These values indicate that thermal conductivity increases with distance from the substrate.

While there are many manufacturing methods (HFCVD, MPCVD, etc.) and conditions which successfully produce diamond growth, the variation of thermal conductivity is significantly dependent on the specific conditions for which the specimen was made. The doping of diamond films is just one condition which is not understood, and therefore doping is the main focus of the present work. Boron doped diamond is an emerging technology which deserves a great deal of attention for future application as semiconductors.

CHAPTER 3

MATHEMATICAL MODEL

Before any experiments can be performed to estimate thermal conductivity, an accurate model must be developed. Without such a model the thermal properties cannot be estimated, and without an accurate account of all heat transfer modes, any results will be meaningless. In this chapter, the radial heat flow model is developed, along with some of the simplifying assumptions used in generating an experimental setup.

3.1 CONDUCTION MODEL

In a solid body that contains variations of temperature, heat flow proceeds from a region of high temperature to a region of low temperature. The term heat flow is the rate of energy (joules/sec) associated with the vibration energy of atoms and molecules in the body, and heat flux is the rate of heat flow per unit area at any point in the body. While heat flux cannot be directly measured, it can be deduced from the temperature distribution inside a solid body if the relationship between temperature and heat flux is thoroughly understood (Beck, 1992). The relationship between heat flux q and temperature T is given by Fourier's law which states that

$$\bar{q}(\bar{r}, t) = -k(\bar{r}, t) \nabla T(\bar{r}, t) \quad (3.1)$$

where k is the effective thermal conductivity, and the minus sign is inserted in accordance with the second law of thermodynamics. In general, heat flux is a vector quantity, and in rectangular coordinates the components are given by

$$q_x = -k \frac{\partial T}{\partial x} \quad q_y = -k \frac{\partial T}{\partial y} \quad q_z = -k \frac{\partial T}{\partial z}$$

To properly model a heat conduction problem, a solution of the heat conduction equation (also called the energy equation) must be derived from the general integral form of the energy equation (Beck, 1992).

$$\int_{c.s.} (\bar{q} \cdot \bar{n}) dA + \int_{c.v.} g(\bar{r}, t) dV = \int_{c.v.} \rho C_p \frac{\partial T}{\partial t} dV \quad (3.2)$$

$$\text{where } q = -k \frac{\partial T}{\partial \bar{r}} \text{ and } \bar{r} \text{ is a vector}$$

In the general equation, the first term on the left hand side represents the net rate of heat flow in, the second term represents the rate of internal heat generation, and the third term represents the rate of heat storage within the system. The general equation accounts for all heat flow processes within a system.

3.2 THE RADIAL HEAT FLOW MODEL

The radial heat flow model was chosen because of its analytic simplicity and small uncertainty in estimation of the thermal conductivity (Herr, 1993). The governing differential equation for the radial heat flow includes the following assumptions

- 1) heat flow dissipated by conduction
- 2) radiation neglected
- 3) no energy storage (steady state condition)
- 4) isothermal in the z-direction ($q_z=0$)
- 5) diamond is isotropic in all direction

which simplifies the heat conduction equation to

$$k \frac{d^2 T}{dr^2} + \frac{k}{r} \frac{dT}{dr} - \frac{2h}{\delta} (T - T_\infty) + g = 0 \quad (3.3)$$

a schematic diagram showing the radial heat conduction model is shown in Figure 3.1

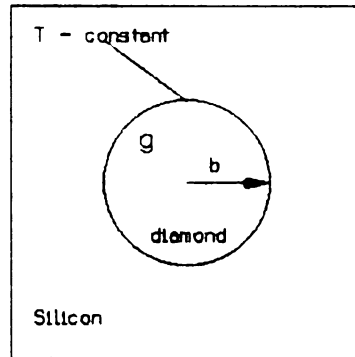


Figure 3.1 Radial Heat Flow Model

The boundary conditions are

$$\left. \frac{\partial T}{\partial r} \right|_{r=0} = 0 \quad \text{and} \quad T|_{r=b} = \text{Constant}$$

The assumption of constant temperature at the boundary is made due to the silicon substrate that remains at the edges of the sample, and the fact that the boundary temperature can be measured directly. The silicon is more than 50 times as thick as the diamond film and has a thermal conductivity of 150 W/m k so that it acts as a thermal heat sink. The large thermal mass at the edges allows the temperature at this boundary to remain at a lower constant value compared to the exposed surface of the film at steady state.

The general solution for the radial heat flow is described by:

$$T(r) = C_1 I_0(m_f r) + C_2 K_0(m_f r) + \frac{g}{m_f^2 k} + T_\infty \quad (3.4)$$

Application of the boundary conditions yields

$$T(r) = \frac{g}{m_f^2 k} \left(1 - \frac{I_0(m_f r)}{I_0(m_f b)}\right) + T_\infty \quad (3.5)$$

where g = volumetric energy generated, $m_f = \sqrt{\frac{2h}{k\delta}}$, b = radius, T_∞ = surrounding temperature, r = radial position, and k = thermal conductivity. Equation 3.5 is the solution for the temperature distribution for radial heat flow with internal heat generation, natural convection losses on both sides, and a constant temperature boundary condition at $r=b$.

3.3 SIMPLIFIED MODEL

The experimental model can be simplified if other modes of heat transfer can be neglected. This section will show that convection and radiation effects can be neglected.

3.3.1 Radiation consideration

Because of the relatively small temperature rise used experimentally (about 10 degrees above room temperature), the effects of radiation can be neglected. The validity of this

assumption can be demonstrated by comparing the heat transfer due to radiation with the total heat generated within the sample. Heat transfer by radiation is described by

$$q_{rad} = 2A\epsilon\sigma(T^4 - T_{\infty}^4) \quad (3.6)$$

where

$$A = \pi r^2$$

for $r=1.5 \times 10^{-3}$ m, $A=7.069 \times 10^{-6}$ m², $\sigma = 5.67 \times 10^{-8}$ W/m² K⁴, $T=305$ K, $T_{\infty}=298$ K, and $\epsilon=0.62$,

$$q_{rad} = 3.88 \times 10^{-4} \text{ W}$$

This value for radiation is small when compared with the heat generated ($P=V^2/R$).

Typical values are $V=1$ volts and $R=1.5 \Omega$, therefore $P=0.667$. This analysis shows that

$$\frac{q_{rad}}{q_{generated}} = \frac{3.88 \times 10^{-4}}{0.667} = 5.8 \times 10^{-4} \text{ W}. \text{ Therefore, heat loss by radiation accounts for about}$$

half of 1% of the heat generated.

3.3.2 Natural convection consideration

Because of the small area and small temperature difference, the heat loss due to natural convection can also be neglected. If the governing differential equation is divided by g/k , the non-dimensional convection term becomes $-2h\theta/g\delta$. This parameter represents the fraction of the total heat lost by convection to the total heat generated (Herr, 1993).

Substituting the radial heat flow solution evaluated at $r=0$ into the non-dimensional convective term yields

$$\left| \frac{2h\theta(0)}{g\delta} \right| = 1 - \frac{1}{I_0(m_f b)} \quad (3.6)$$

where $m_f = \sqrt{\frac{2h}{k\delta}}$

evaluating the non-dimensional convective term using

$k=200 \text{ W/m K}$, $h=10 \text{ W/m}^2 \text{ k}$, $\delta=2.1 \times 10^{-6} \text{ m}$, and $b=1.5 \times 10^{-3} \text{ m}$

yields 0.026. This analysis revealed that 2.6% of the heat generated is lost to convection,

therefore heat lost by convection is small and can be neglected. With the effects of

radiation and convection neglected the governing differential equation can be written as

$$k \frac{\partial^2 T}{\partial r^2} + \frac{k}{r} \frac{\partial T}{\partial r} + g = 0 \quad (3.7)$$

with boundary conditions

$$\left. \frac{dT}{dr} \right|_{r=0} = 0 \quad \text{and} \quad T|_{r=b} = \text{Constant}$$

The solution to this problem is

$$T(r) = T_h + \frac{gb^2}{4k} \left[1 - \left(\frac{r}{b} \right)^2 \right] \quad (3.8)$$

This is the simplified model for the radial heat conduction problem.

CHAPTER 4

SAMPLE DESIGN

Diamond films are one of the most difficult materials to analyze thermally. Due to their microstructural size and fast thermal response, they pose problems in the space and time domains (Herr, 1993). Because of these problems, optimum sample design is extremely important in order to comply with the experimental model discussed previously. This chapter discusses the complete fabrication of the diamond film sample from the wafer preparation to gold deposition, and explains why each procedure is necessary to run the experiment and acquire accurate temperature data.

4.1 WAFER PREPARATION

The first step in the design of the samples is to prepare the wafer for diamond deposition. This part is crucial because if the silicon wafer is not properly cleaned and pre-treated, diamond will either not be deposited or it might not adhere to the silicon surface. The 4 inch diameter wafer (with silicon dioxide) is thoroughly cleaned using pure acetone and then methanol. It is then rinsed with (distilled) water before it is dried with nitrogen gas. This procedure is performed to verify that there are no debris or dust

particles on the silicon wafer. In order to ensure that no water droplets remain, the wafer is placed in an oven at an elevated temperature of 200°C for 20 minutes. After the wafer has been properly cleaned and dried, a solution called photoresist is applied to the surface of the SiO₂ (the silicon dioxide is important because it serves as insulation between the silicon and diamond when an electric current is passed through the diamond). Since photoresist is applied in droplets, the wafer is placed in a spin cycle for about 2 minutes at 2300 rpm. Spinning the wafer at this rate allows the photoresist to be distributed evenly across the surface. Finally, the wafer is placed in an oven preheated to about 400 °C for approximately 30 minutes. The heat treatment is included to ensure that the photoresist adheres to the surface. The application of the photoresist is very important in the deposition of diamond because it is this solution which contains diamond powder and other elements necessary to grow diamond crystals. This completes the pre-deposition phase of the silicon wafer.

4.2 MASK

While the mask is not needed for diamond growth, it is necessary for selective growth. In order to grow diamond in some areas and not in others, a mask was patterned which allowed for the exact shape and size of the diamond films.

Masking (or photolithography) takes place in two basic steps. First, the pattern on the mask is transferred onto the thin layer of photoresist. Photoresist is a light sensitive

solution similar to the coating on a regular photographic film. It changes structure and properties when exposed to light. Second, the transfer of the pattern takes place from the photoresist layer into the wafer surface layer (Van Zant, 1990). Therefore, the mask actually blocks UV rays which bombard the photoresist after it has adhered to the surface of the wafer. By exposing the photoresist to UV radiation, diamond growth occurs in regions shielded by the mask and is eliminated in the exposed regions (Herr, 1993).

4.3 DIAMOND DEPOSITION

After the wafer has been properly prepared and the mask generated, diamond can now be deposited on the silicon substrate (with SiO_2). This section provides a brief description of the hot filament chemical vapor deposition system used to grow diamond crystal on silicon substrate. Also in this section, the conditions and procedures specific to the diamond films used in the present work to experimentally determine thermal conductivity are described.

The Hot Filament Chemical Vapor Deposition system(HFCVD):

The HFCVD reactor used here was a modified version of the system originally built at Ford research lab and located in Microstructures Materials Laboratory at Michigan State University (under the supervision of Dr. Aslam, Dept of Electrical Engineering). A schematic diagram of the system is shown below

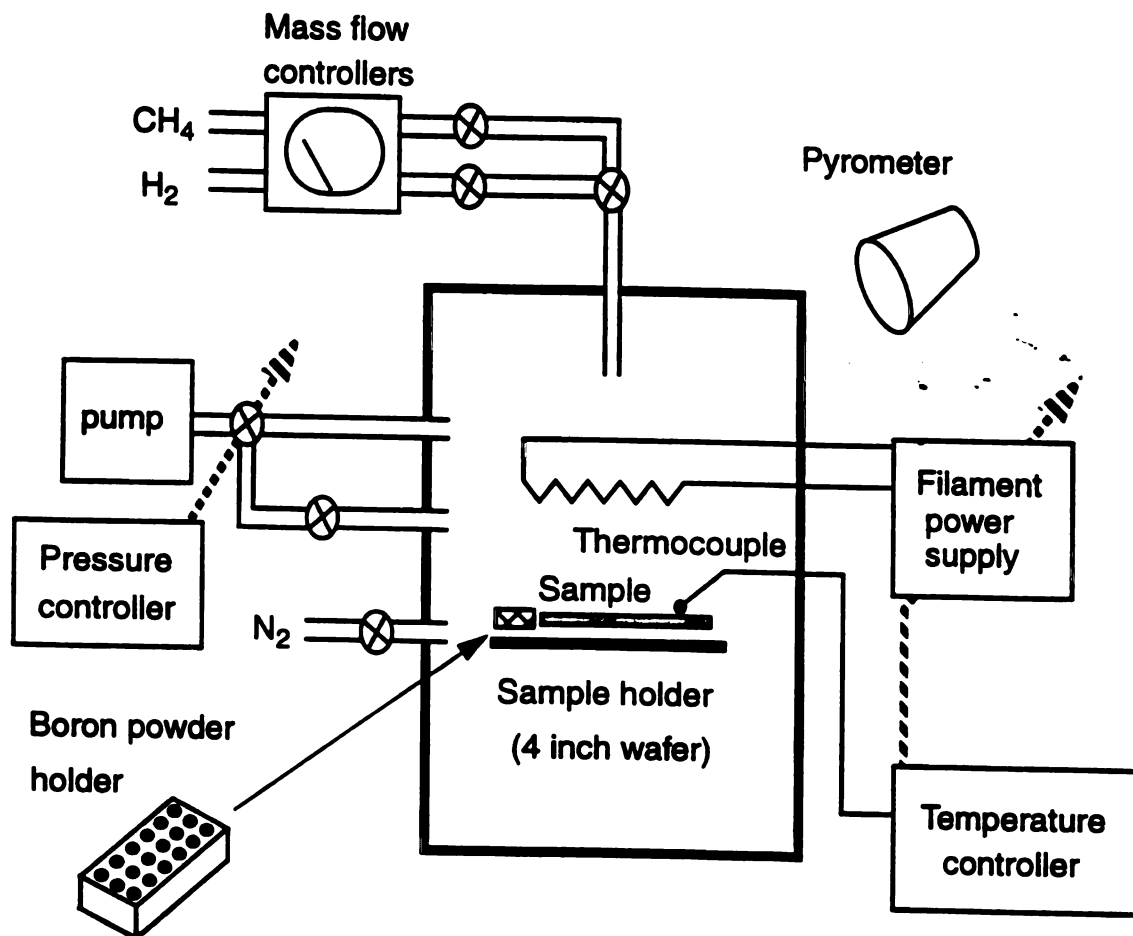


Figure 4.1 Schematic of the HFCVD system (Microstructures Lab)

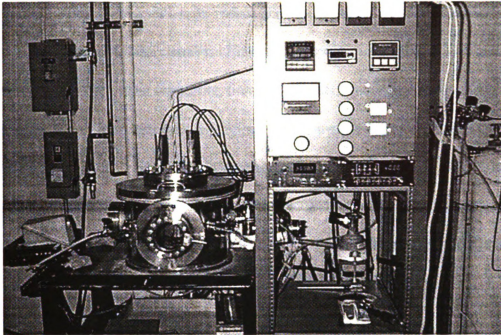


Figure 4.2 Photograph of the HFCVD system

The HFCVD reactor consists of an 18 inch diameter stainless steel chamber with a 10 inch access door. Inside the chamber are ten tantalum (Ta) filaments supported by a square frame. The filament is design to ensure uniform deposition over a 4 inch wafer. The filament typically draws 20-23 amps of current at temperatures of approximately 2300 °C. The filament temperature is monitored by an optical pyrometer through a 6 inch glass port. The gas mixture inside the reacting chamber consists of ultra-pure grade (99.995%) methane (CH₄) and hydrogen (H₂). The flowrates of these gases are independently controlled by MKS 250 pressure controllers. The operating pressure is measured by a MKS type 122A baraton pressure gauge and is controlled by a MKS 250 pressure controller via a type 248A upstream valve. The base pressure is measured by a MDC thermocouple vacuum gauge with a range of 1-1000 mtorr. A Varian SD-200

rotary pump is used for evacuation (to reduce chamber pressure). In addition, nitrogen is used to purge and backfill the chamber. Either 4 inch wafers or graphite plates can be used as sample holders. The supporting frame for the filament is specifically designed with a vertical movement mechanism to adjust the separation distance between the filament and the substrate. Two type K thermocouples are used to measure the temperature of the top and bottom side of the substrate during the deposition process. Since a large amount of heat is generated by the square filament array, no additional substrate heating is required to maintain an average substrate temperature of approximately 900 °C (Yang, 1996).

Operating procedure:

The properly cleaned and dried silicon wafer, along with the mask, is placed inside the reacting chamber. The doping source (Boron powder) is positioned precisely on the silicon wafer. A diagram showing the silicon wafer, which is masked for sample configuration, and boron source location is shown in Figure 4.3

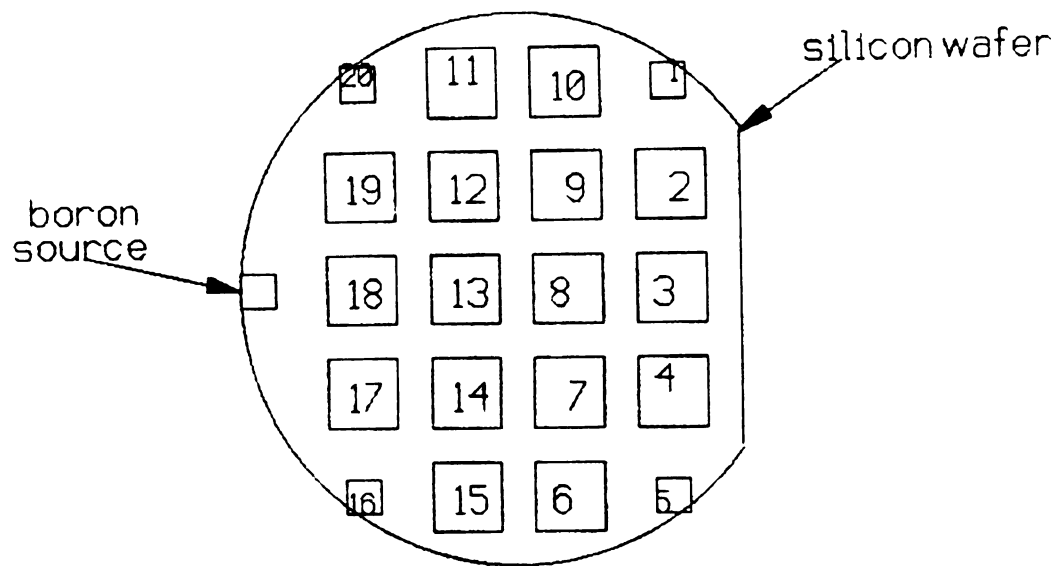


Figure 4.3 Silicon wafer with mask

The numbers correspond to each sample and were chosen for simplicity. The sample number described later corresponds to each film location on this figure. The silicon substrate and the boron source are loaded on the sample holder. The distance between the filament and the substrate is then adjusted so that the filament is only a few centimeters above the substrate. The chamber is then sealed and evacuated to a base pressure less than 10 mtorr. Hydrogen is then introduced into the chamber. The addition of hydrogen causes the chamber pressure to rise. When the chamber pressure is above 20 torr, the current to the filament is adjusted in order to raise the filament temperature to about 2300C. A slow adjustment of the current is desired to avoid damage to the filament. The methane (CH_4) is turned on after the substrate temperature reaches the desired value of 900C. With the desired settings, the chamber is left without any adjustments for the time of deposition. Previous studies have shown that the deposition rate is approximately 0.2 micron/hour depending on the settings. After the desired deposition time has elapsed, the

next step is the shut down of the system. The process is terminated by first turning off the methane, while the hydrogen remains on for another 5 to 10 minutes. During this period, the hydrogen is the preferential etchant to remove a thin carbonaceous layer on the surface of the CVD diamond films (Yang, 1996). The applied filament current is slowly decreased to zero amps. The chamber is then returned to atmospheric pressure and cooled. Samples can then be removed from the system.

Operating Conditions: (Typical range is specified and actual conditions used are given in parenthesis.)

1. Gas Composition: $\text{CH}_4:\text{H}_2=0.5\% - 1\%$ (1%)
2. Gas flow rate: $\text{CH}_4=1-5$ sccm (4sccm)
 $\text{H}_2=200-500$ sccm (400sccm)
3. Filament Temperature: 2200-2350 °C (2300 °C)
4. Substrate Temperature: 850-950 °C (900 °C)
5. Operating Pressure: 40-50 torr (50 torr)
6. Substrate to filament distance: 0.5 - 1.5 cm (1 cm)
7. Doping source: Boron powder or plane boron source or boron gas (Boron Powder)

4.4 ETCHING

Continuing with the sample design part of the experiment, the samples must now be shaped and etched in order to have a free standing diamond area (with no silicon backing). Since the silicon substrate is 4 inches in diameter and a mask was used which allowed for many separate films on one substrate, it is necessary to separate each film. The cutting was done by simply scribing with carbon tip pen and then breaking the silicon along each of the masked regions. With each sample now separated from the bulk wafer, the resistivity and thickness measurements can be performed. The measurement of resistivity and some of the thickness measurements pursued are described in the next chapter (some techniques for measurement of thickness were performed before etching of the silicon).

The silicon is removed by chemical etching using a combination of acids. The etchant used is a modified version of the well known HNA (Hydrofluoric acid, Nitric acid, and Acetic acid). The HNA etchant was chosen due to its rapid etch rate and versatility. HNA is a very complex etch system with variable etch rate and etching characteristics which depend on the silicon dopant concentration, the mix ratios of the three etch components, and the degree of etchant agitation. The basic principles of etching take place in four basic steps (Peterson, 1982). These steps are:

- 1) injection of holes into the semiconductor to raise the silicon to a higher oxidation state Si^+
- 2) the attachment of hydroxyl groups OH^- to the positive charge Si^+
- 3) the reaction of the hydrated silicon with the complexing agent in the solution
- 4) the dissolution of the reacted products into the etchant solution.

The four steps imply that any etching solution must provide a source of holes as well as hydroxyl groups, and must also contain a complexing agent whose reacted species is soluble in the etchant solution. In the HNA system, both the hole and the hydroxyl groups are effectively supplied by the strong oxidizing agent (HNO_3), while the fluorine from the HF forms the soluble species (Peterson, 1982).

Based on the chemistry described above, the modified version used consisted of Nitric acid and Hydrofluoric acid in a 3 to 1 ratio. This combination was primarily used in the initial phase of the etching process, while 2:1 combination of nitric and hydrofluoric acids were used as a second step when it became apparent that the diamond was exposed.

The etching procedure itself is quite simple, however it is rather time consuming and must be performed meticulously. The solution is applied to the silicon side in small droplets using a micro pipette. It's important that the solution is applied to the same region each time, where it attacks the exposed silicon. Since the solution is applied to the

silicon in tiny amounts, it acts as a limiting reagent. Therefore, after a short time the reacted mixture is carefully removed and small droplets of the solution are reapplied. The process is repeated for several hours (10-16) until the diamond is exposed. The etching process is only terminated after a 3mm diameter of free standing diamond is produced. The entire process is tedious, and while the solution is being added and removed numerous times, each movement must be done very carefully in order not to damage the even more delicate sample. Figures 4.4 and 4.5 show the sample after the etching is completed. The samples are approximately 2.0 cm × 2.0 cm with the diamond film occupying 1.5 cm × 1.5 cm. The etched region is about 3mm in diameter. The etched angle vary depending on how the solution was applied.

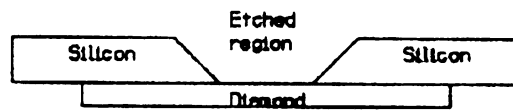


Figure 4.4 Side view (cut away) of the etched diamond sample

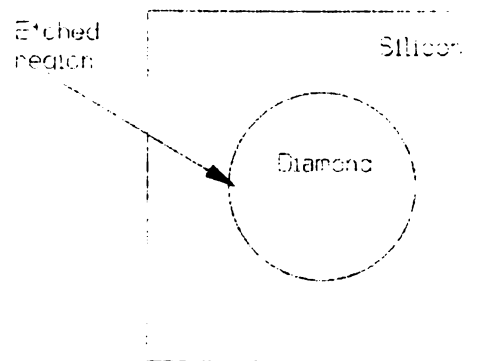


Figure 4.5 Top view of the etched diamond sample

4.5 SAMPLE PREPARATION

With the completion of the etching, it becomes necessary to produce the temperature rise within the diamond region. This is done by creating an electric circuit within the diamond. Two strips of electrically conducting tape (manufactured by Electrolock Inc in Chargrin Falls, OH) are fabricated for placement on the diamond surface. Because of the miniature size of the diamond sample, the width of the conducting tape was made smaller at one end. A diagram showing the shape of the conducting strip is given in Figure 4.6.



Figure 4.6 Conducting strip

The conducting tape, with one adhesive surface, is then attached to the surface of the diamond. Lastly, to ensure good electrical contact between the tape and the diamond, electrically conducting silver paint manufactured by Dynaloy Corporation (“340”) is added to the diamond-tape interface. Figure 4.7 below illustrates the sample setup and Figures 4.8 and 4.9 show photographs of the sample from both sides.

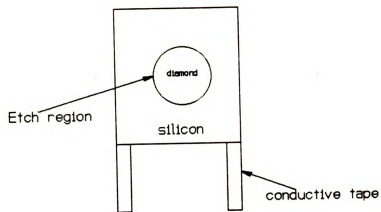


Figure 4.7 Sample setup

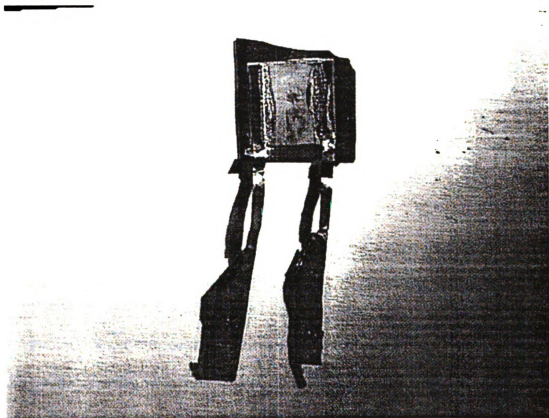


Figure 4.8 Photograph of sample viewed from diamond side

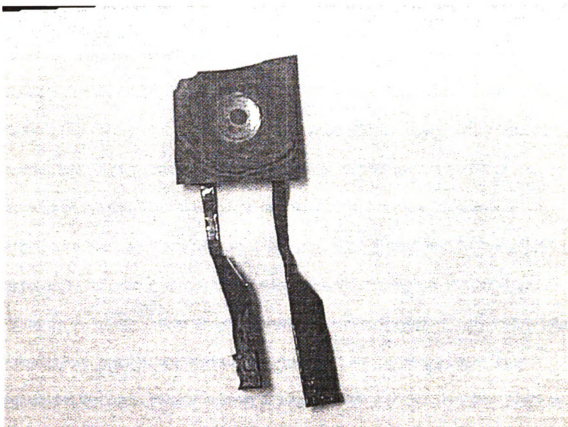


Figure 4.9 Photograph of diamond sample viewed from the silicon side

4.6 GOLD DEPOSITION

Due to the spectral characteristics of diamond and the use of infrared thermography to acquire temperatures, one additional requirement must be satisfied in the sample design. In order for infrared thermography to yield accurate temperatures, the sample must be opaque in the infrared and the emissivity must be known. The determination of the emissivity of CVD diamond is explained in the next chapter. In this section, the method used to ensure that an opaque sample is achieved is discussed.

The sample is made opaque by overlaying a thin layer of gold on one side of the diamond. The added layer serves two purposes, 1) it reduces the sample electrical resistance (not the diamond), therefore allowing for electrical resistance heating with a relatively low voltage input, and 2) it creates a sample which is opaque in the infrared, therefore allowing for accurate temperature readings with the use of an infrared thermograph system. Without an opaque sample, the scanner would be measuring temperatures which are a combination of the diamond temperature and the background temperature. In lowering each sample's electrical resistance, the coated layer allows heating for all levels of boron doped diamond. Without such a feature, only a small range of doping level could be investigated for thermal conductivity using the techniques discussed in this report because at lower doping levels the electrical resistance would be too high.

The procedure for precise sputtering of a thin gold layer is simple. The Emscope SC500 Sputter Coater (located in the Center for Electronic Optics at Michigan State University under the supervision of Dr. Flegler) is used with a gold target (photograph shown in Figure 4.10).

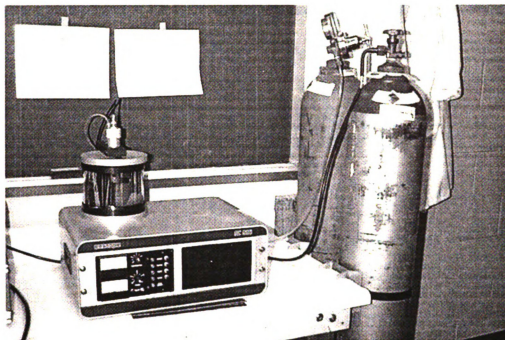


Figure 4.10 Photograph of the Emscope SC 500 sputter coater

A mask is used to ensure gold deposition on the diamond, and not on the silicon substrate. It is imperative that the gold generate energy in the diamond and not in the silicon, otherwise the heat sink characteristics of the silicon wafer necessary for the experimental model will not occur. Since the gold is deposited using a sputter coater, the mask simply involves any material which shields the silicon wafer from falling atoms. The masked sample is placed in the sputter coater chamber where a vacuum is created. The instrument is allowed to coat at 20 mA and 0.1 torr. At this setting, the Emscope SC500 coats at 70 angstroms per minute. The instrument was allowed to coat for 14 minutes producing a predicted total thickness of 980 angstroms. This thickness was not verified experimentally. Because the coated layer is only a small fraction (less than 4%)

of the diamond's thickness, its effect on the measured thermal conductivity is assumed to be small.

CHAPTER 5

EXPERIMENTAL METHODS

The previous chapters describe the sample setup and the experimental model. In this chapter, the equipment and method used to acquire temperatures and estimate the thermal conductivity are discussed. However, before experiments can be performed, thickness and resistance measurements must be made. Also, it is necessary to understand the basic concepts needed for accurate temperature measurements using an infrared thermography system (this includes knowing the emissivity of diamond). Once accurate temperatures are determined experimentally, the methods of parameter estimation are used to determine the thermal conductivity.

5.1 EXPERIMENTAL SETUP

Due to the extensive requirements involved in the design of the samples, very few items are needed for the experimental setup. The setup consists of:

- 1) Power supply
- 2) Digital multimeter
- 3) Diamond sample
- 4) Adjustable clamp

5) Electrical lead wires

6) Infrared camera and control unit

7) Jiffy Jack

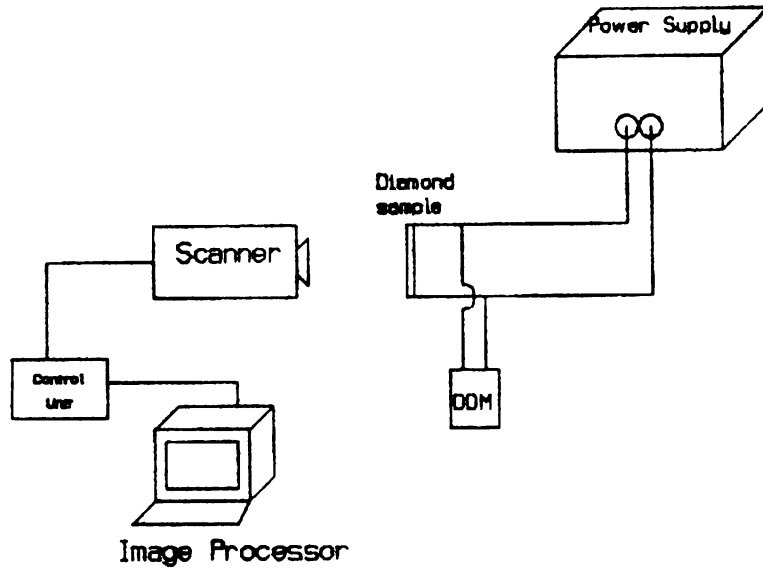


FIGURE 5.1 Schematic diagram of experimental setup



Figure 5.2 Photograph of data acquisition system

The setup, shown schematically in Figure 5.1 and photographed in Figure 5.2, consists of two main regions. One region serves as the heat generation area within the diamond, and the other region serves as the temperature sensing area. The energy generated within the diamond is accomplished through the use of an electrical circuit formed with the diamond. This region consists of the diamond sample, the electrical lead wires, and the power supply. Figure 5.1 (right hand side) shows the necessary connection required for energy generation in the diamond. The temperature sensing area consists of the infrared camera (scanner) and control unit. The scanner is focused on the diamond window where internal energy generation takes place, while appropriate settings to acquire accurate temperatures are selected on the control unit. The remaining items are used to aid in the setup and data acquisition.

5.2 INFRARED THERMOGRAPHY

Because of the miniature size and fragility diamond films, conventional methods such as the thermocouple and the resistance thermometer are unreliable to acquire temperature. As a result, an infrared imaging camera was used to image microstructural areas. In this section, the basic components of an infrared system and all equipment used to acquire temperatures, along with parameter settings used while performing the experiments are discussed.

The system used is the model 600L imaging radiometer (Figure 5.3). This system is designed for applications requiring accurate real time analysis of static or dynamic thermal patterns. The high performance system combines superior image quality and thermal sensitivity with true temperature measurement display, digital remote control, and automatic emittance and background correction. The system can be combined with a video cassette recorder (VCR) for later analysis on playback. While operating, the thermal reference target is viewed by the detector 60 times per second. A mercury/cadmium/telluride detector, while being cooled by liquid nitrogen to 77 K within an evacuated metal cryogenic dewar, is used to produce maximum thermal sensitivity and high spatial resolution (Inframetrics Operator's Manual, 1988).

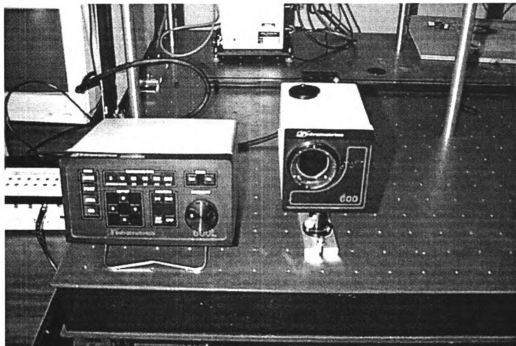


Figure 5.3 Photograph of the Model 600L (Scanner and Control Unit)

The Model 600L scanner incorporates electromechanical servos (galvanometers) to perform horizontal and vertical scanning. This scan concept produces the highest scan speed or frame update rate of any imaging radiometer, permitting fast moving targets to be viewed without significant distortion. The optical path of the scanner is shown in Figure 5.4.

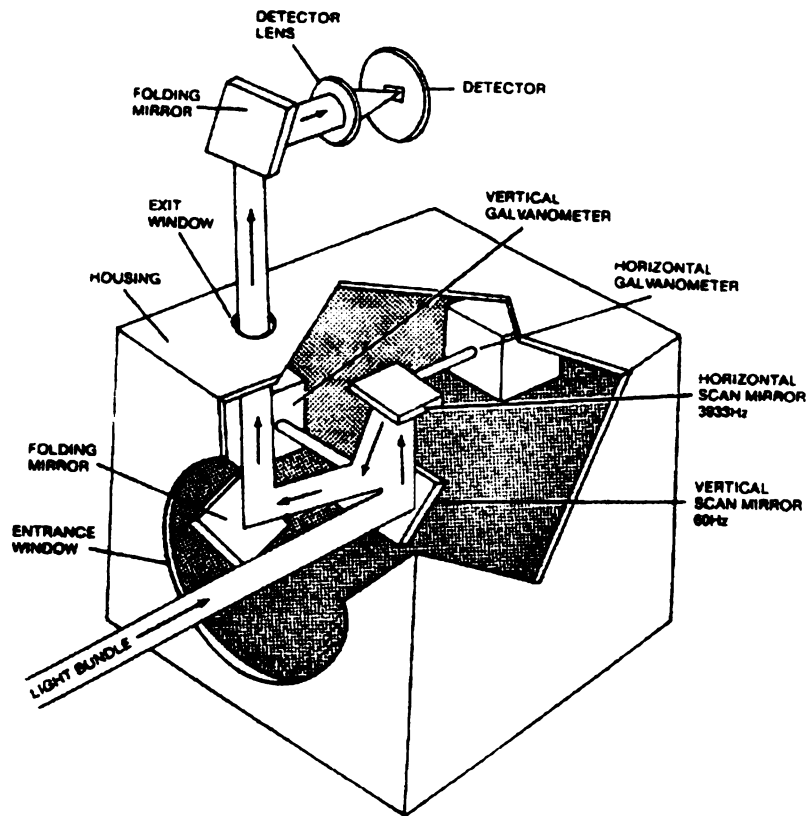


Figure 5.4 Optical Path of the Scanner (Inframetric Operator's Manual, 1988)

Thermal radiation enters the evacuated scan module through a germanium window, is deflected by horizontal and vertical scan galvanometers, and exits through a second window to pass through the focus lens on the detector. During system operation, a magnetic field oscillates a mirror against a torsional spring shaft under closed-loop electrical control. Horizontal scanning is performed at a very high rate (4 KHz) in a resonant (sinusoidal) mode. Vertical scanning is done in a sawtooth pattern similar to standard TV formats (Inframetrics Operator's Manual, 1988).

The model 600 control unit contains circuits to process, digitize, reformat, and otherwise prepare the IR signal for display. A microprocessor performs internal calibration as the scanner temperature changes, filters are installed, or settings are altered. The microprocessor accesses individual picture elements (pixels), then calculates temperatures using internal calibration tables corresponding to the optical filters/lens combination in use. A pulse-width modulated switching power supply accepts a wide range of DC input voltages with excellent noise immunity (Inframetrics Operator's Manual, 1988).

Two additional lenses are used to improve the spatial resolution necessary for the 3mm diamond area. The afocal 3X telescope uses four germanium optical elements which reduces the system field of view (FOV) and resolution element size by a factor of 3. The bayonet-type mounting is equipped with Hall-effect sensors which reinvert the image for proper display. Attached to the 3X lens is a 6 inch closeup lens which can resolve objects smaller than 100microns (Herr, 1993). Photograph below, Figure 5.4, shows each lens used. The lens on the left is the 3X telescopic lens. The lens on the right is the 6 inch closeup lens.



Figure 5.5 Photograph of Lens

5.3 DETERMINATION OF EMISSIVITY

One of the difficulties encountered when using the infrared thermography system to measure temperature is knowing the emissivity of the object being measured. In this section, the importance of knowing the emissivity is discussed, along with the experimental setup, techniques, and results used to determine the emissivity of CVD diamond.

In order to convert the emissive power measured by the radiometer to surface temperatures, the emissivity of the diamond window needs to be pre-determined. As

described in the sample design, the diamond window consists of CVD diamond and a very thin layer of gold. Therefore, the emissivity of this combination (diamond and gold) is required. Without an accurate measurement of the emissivity, temperature measurements from the radiometer will be erroneous.

The experimental setup consists of a black aluminum plate heated with a constant heat flux on the backside. A thin (2mm) aluminum plate is sprayed uniformly with black paint (Champion sprayon high heat 1200 °F) on both sides. A flat plate heater is then attached to the aluminum plate using conductive thermal paste (Omegatherm “201”). Figure 5.6 illustrates the black plate with attached heater.

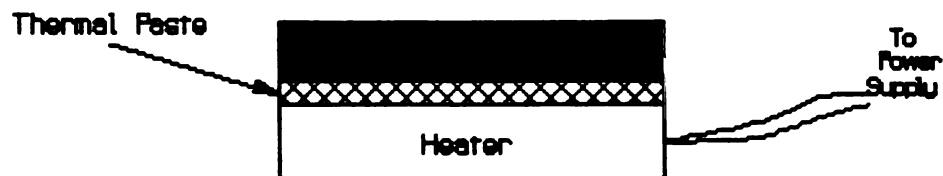


Figure 5.6 Black plate with heater attached

A thermocouple is then attached to the front side of the plate using an epoxy (Devcon 5 minute epoxy). The sample is then suspended in front of the scanner to check the isothermal nature of the plate, and subsequently used to determine the emissivity.

The first step is to check the isothermal nature of the black plate across a region of interest, and then verify that a steady state condition has been reached. The latter is checked by simply applying a voltage and then monitoring the temperature changes for a period of time. While several voltage settings were tested, a power supply reading of 7 volts worked best. With this applied voltage, a steady state temperature was achieved quickly, and the temperature was monitored for 20-25 minutes. Steady state temperatures remained fixed (within the radiometer's uncertainty of 0.1 °C) if not affected by forced convection. Therefore, in order to avoid sudden changes due to air circulation in the laboratory, the sample was properly shielded by placing cardboard around the sample. Constant temperature across the plate was investigated by focusing a region of the black plate on the RGB monitor. While using a temperature span of 10 degrees, the electronic ruler of the ThermaGram software program was used to show the temperature distribution across the region. This method was first used, however in order to verify what is seen on the monitor, temperatures were extracted. Because of the noise level involved in using infrared thermography, data for the black plate at room temperature were first extracted. The temperatures were measured over a length of about 1.5 inches along the black plate. A plot of these data is given in Figure 5.7. The room temperature data is important because it shows the best possible accuracy to which data can be obtained (average=24.01 ± 0.08).

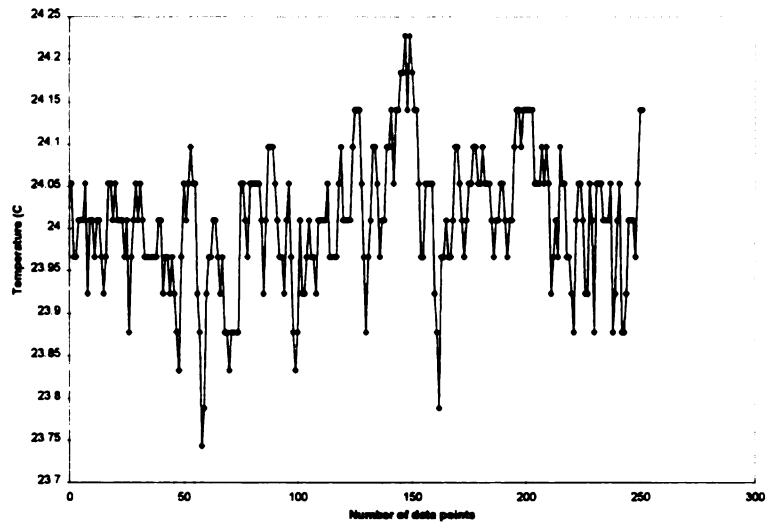


Figure 5.7 Black plate at room temperature

The heated black plate at steady state is then extracted, and shown in Figure 5.8.

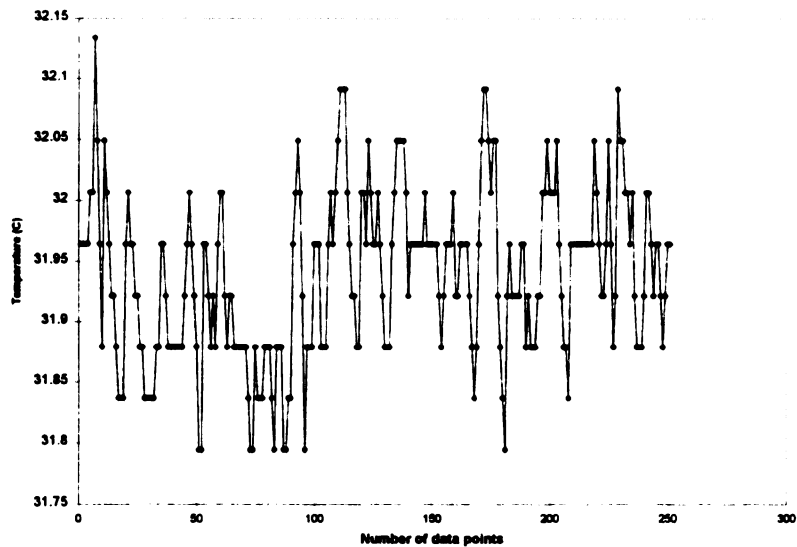


Figure 5.8 Temperature distribution of heater black plate

Observation of temperature data for Figures 5.7 and 5.8 shows a similar peak to peak noise level of ± 0.25 °C. Figure 5.8 shows that the heated plate is isothermal with a measurement uncertainty of 0.25 °C. This corresponds to a mean of 31.93 and a standard deviation of 0.07.

A diamond sample is subsequently etched and coated with gold as described previously. The sample is then attached to the plate using a high conductive thermal paste. Figure 5.9 below shows the diamond sample attached to the black plate (with heater on the backside), along with a type E thermocouple. The black plate is 3 inches in diameter. The thermocouple was located about 0.5 cm from the sample.

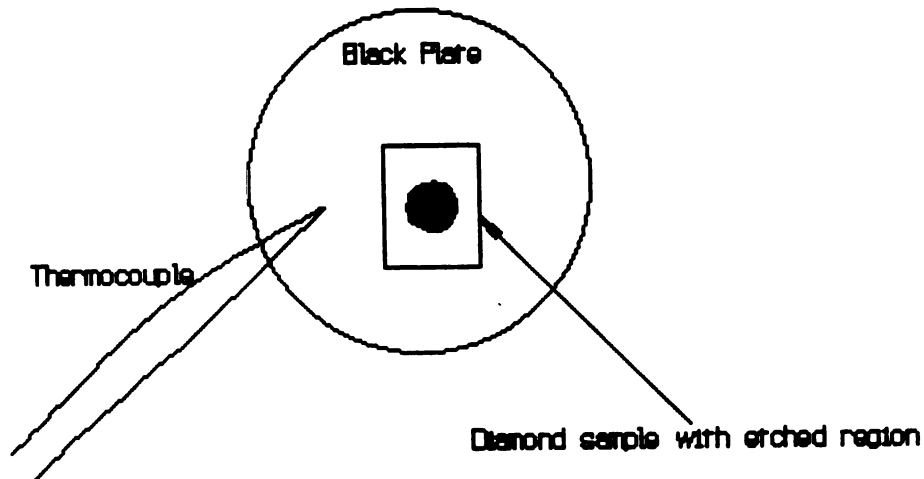


Figure 5.9 Black plate with attached sample

With the black plate suspended in front of the IR scanner, the point mode function (used to measure temperature at a given location on the object) on the radiometer control unit is used to measure the emissivity of both the black paint and the diamond/gold region

(which faced the scanner) of the sample. The premise used to find the emissivity is to match the temperature measured by the radiometer to the “true” temperature of the body (as measured by the uncalibrated type E thermocouple). The first step is to find the emissivity of the black paint. This is accomplished by adjusting the emissivity setting on the control unit until the temperature of the scanner at a point close (<0.5 mm) to the thermocouple matches the temperature measured by the thermocouple. Based on the experimental data in Table 5.1, the emissivity of the black paint was taken to be 0.98.

Emissivity	Thermocouple	Scanner
	Temperature (C)	Temperature (C)
1	37.1	36.7
0.99	37.1	36.9
0.98	37.1	37.1
0.97	37.1	37.2
0.96	37.1	37.3
0.95	37.1	37.5

Table 5.1 Emissivity of black paint

With this value of emissivity for the black paint input into the control unit, the correct temperature of the black plate can be read from the RGB monitor using the point mode function. Still using the point mode function, the emissivity of the diamond window for the attached sample is determined. The procedure is similar to that used for the black paint, however the reference temperature (true temperature) is that of the black paint with an emissivity of 0.98. The emissivity of the diamond is then adjusted until the temperature of the diamond matches that of the black plate ($e=0.98$). Tables 5.2 to 5.5 below show that the temperatures match closely at emissivity values (of the

diamond/gold region) in the range of 0.61 to 0.63. Due to noise level in the system, four experiments were performed and an average emissivity was found to be 0.62.

Emissivity	Black Plate	Diamond
	Temperature (C)	Temperature (C)
1	35	30.9
0.99	35.3	31
0.98	35.6	31.2
0.97	35.8	31.4
0.96	35.9	31.5
0.95	36.1	31.6
0.65	40.8	34.6
0.64	41.4	34.9
0.63	41.9	35.3
0.62	42.3	35.4
0.61	42.6	35.7
0.6	42.8	35.9
0.59	43	36.1
0.58	43.3	36.2
0.57	43.6	36.6
0.56	44.1	36.8
0.55	44.5	37.2

Table 5.2 Emissivity of diamond (test #1)

Emissivity	Black Plate	Diamond
	Temperature (C)	Temperature (C)
1	48	40.1
0.99	48.6	40.3
0.98	48.9	40.7
0.97	49.1	40.9
0.96	49.5	41.2
0.95	49.7	41.3
0.65	60.3	48.2
0.64	60.7	48.5
0.63	61.2	48.8
0.62	61.8	49.2
0.61	62.5	49.5
0.6	63	50
0.59	63.5	50.4
0.58	64.1	50.8
0.57	64.6	51.3
0.56	65.3	51.7
0.55	65.9	52.1

Table 5.3 Emissivity of diamond (test #2)

Emissivity	Black Plate	Diamond
	Temperature (C)	Temperature (C)
1	40.6	35.1
0.99	40.8	35.2
0.98	41	35.4
0.97	41.2	35.5
0.96	41.3	35.6
0.95	41.6	35.7
0.65	48.6	40.5
0.64	48.8	40.7
0.63	49.2	41
0.62	49.7	41.2
0.61	50.1	41.6
0.6	50.5	41.8
0.59	50.9	42.2
0.58	51.4	42.4
0.57	51.7	42.6
0.56	52	42.8
0.55	52.4	43.2

Table 5.4 Emissivity of diamond (test #3)

Emissivity	Black Plate	Diamond
	Temperature (C)	Temperature (C)
1	55.3	
0.99	55.7	
0.98	56	
0.97	56.5	
0.96	56.8	
0.95	57.3	
0.94	57.7	
0.93	58.1	
0.92	58.4	
0.91	58.8	
0.9	59.2	
0.65		54.6
0.64		55
0.63		55.4
0.62		56
0.61		56.4
0.6		56.9

Table 5.5 Emissivity of diamond (test #4)

The determination of the emissivity of diamond/gold window using the above technique is advantageous because it measures temperatures from an infrared system similar to those that would have been obtained had a type E thermocouple been placed on the diamond window. The emissivity of 0.62 compares well with Herr's measurement of 0.63. Herr's (1993) experimental setup measured the diamond with the silicon backing present, while this work measured the diamond/gold combination. This would indicate that the radiometer is only detecting emitted energy from the surface of an opaque object.

5.4 MEASUREMENT OF RESISTIVITY

While there are different techniques to measure the resistance of diamond, the four probe method was chosen due to its ease in measuring resistance at local areas on each sample. A brief description which explains how the method is applied and how resistivity is calculated is given in this section.

In the four probe method (shown in Figures 5.10 and 5.11), four equally spaced point probes are brought into contact with the diamond surface (before any preparation conditions are performed), and a known DC current is passed through the outer probes. The two inner probes are connected to a high impedance voltmeter.

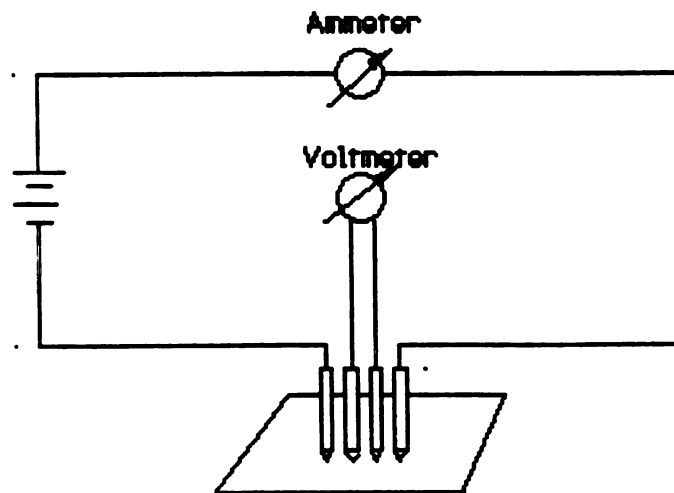


Figure 5.10 The Four Probe method



Figure 5.11 Photograph of the Four Probe instrument

This arrangement largely eliminates contact resistance effects, since the voltage-measurement probes draw negligible current (Reinhard, 1987). The relationship between sheet resistivity, R_D (ohms), voltage, V (volts), and current, I (amps), is given by

$$R_D = C \frac{V}{I} \quad (5.1)$$

where C is a constant which depends on the ratio d/s and a/d (d is the sample length, a is the width, and s is the space between the probes). Based on these ratios, values of the

constant C are extrapolated from Table 7.1 (p.346) of Introduction to Integrated Circuit Engineering by Reinhard. The resistivity, ρ (Ω cm), is calculated using

$$\rho = \delta R_D \quad (5.2)$$

where δ =average sample thickness and R_D =sheet resistivity.

The procedure is quite simple. Each sample is placed individually across the four probes, and a known voltage is applied (about 10^{-6} amps). The voltage across the inner probes is subsequently recorded, and used to calculate resistivities. Values measured for all samples used are given in Table 5.6.

Sample Number	Average Resistivity (ohm cm)	Local Resistivity (ohm cm)
17	1.62	1.63
19	3.98	2.20
8	6.77	5.51
7	8.07	6.73
6	11.68	9.82
3	18.40	14.96
4	28.53	21.85
2	31.68	28.38
1	80.14	68.43

Table 5.6 Resistivity of samples

While the four probe method measures local resistivity, its possible to calculate global resistivity by measuring the resistance for a known length and subsequently calculating

the resistivity. The DMM probes were placed in contact with the electrical conducting tape. The measured resistance was then recorded along with the samples width, length, and thickness. These values were then used to calculate global resistivity ($\rho=RL/A$) This was done for sample #2 and #3, and the global resistivities are shown in Table 5.7 below.

Sample Number	Resistivity (Ω cm)
2	20
3	16.8

Table 5.7 Global resistivity using a DMM

Comparing the global resistivity to the local and average from Table 5.6, it can be seen that for sample #2 the global is somewhat lower, however for sample #3 the global value is between the average and local values. Because only two samples were used and the variability of doping when local measurements were made, little information can be deduced from the comparison.

5.5 MEASUREMENT OF FILM THICKNESS

The measurement of diamond film thickness was necessary because accurate estimate of thermal conductivity depends on accurate measurements of all parameters. This proved to be challenging since the films were on the order of a few microns. Several methods were pursued in order to accurately determine the thickness and thickness profile of each diamond sample. In this section, a brief description of each method is given, along with results and explanations of the accuracy of each method.

The first instrument tried was the Sloan Dektak IIA profilometer which is located in the Physics Department at Michigan State University (under the supervision of Dr. Golding). This instrument is basically a surface roughness measuring device. The basic theory behind this instrument involves detecting the step change between two surfaces, in this case diamond and silicon. Figure 5.12 illustrates how the Dektak actually measures thickness.

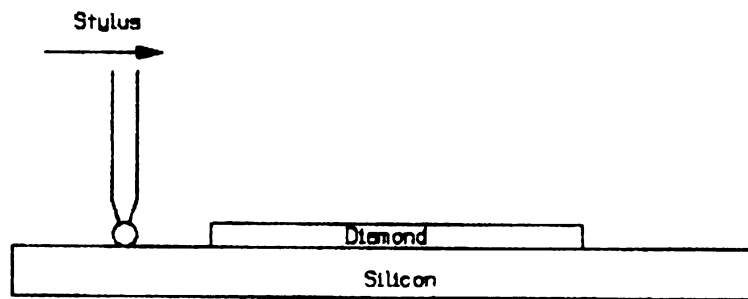


Figure 5.12 Sloan Dektak IIA

Since the diamond was deposited on the silicon using a mask, the step change which occurs at the edge of the diamond-silicon interface can hopefully be measured. While the idea is rather simple, the application presented uncertainty in the uniformity of the diamond's thickness. One source of problems encountered when using the instrument was the leveling of the reference surface. Since the silicon surface assumes the slope of the surface on which it sits, a small slope in this surface will cause a sloping of the silicon, and consequently the diamond. This unevenness will be detected and affect the results. Therefore it is difficult to distinguish whether the thickness is uniform. Another

problem encountered was in the use of the silicon as reference. Because of the fabrication techniques used to separate each sample from the bulk wafer and the heat treatment necessary to grow diamond, the silicon possesses a spherical shape, and could not serve as a reliable reference. These are just some of the problems encountered in using the Dektak to measure thickness.

Fairly accurate results can be obtained if it is assumed that the thickness of the diamond is uniform over small regions (2 mm). Based on this assumption, the leveling feature can be used to distinguish the diamond surface height from the silicon reference. The step change can then be measured using calibrated scales within the instrument. Results from the Dektak are given later.

Another instrument used with a great deal of success is the WYKO RST-PLUS rough surface/step tester. The tests were performed at Wyko Corporation in Tucson, AZ by Tom Stoudt. The RST-Plus is a non contact profiler capable of measuring step height from 100 angstroms to 500 microns. Along with thickness, the RST-Plus is capable of detecting the thickness profile of both the silicon and the diamond.

The technique used by the RST-Plus for determining surface height using phase-shifting interferometry typically involves sequential shifting of the phase of one beam of the interferometer relative to the other beam by a known amount, and measuring the resulting interference pattern irradiance. The phase data are then processed by an

algorithm that removes phase ambiguities between adjacent pixels. The surface height can then be determined from the phase data. One disadvantage of this technique is its limitation to smooth continuous surfaces, because reliable removal of discontinuities depends on the phase not changing by more than Π (Caber, 1996). Measurement of step heights for two samples (#17 and #3) are shown in Figure 5.13 and 5.14 below.

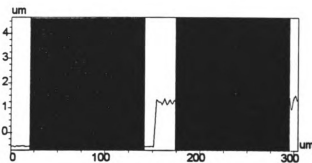


Figure 5.13 Step heights using RST-Plus (Sample #17)

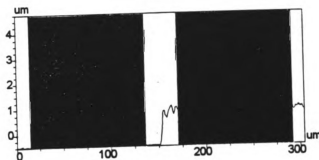


Figure 5.14 Step heights using RST-Plus (Sample #3)

The measurements were obtained using a 20X objective. The 20X objective permits sampling a $228\mu\text{m}$ by $304\mu\text{m}$ area with a spatial sampling interval of 0.8 microns. The thicknesses obtained are shown in Table 5.8

Sample Number	Thickness (microns)
17	1.74
3	1.34

Table 5.8 Thickness measurements using RST-Plus

To measure the thickness profile, an alternative method of determining surface height using white light as the source in an interferometer is used. The method measures the degree of fringe modulation, or coherence, instead of the phase of the interference fringes. The principle behind white light vertical-scanning interferometry utilizes the idea that when white light is used as a source in an interference microscope, the modulation, or visibility of the fringes, drops off rapidly from its maximum value at minimum OPD (Optical Path Difference). If the modulation signal is extracted from the intensity signal as the OPD is varied through focus and its peak is detected, a measurement of relative surface height at that point can be obtained (Caber, 1996). If this procedure is done for each point, a three dimensional surface map can be obtained. The 3-D plot represents the thickness profile of the surface.

In order to verify the profile over the entire surface, measurements were taken at the corner of each sample (Figure 5.15 and 5.16) as well, and this confirmed that the shape of the diamond was due to the silicon substrate. The fringe patterns shown in Figures 5.15, 5.16, and 5.17 is due to surface heights at each point on the sample. The curvature indicates that constant height occurs at regions which form a circle (similar to a cone).

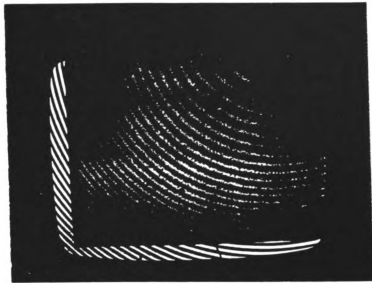


Figure 5.15 Corner profile of thickness (Sample #17)

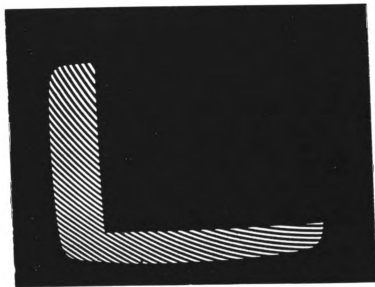


Figure 5.16 Corner profile of thickness (Sample #3)

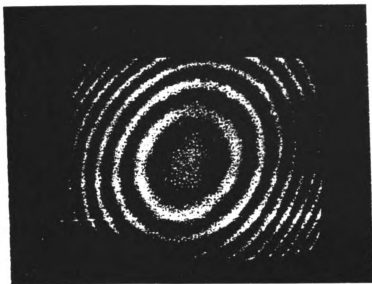


Figure 5.17 Bullseye at the center for spherical shape (Sample #3)

The interferogram at the center of the silicon (sample backside) for samples 1 shows a circular “bullseye” fringe pattern which indicates a spherical surface (Figure 5.17), convex in this case. The Figures shown above were measured with a 1.5X magnification objective and a 0.5X converter. This combination is equivalent to a 0.75X objective that profiles a 5.5 mm by 7.4 mm area with a spatial sampling interval of 20 microns. The results clearly show a convex shape (Figure 5.17) of the diamond film and silicon substrate.

A Laser Scanning Confocal Microscope (LSM), located in the Laser Lab in the Crop and Soil Sciences Dept. at Michigan State University under the supervision of Dr. Whallon, was another instrument which was used in order to accurately measure the

thickness or step change of the diamond. The words “laser” and “scanning” refer to the method of illumination, while “confocal” refers to the method of image formation (not all confocal microscopes use laser or scan the sample). A confocal microscope is aligned so that the illuminated spot and the image spot coincide precisely. This alignment is not present in all microscopes, therefore light reaches the observer frames from all parts of the sample within the field of view. Light from out of focus areas severely degrades the focal plane image, thereby limiting the depth to which a sample can be examined. In a confocal microscope, the sample is scanned point-to-point with a finely focused laser beam, and a pinhole aperture is placed directly in front of the detector at the focal point of light coming from the in-focus part of the sample. The effect of these modifications is to block light from out-of-focus regions because the focal point of such light falls either in front of or behind the pinhole aperture (Whallon, 1996), as shown in Figure 5.18.

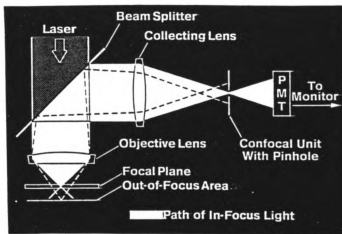


Figure 5.18 Focal plane of LSM

The result of this instrument configuration on the final image is a dramatic increase in resolution and contrast.

One particular feature of the LSM which allows for microscopic thickness measurements is a feature known as optical sectioning. In this process, the microscope collects a series of optical sections at intervals along the z-axis. The application of a feature known as phi-Z section produces an image of the sample as it would appear if cut in the vertical plane. This image is then fit to calibrated length scales within the system, where the distance from the top of the diamond to the top of the silicon is measured. Figures 5.19 and 5.20 show thickness measurement along with confocal images of the diamond surface.

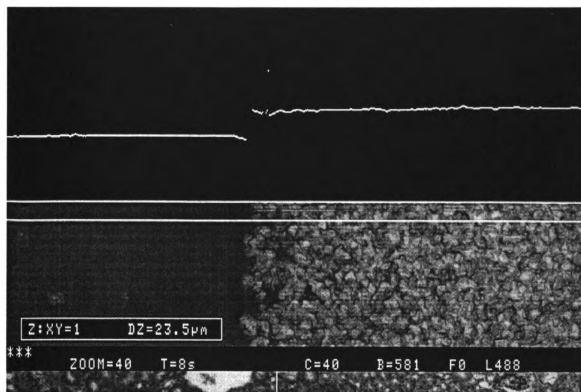


Figure 5.19 Thickness measurement on the left edge of Sample #3 ($\delta=3.1 \mu\text{m}$) using LSM

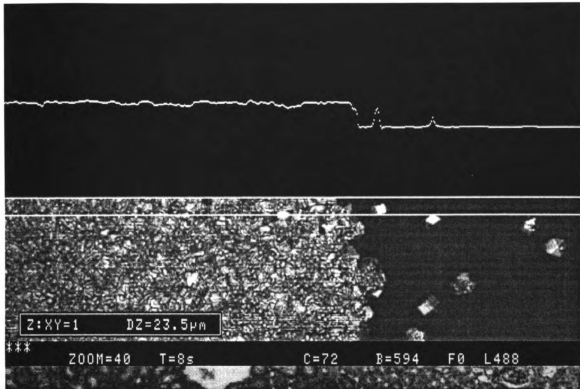


Figure 5.20 Thickness measurement on the right edge of sample #3 ($\delta=3.0 \mu\text{m}$) using LSM

One disadvantage of using the LSM was the uncertainty involved. The 100X objective used had an uncertainty of about 1 microns. This poses a problem since the samples range in thickness from 1.5 to 3 microns, therefore the relative uncertainty ranges from 33% to 66% making the measurements meaningless. Also, the LSM was not successful in detecting the thickness profile of the diamond and/or the silicon because of the limited field of view (approximately 0.5 mm) capability of the 100X objective.

The NEWVIEW 100 by Zygo Corporation in Middlefield, CT (tests performed by John Roth) was used to analyze the shape profile and determine film thickness. The overall results were mixed. The Newview100 was successful in determining the thickness profile, however its measurements of film thickness exceeded values measured by other instruments. The measurements of film thicknesses were approximately 6 microns which is 2 to 3 times that of the RST-Plus (1.5-2 μ m), LSM (~3 μ m), and Sloan Dektak (2 μ m).

The Newview 100 is a scanning white light interferometer. It works by using traditional techniques in which a pattern of bright and dark lines (fringes) result from an optical path difference between a reference beam and a sample beam. A simple mechanism is used to split incoming light inside an interferometer, one beam going to the internal reference surface and the other to the sample. After reflection, the beam recombines inside the interferometer, undergoing constructive and destructive interference and producing a light and dark fringe pattern. In the system, a translation stage and a CCD camera work together to generate a 3-D interferogram of the object. This interferogram is stored in the computer's memory and then transformed into a quantitative 3-D image of sample thickness over a specified area (Zygo, 1996).

Analyses of two samples (#4 and #5) were performed using the Newview 100. The thickness data are shown in Figures 5.21 and 5.22. Oblique plots are also given in Figures 5.23 and 5.24.

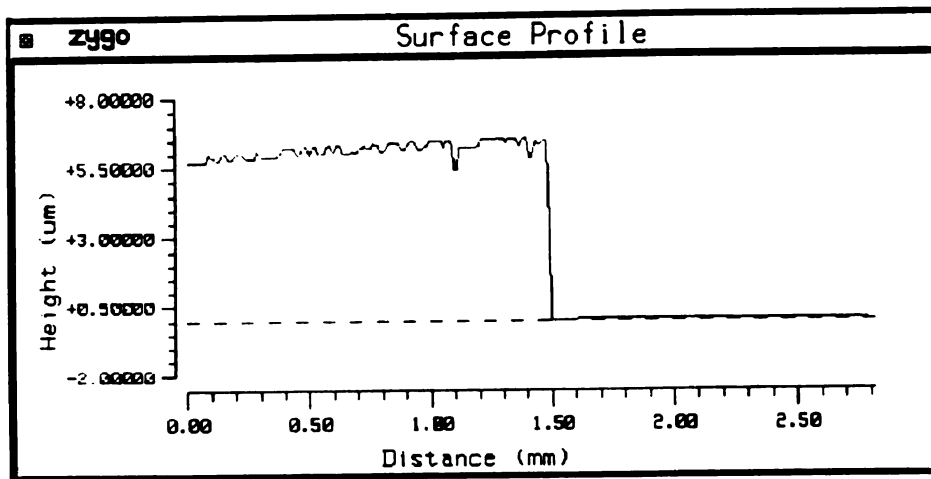


Figure 5.21 Thickness measurement on Sample #4 using Newview 100

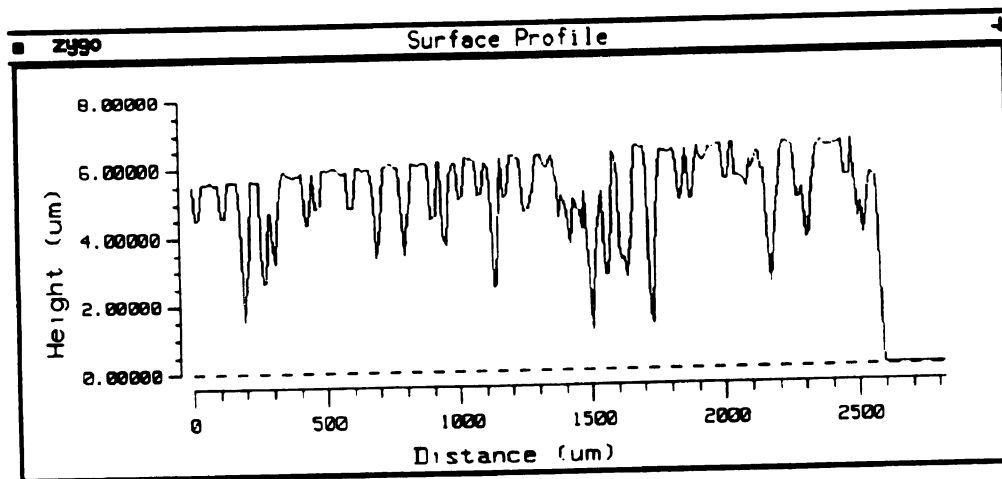


Figure 5.22 Thickness measurement on Sample #5 using Newview 100

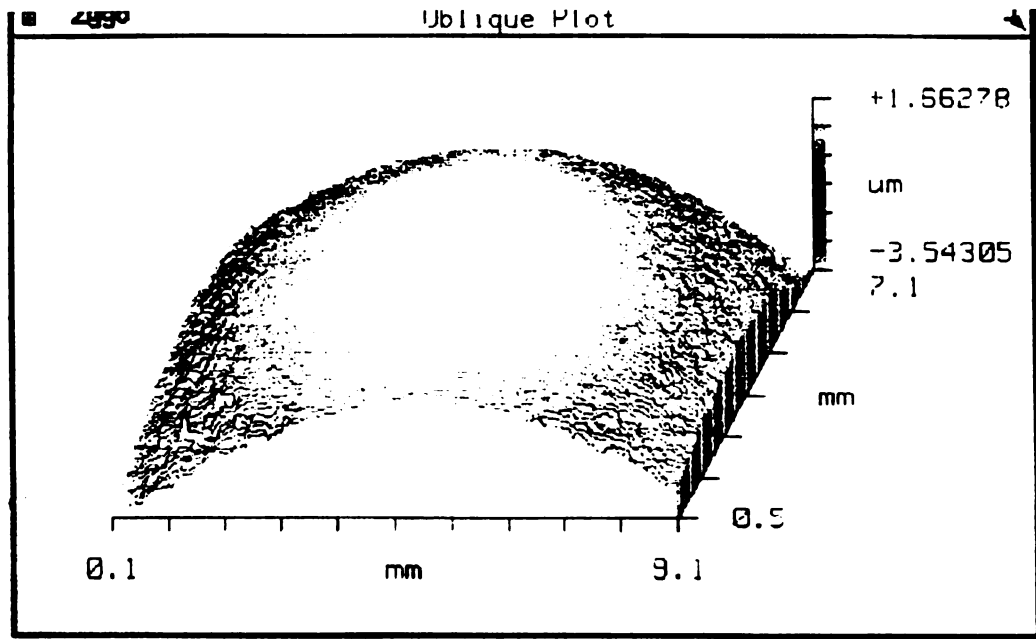


Figure 5.23 Oblique plot of surface for sample #5

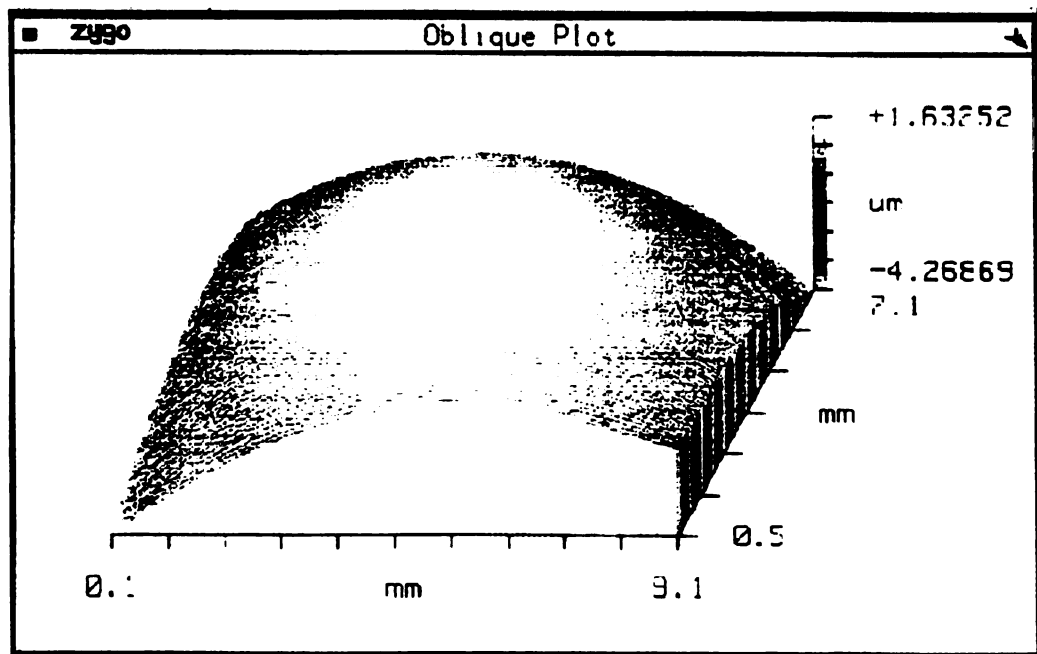


Figure 5.24 Oblique plot of surface sample #4

The measurements show a step change from the silicon surface to diamond of about $6\mu\text{m}$ for each sample. These values are 2 to 3 times larger than other instruments used. The surface profile of each sample is shown in Figures 5.25 and 5.26.

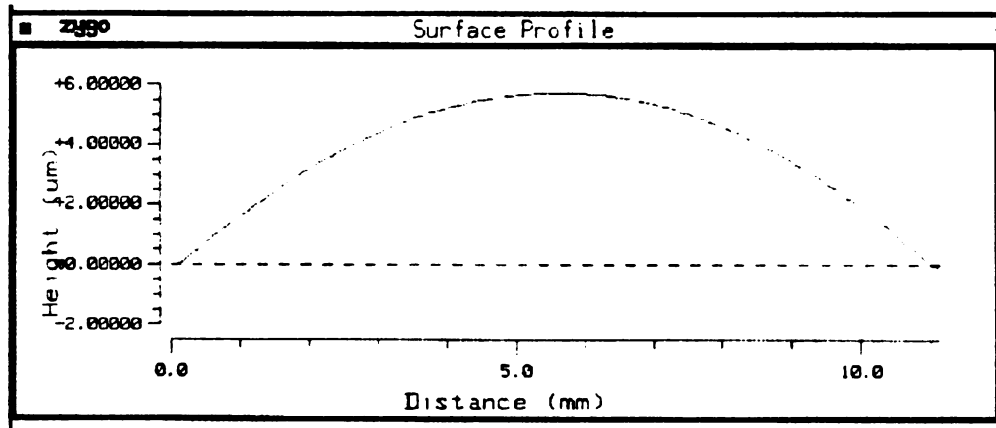


Figure 5.25 Surface profile of sample #4

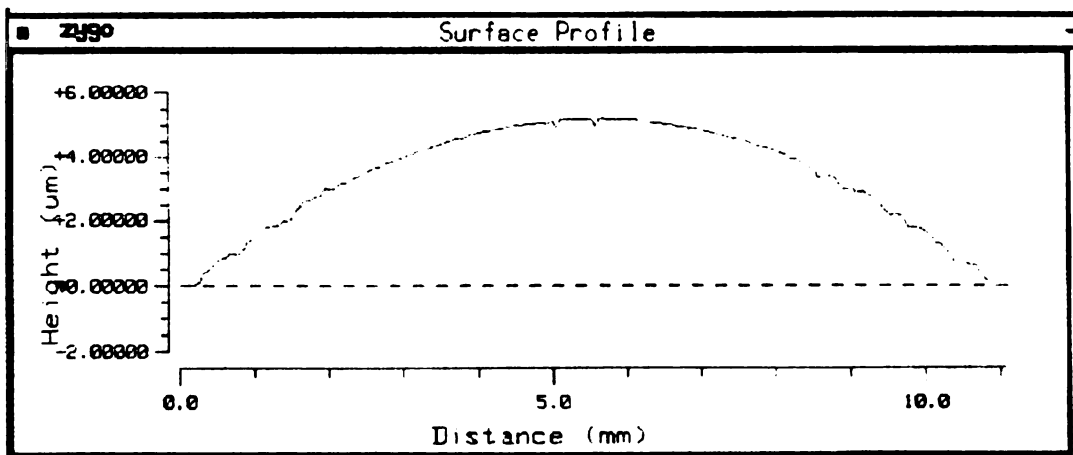


Figure 5.26 Surface profile of sample #5

While these profiles indicate a parabolic shape for the diamond film, it doesn't distinguish whether the shape is due to the silicon or the diamond. The results from the Newview 100 indicate that it is an instrument with a great deal of promise. However, because of its high values for thickness and uncertainty in showing whether the shape is due to the silicon or the diamond, further analysis was discontinued.

An Environmental Scanning Electronic Microscope (ESEM) was another instrument used to measure thickness. The ESEM has the advantage of showing the various layers comprising the sample. Therefore, it is easy to measure all layers (Silicon, SiO₂, Diamond) of the sample using calibrated scales within the microscope. The results from the ESEM for samples # 5 and #14 are shown in Table 5.6.

Test Number	Sample #5	Sample #14
1	2.0	1.48
2	1.78	1.6
3	1.85	1.7
4	1.74	
5	1.7	
Average	1.814	1.593
Standard Deviation	0.119	0.110

Table 5.9 Thickness measurements using ESEM

One disadvantage of the ESEM has to do with the preparation conditions necessary for accurate measurements. The ESEM needs to examine the samples on its edge so all layers can be viewed. In order to view the samples on edge, they must be broken along a region. This limitation makes the technique destructive, therefore samples measured by the ESEM cannot be used to determine thermal conductivity. For this reason, thickness measurements using the ESEM was discontinued.

In summary, measurement of film thicknesses were investigated using four separate instruments. Each instrument was used to measure film thickness and determine uniformity over the film surface. The RST-Plus by Wyko Corporation gave reasonable results for both thickness and thickness profile over the surface. However, the values for film thickness were lower than all other instrument. The Newview 100 by Zyko corporation also displayed excellent capabilities in generating 3-D thickness profile and thickness measurements. However, measurements of thicknesses were higher than other instruments, and the parabolic thickness profile did not distinguish whether the shape is

due to the silicon or the diamond. The LSM measured thicknesses of about 3 microns, however due to its large error (1 micron) and the sensitivity of thermal conductivity to film thickness (described in uncertainty analysis) the results were not used. The Sloan Dektak IIA presented difficulty due to the spherical shape of the sample (as shown by Wyko RST-Plus). Because it was understood that the parabolic shape of the sample was due to the silicon substrate, the leveling feature can be successfully used to detect step change in height. This procedure was performed and thicknesses (step change) were measured. Figures showing some of the measurements performed, along with Table 5.6 of other tests are shown below. Based on the measurements from the Dektak, it was assumed that all samples were 2 μm thick. The “spikes” in the Dektak measurements could be due to dust particles on the surface. The table of thickness (Table 5.6) shows measurements performed on sample #8 (test #2,6,8), sample #4 (test# 1,4, 5), and sample #3 (test # 3, 7,9).

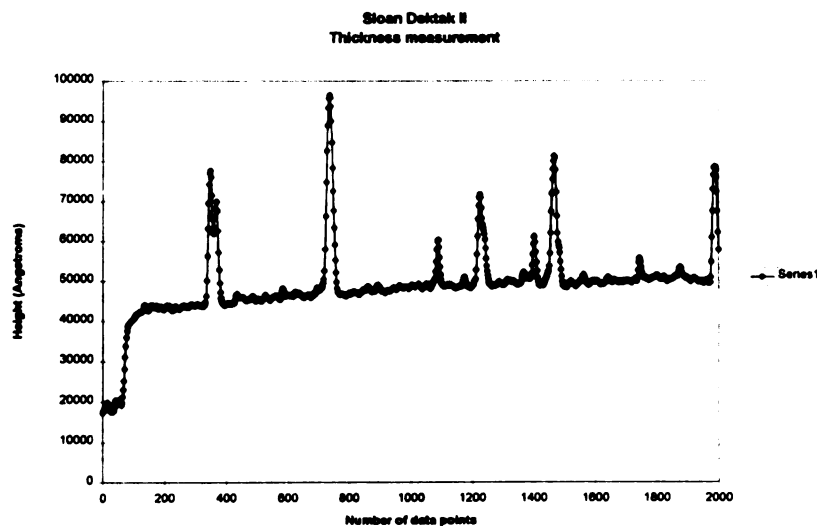


Figure 5.27 Thickness measurement (test#3)

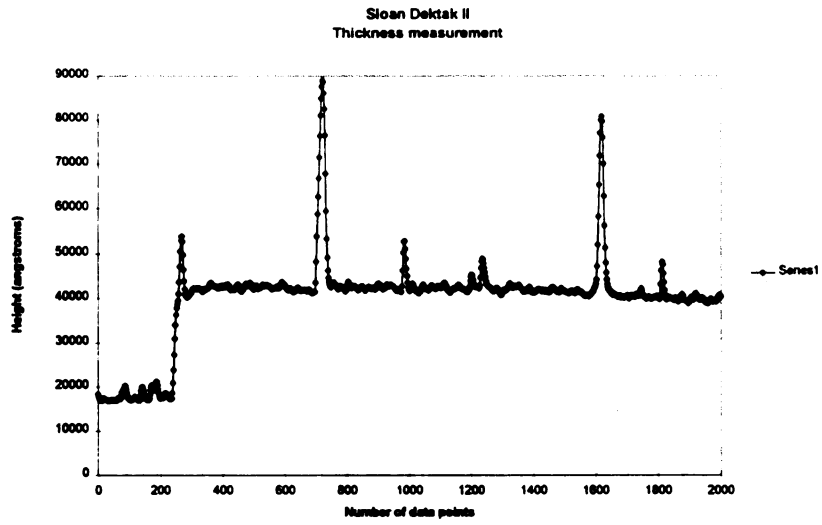


Figure 5.28 Thickness measurement (test #7)

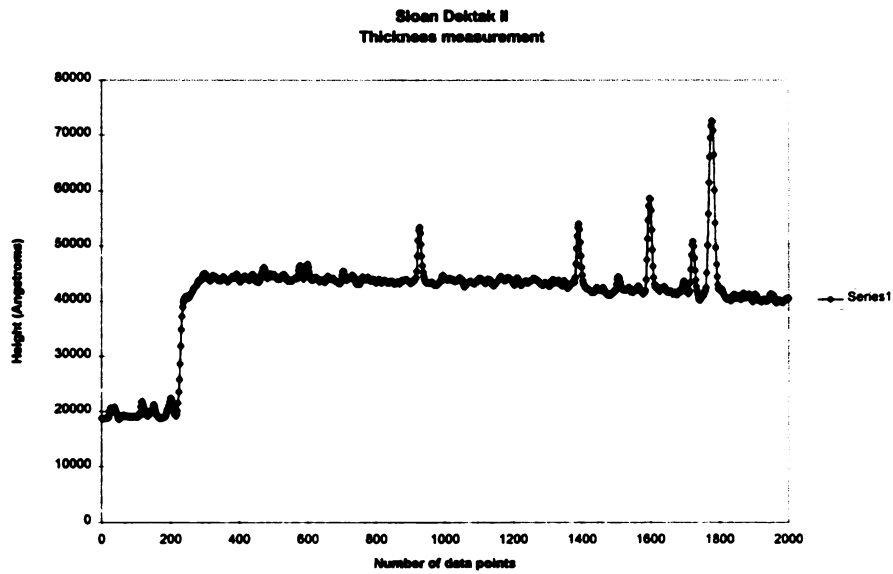


Figure 5.29 Thickness measurement (test #9)

Sample Number	Average Thickness (μm)	Standard Deviation (μm)
3	2.38	0.1
4	2.31	0.37
8	1.98	0.07

Table 5.10 Thickness measurements using Sloan Dektak IIA

Lastly, all measurements of thicknesses are compiled in Table 5.11. One factor which might affect the measured results for the Dektak was the condition of the sample when measurements were made. Sample #3 and #4 were performed after various preparation condition necessary to estimate the thermal conductivity were applied and then removed. This condition could lead to higher values for thickness since residue from the paint, gold, and chemicals could affect the results.

Sample Number	RST-Plus (μm)	DekTak IIA (μm)	LSM (μm)	ESEM (μm)	NewView 100 (μm)
3	1.34	2.4	3.0		
4		2.3			6.0
5				1.81	6.0
8		2.0			
14				1.59	
17	1.74				

Table 5.11 Summary of thickness measurements

All other measurements were performed before any preparation condition were applied to the samples. In order to compare the results of all the instruments used, the measurements must be compared with consideration to measured standard deviation and instrument precision. Table 5.12 shows each instrument measured standard deviation and uncertainty.

	Measured Standard Deviation	Uncertainty (μm)
Dektak IIA	0.233	0.01
RST-Plus	0.283	0.05
NewView 100	0	0.5
ESEM	0.156	0.1
LSM	0.1	1.0

Table 5.12 Uncertainty and standard deviation of each instrument

Table 5.12 shows that when standard deviation and uncertainty are considered, the samples are within the range of the measured values predicted by the Sloan Dektak IIA except for the newview 100 which is high due to the belief that it measured both the diamond and the silicon dioxide (about 3 μm). Also important in comparing the various instruments is accessibility and cost. The Dektak is easily accessible and free of charge. The LSM is also accessible (on the Michigan State University campus), however cost \$34 per hour for operation. The Newview 100 and RST-Plus are not easily accessible and cost approximately \$300 per hour for operation. The ESEM is also easily accessible, but cost \$40 per hour. In comparing all the instruments, the Dektak can give a good approximation of the thickness at the edge of the diamond. However, the RST-Plus gives the best and most complete results because of its ability to show how uniform the diamond thickness is at all locations with an uncertainty of about 0.05 microns.

5.6 TEMPERATURE ACQUISITION

The acquisition of temperatures involves capturing thermal images of the diamond window in steady or quasi-steady state, and then extracting the desired temperatures, in this case along a 3mm line. However, before the images can be captured, it is necessary to properly align the sample in the desired field of view because the 3mm diamond window on an opaque surface can be misread easily when viewed through the telescopic zoom lens. The process of aligning and focusing the 3mm diamond window is a difficult and time consuming task. Once the diamond window can be viewed properly through the telescopic zoom lenses, a calibration must be made to

relate physical distance on the sample to radiometer distance as seen on the RGB monitor. The procedure necessary to accomplish these tasks is explained in the following paragraphs.

The setup of the sample to capture thermal images is carefully performed since handling can easily damage the diamond window. First, the sample is placed between the jaws of an adjustable clamp. The jaws are then tightened so that the sample is immobile and suspended. The upper left or right corner is the only area where the sample is in contact with the clamp. This positioning is convenient because the electrical tape at the bottom of the sample must hang for easy access to the electric lead wires. The clamp and sample (shown in Figure 5.30) are then placed on a flat vertical motion jack.

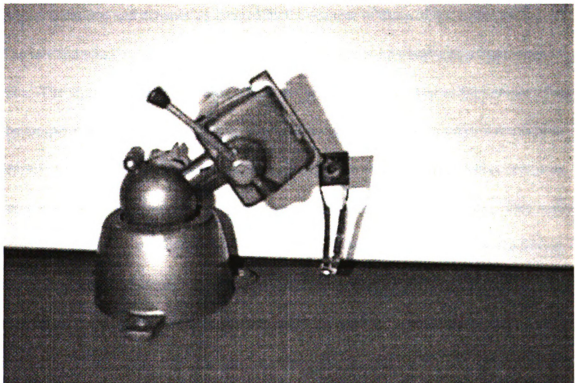


Figure 5.30 Adjustable clamp with sample

This jack was used because positioning the sample in the desired field of view requires many movements of the sample in the horizontal and vertical directions, Therefore the flat surface allows for easy horizontal motion of the clamp and the adjustable nature of the jack allows for easy vertical movements. These precautions are necessary because extensive movement (and handling) of the sample might lead to destruction. Care must be taken to assure only a small portion of the sample is in contact with the clamp, otherwise heat conduction might occur through the clamp and ultimately affect the experimental model.

Once the sample is suspended in front of the scanner, the next step is to relate precise locations and distance as imaged by the scanner to those of the actual sample. The relation was defined by using a machined thin aluminum plate with a 3mm open area. The aluminum plate was then placed in the same field of view as the sample where the temperature of the open area was elevated for clarity. Two procedures were used to identify the 3mm region. One technique was to use the electronic ruler and coordinates (on the image processor) to identify the number of pixels equivalent to 3mm. This really involves identifying the silicon/diamond interface. This procedure involves identifying the silicon/diamond interface. Another technique was to record the image corresponding to 3mm on videocassette using the VCR (Panasonic AG-2400). Recording the image is important if other methods (such as image processing software) are to be used to extract

temperatures from the thermal images. Once the calibration scale has been determined, the control unit is set to the desired settings (emissivity, image average, and temperature span, etc.). The electrical wires are then connected to the sample, and a constant voltage is applied. The temperature of the sample increases immediately, and the image of the sample in quasi-steady state is captured. The shape profile or temperature gradient across the 3mm diamond window is the same in quasi-steady state as it is for steady state.

Two methods were used to capture the diamond window in quasi-steady state. One method involves using the freeze frame function on the image processor. This involves simply freezing the image and subsequently saving the still thermogram on disk. The other method is to record the entire heating process on video, and later capturing the desired image on playback.

After the thermal images have been acquired using the appropriate control setting on the radiometer, the temperatures can be extracted using the File_Access program run by the gwbasic interpreter with the ThermoGram card or the software Image Pro Plus (IPPlus). The File_Access program, which is part of the thermal image processing software, extracts data from a particular line of the thermal image and converts the individual pixel intensity to temperatures using calibration tables stored in the ROM of the radiometer's microprocessor. The program prompts the user for the filename of the thermal image and the desired line number within that image. The temperatures corresponding to the pixel location across the entire image are then written to a data file.

Another method to extract temperatures is to use the software Image Pro Plus with a VCR and the recorded heating process. Since IPPlus is not a thermal image processing software, it must first be calibrated in order to convert pixel intensity to temperature. A calibration scale corresponding to the temperature span of the radiometer was used. Therefore, once the 3mm region is known (through the use of the electronic ruler or recorded calibration scale), the corresponding pixel intensity (and then temperature) can be extracted by simply selecting the 3mm line corresponding to the diameter of the diamond window. Two methods were used because equipment failure by the ThermoGram card forced the use of IPPlus. Therefore, experiment performed in the latter phase of the project were processed using IPPlus. Samples #1,2,3 and 17 experiments were processed using IPPlus, while samples #19,7,8,6, and 4 were processed using the ThermoGram card. With the desired temperatures obtained, it is now necessary to estimate the thermal conductivity of the sample.

5.7 DATA PROCESSING AND ESTIMATION OF THERMAL CONDUCTIVITY

Parameter estimation is a discipline that provides tools for the efficient use of data in the estimation of constants appearing in mathematical models and for aiding in modeling of phenomena (Beck, 1977).

With the appropriate temperature distribution and the governing equation, the program NLIN (design by Dr. Beck) is used to analyze the data and estimate the thermal conductivity. The FORTRAN program NLIN uses the method of least squares

$$S = \sum_{i=1}^N (Y_i - T_i)^2 \quad (5.3)$$

where N is the number of temperature measurements, Y_i is the measured temperature, and T_i is the calculated temperature represented by

$$T_i = T_b + HK \left(1 - \left(\frac{r_i}{b} \right)^2 \right) \quad (5.4)$$

where $H = \frac{V^2 b^2}{4RLW(\delta_d + \delta_g)}$, $K = \frac{1}{k}$

and V=applied voltage (volts), b=radius (meters), R=resistance of gold coated sample (ohms), L=length of circuit (meters), W=width of circuit (meters), δ_d =thickness of diamond (meters), δ_g =thickness, of gold (meters), k=thermal conductivity (Watts per meter Kelvin), T_b =temperature at the boundary.

Using the method of least squares, NLIN simultaneously estimates T_b and k to calculate T_i such that the error in S is minimized. In order to minimize the error in S, NLIN uses the system of equations

$$\frac{\partial S}{\partial T_b} = -2 \sum_{i=1}^N (Y_i - T_i) = 0 \quad (5.5)$$

$$\frac{\partial S}{\partial k} = -2 \sum_{i=1}^N (Y_i - T_i) H \left(1 - \left(\frac{r_i}{b} \right)^2 \right) = 0 \quad (5.6)$$

While these equations form the basis of the linear estimation problem, NLIN is actually a sequential nonlinear estimation program with more complex calculations than those shown above. Not only does NLIN fit the experimental data to the mathematical model, but it also calculates the residuals which are the difference between the measured and calculated temperatures ($Y_i - T_i$). The estimation of K and the calculation of the residuals are carried out with the input $H = \frac{V^2 b^2}{4RLW(\delta_d + \delta_g)}$, initial guess of T_b and $K = \frac{1}{k}$, and the temperature distribution (Herr, 1993). Typical input and output files are shown in the appendix.

CHAPTER 6

RESULTS AND DISCUSSION

The techniques and procedures discussed in the previous chapters were used to acquire accurate temperatures and estimate the thermal conductivity of each sample. There were a total of 9 samples. All samples were fabricated in a similar manner, therefore the only significant difference from sample to sample was the level of doping as measured by the electrical resistivity. The purpose of the research was to investigate what effects the measured resistivity (doping level) has on the thermal conductivity of boron doped diamond films. In this chapter, the results of the experimental measurements are shown, along with a discussion of the factors which contributed to each sample measured thermal conductivity. The measured thermal conductivity and electrical resistivity are presented with experimental uncertainty to indicate the confidence (or certainty) to which the results are known.

6.1 THERMAL CONDUCTIVITY AS A FUNCTION OF ELECTRICAL RESISTIVITY

The estimation of the thermal conductivity was performed using the program NLIN. Representative results of an experimental test for sample #17 showing

temperature distribution, residuals, and sequential estimation is given below. A complete set of results for all samples is given in Appendix A.

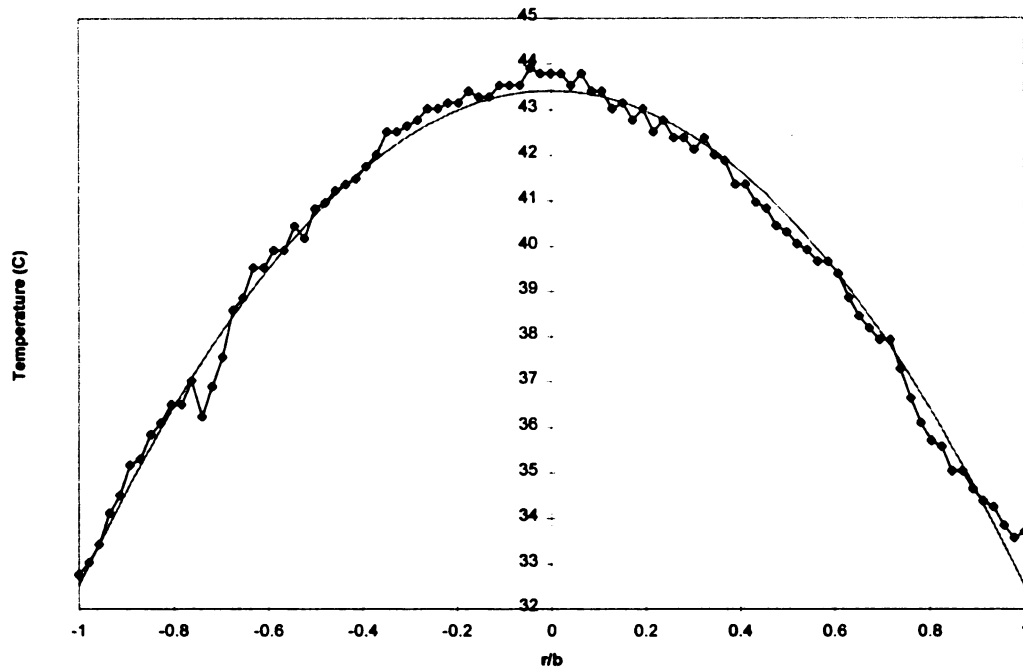


Figure 6.1 Measured versus calculated temperatures (Sample #17)

Figure 6.1 shows a plot of the measured temperature (diamond symbol) across the 3mm diamond window, along with the calculated temperatures as predicted by the simplified governing equation (solid line). From the figure, it's easy to see that the temperatures match fairly well except for measurement noise inherent in the infrared thermograph system. A better indication of how accurate the measured temperature is compared to the calculated temperature is shown in Figure 6.2. This figure is the residuals ($Y_i - T_i$), and it

represents the calculated temperature minus the measured temperatures at each location along the 3mm diamond window.

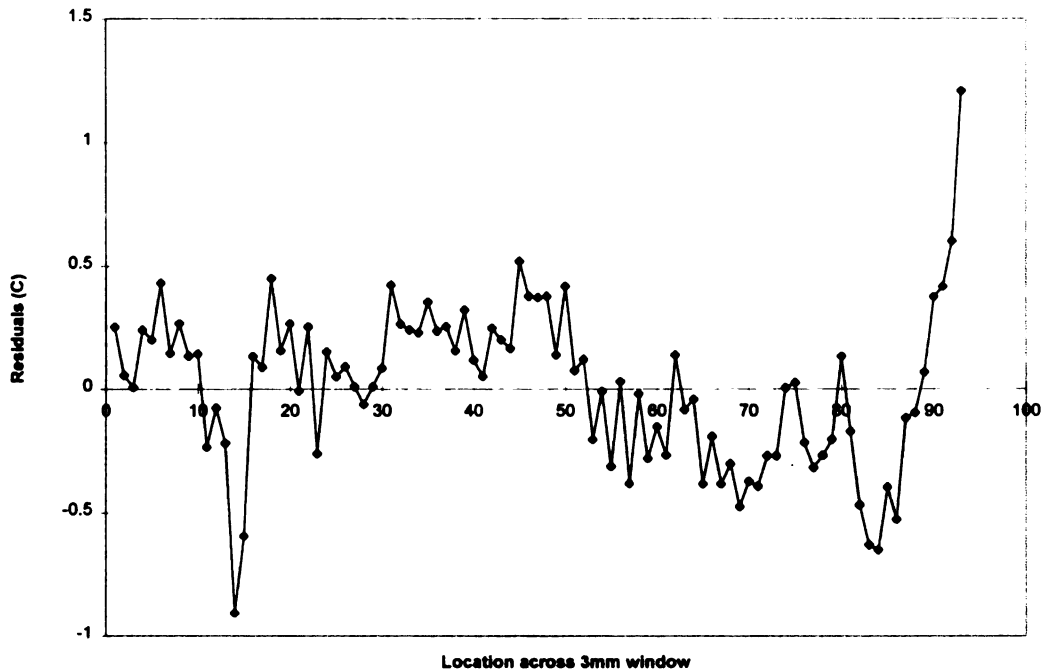


Figure 6.2 Residuals (Sample #17)

Figure 6.2 shows a noise level of about 0.5°C . This measurement is fairly accurate considering that a noise level of 0.25°C was measured at room temperature and is the best accuracy to which the infrared camera can measure the diamond surface. Also, a noise level of 0.5°C is small when compared to the maximum temperature gradient of about 10 degrees from $r=b$ to $r=0$ across the diamond window. The residuals are calculated for each measurement from $r=-b$ to $r=+b$, therefore data point #1 corresponds to $r=-b$ (-1.5mm) and data point #93 corresponds to $r=+b$ (+1.5mm).

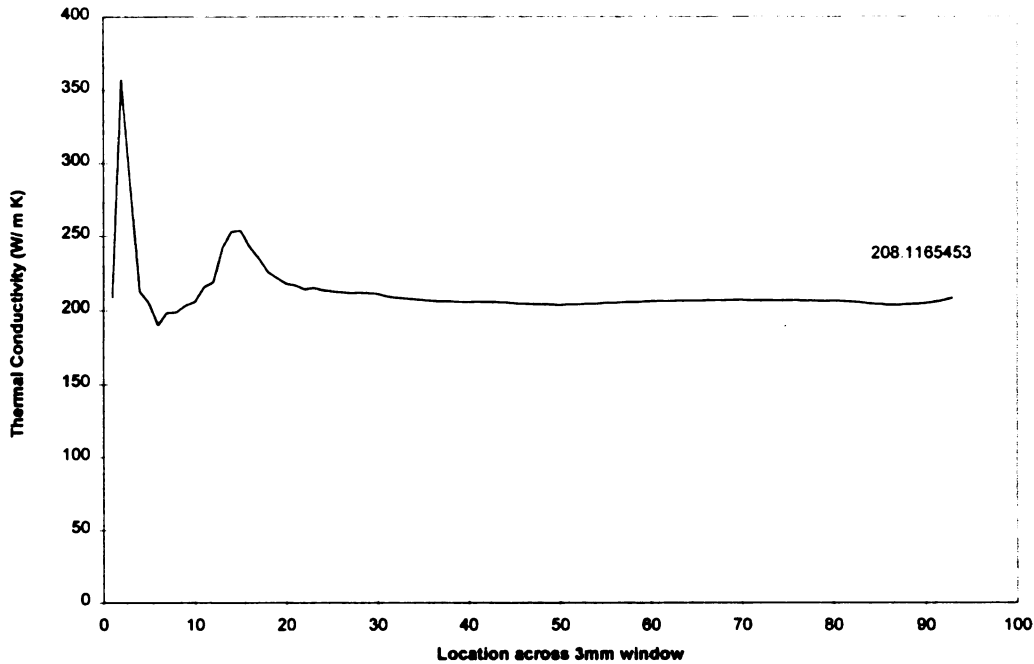


Figure 6.3 Sequential estimation of thermal conductivity (Sample #17)

The measured temperatures are then used to estimate the thermal conductivity. Figure 6.3 shows the sequential estimate as each data point is added. It's easy to see that with only a small amount of temperature measurements the estimate fluctuates. However, as more temperature measurements are considered an asymptotic value is approached. In this case, thermal conductivity is estimated to be 208.1 W/m K. The estimate was performed from $r=-b$ (-1.5mm) to $r=+b$ (+1.5mm), and the data points are numbered similar to that for the residual data.

The overall results show that thermal conductivity increases as doping level decreases (electrical resistance increases). Figure 6.4 shows that there exists an

“exponential” type relationship between thermal conductivity and average electrical resistivity.

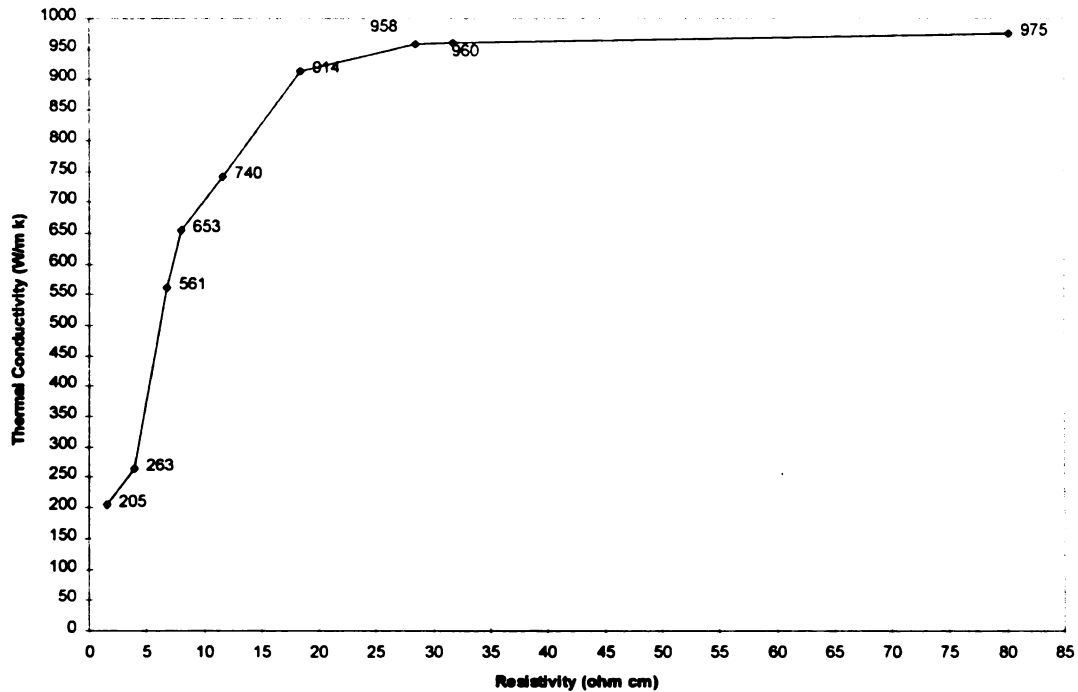


Figure 6.4 Thermal conductivity as a function of average resistivity

Based on the distribution of boron powder which substitute into the diamond lattice as diamond crystals nucleate from the surface of the silicon, and the notion that samples close to the boron source is exposed to a higher concentration of boron atoms, the results shown in Figure 6.4 is consistent with doping levels and it's effect on diamond. The above graphs indicate that samples with high levels of boron doping (low resistivity) posses relatively low thermal conductivity, while low doping levels (high resistivity) samples posses relatively high thermal conductivity. Also present in the “exponential”

nature of the curve, which has a steep slope at low resistivity values which subsequently decreases as resistivity increases, is the approach of a limit. This would indicate that a particular value of thermal conductivity is being approached as the resistivity increases to infinity. Such trends imply that the effects are entirely due to the addition of boron during synthesis, and had synthesis been carried out without boron (infinite resistance) an average value consistent with infinite resistance would be measured for all samples considered. Likewise, had an infinitely large amount of boron been used, it is presumed that the thermal conductivity would approach that of boron which is about 27 W/m K (Kittel, 1996). One method commonly used to characterize the doping level is to use a Secondary Ion Mass Spectroscopy (SIMS). This was done by Malta, Windheim, and Fox (1986) and it was discovered that polycrystalline boron doped diamond at 300K with a measured resistivity of approximately 600 Ω cm possesses atomic boron concentration of 2×10^{18} cm^{-3} . If it is assumed that there exist a linear relationship between atomic concentration and resistivity, it can be concluded that samples used in the present work with average resistivity which range from 1.63 to 80 Ω cm possess boron concentrations at least 7.5 times greater than the Malta et al. sample. In order to fully understand the relationship between atomic boron concentration and the measured resistivity reference is made to a 1996 paper by Werner et al. In their work a four point probe was used to measure resistivity and a Secondary Ion Mass Spectroscopy (SIMS) was used to determine the amount of boron atoms present. In Figure 6.5 below (Irvin Curve), the relationship between resistivity, Hall measurements, and effective doping concentration is given for single and polycrystalline diamond.

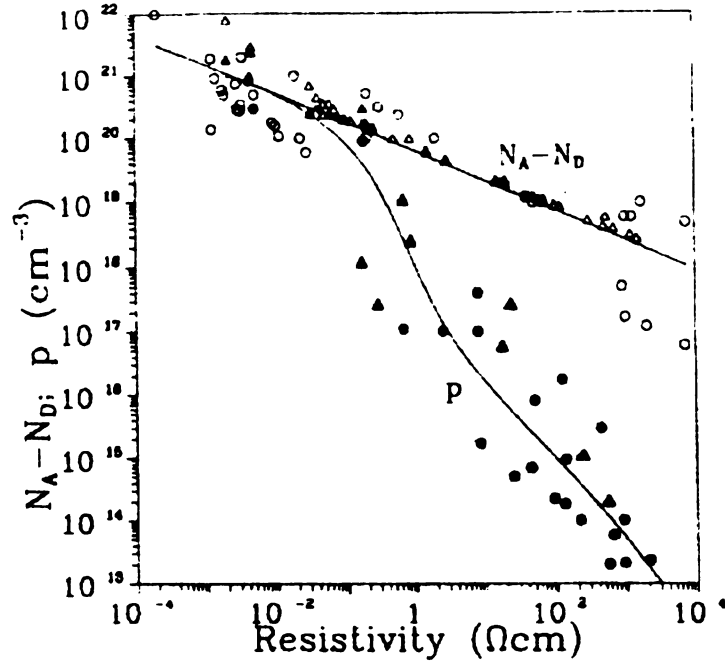


Figure 6.5 Irvin curve for diamond (Werner et al. 1996)

Circles are for single crystal and triangles are for polycrystalline diamond, with open symbols representing effective doping concentration, $N_A - N_D$, and filled symbols representing free hole concentration. From the figure, it was concluded that the current mechanism depends on the doping level and a simple room temperature resistivity measurement is required to estimate the doping level. Based on the above graph, it is possible to estimate the amount of boron for local resistivities used in this work. Table 6.1 gives an estimate of the doping level for all samples.

Local Resistivity (Ω cm)	Estimated Atomic Concentration $\times 10^{19}$ cm ⁻³
1.63	8.0
2.2	6.0
5.51	3.5
6.73	3.0
9.82	2.9
14.96	2.3
21.85	2.0
28.38	1.6
68.43	1.1

Table 6.1 Estimated doping level for all samples

One difficulty commonly encountered in using boron powder as the doping source in diamond synthesis is the variability of resistivity over relatively small areas of each film. For this reason, the above graph of thermal conductivity is plotted versus average resistivity. Another way of representing the results is to plot thermal conductivity versus local resistivity. The local value of resistivity was measured in the center of the sample prior to etching (i.e. in the etched region where temperatures were measured during experimental runs). This was done to investigate if there exist significant differences between the local region of interest and the overall expected value of film resistivities. Figure 6.6 shows the thermal conductivity vs. local resistivity (measured at the center).

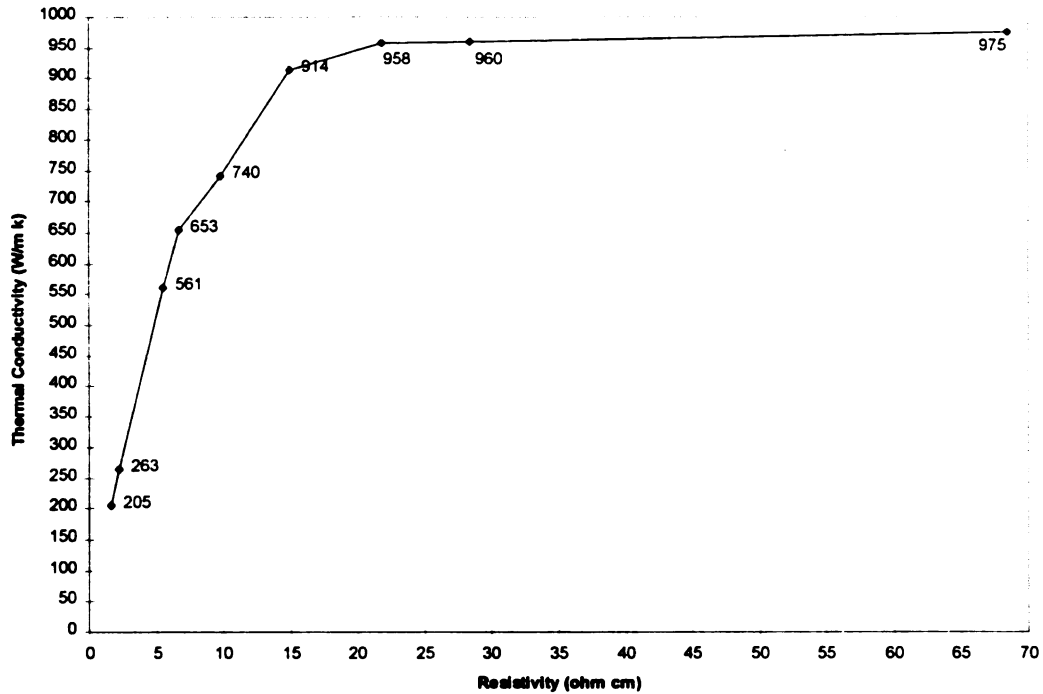


Figure 6.6 Thermal conductivity as a function of middle resistivity

Comparison of the thermal conductivity graphs (Figure 6.7 combine plot of average and local resistivity) indicates little variation, therefore it can be concluded that conductivity of each sample is unique to the range of resistivity measured using the four probe method and the overall shape of the thermal conductivity-resistivity data does not change.

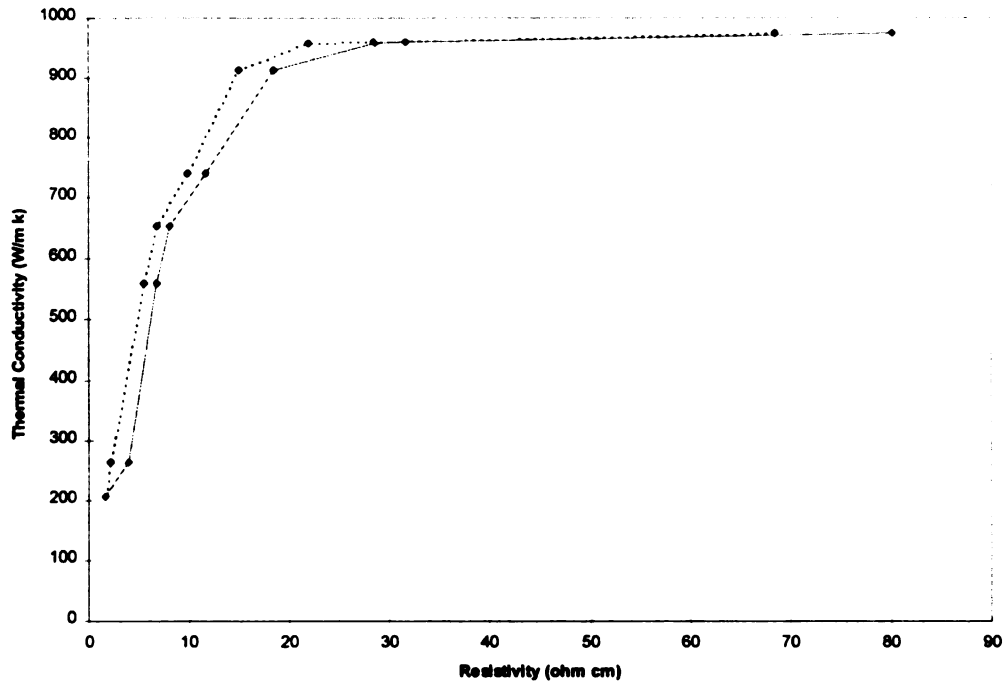


Figure 6.7 Combined plot of measured thermal conductivity

Another important point in the measurement of resistivity of each film is that while there were variations within each sample, there was no overlapping among the measured values for different samples. The non overlapping indicates that each sample possesses a unique range of resistivities. Along with knowing the range of resistivities for all samples, it is necessary to understand the variability within a given sample. The standard deviation of the measured resistivities within each sample was calculated and shown in Table 6.2

Sample #	Measurements	Average resistivity (ohm cm)	Standard Deviation	Coefficient of Variation
17	8	1.621	0.352	0.217
19	4	3.98	2.386	0.599
8	3	6.765	1.22	0.180
7	5	8.065	1.342	0.166
6	3	11.68	2.806	0.240
3	3	18.395	3.668	0.199
4	3	28.5	5.845	0.205
2	3	31.678	6.545	0.207
1	3	80.142	10.18	0.127

Table 6.2 Average resistivity and standard deviation

The estimated values of thermal conductivity shown in Figure 6.4 and Figure 6.6 are average values for multiple experimental runs. The experiments were performed under similar conditions except for slight variation in power setting which has shown no effect on the estimated conductivity. While the average value gives some indication of the expected value, the variability of the estimates must also be understood. For this reason, the standard deviation of all estimates used to calculate an average value is given in Table 6.3.

	Sample 17	Sample 19	Sample 8	Sample 7	Sample 6	Sample 3	Sample 4	Sample 2	Sample 1
	210.89	280.84	584.6	619.75	730	915.3	981.32	1002.94	987.4
	200.76	266.97	576.5	667.9	862	900.5	918.99	970.35	1009.5
	202.62	259.5	541	683	744	932.26	963.46	958.38	1002.1
	209.08	254.46	542.5	654.7	709	915.16	882.72	949	964.09
	208.13	255.68	557.77	622	715	906.77	1043.2	936.07	947.9
	205.66		538.7	673	682				958.1
	207.54		588.3						958.78
	203.51		558.7						
	198.04								
N	9	5	8	6	6	5	5	5	7
Average	205.14	263.49	561.01	653.39	740.33	914.00	957.94	963.35	975.41
Stdev	4.22	10.86	19.99	26.80	63.17	11.95	61.28	25.45	24.08
CoV	0.02	0.04	0.04	0.04	0.09	0.01	0.06	0.03	0.02

Table 6.3 Estimates of thermal conductivity with average and standard deviation

The data from Table 6.3 indicates that as the measured value increases so does the standard deviation. This trend implies that samples with low thermal conductivity can be measured with a great deal of precision. However, as the estimated thermal conductivity

increases, the standard deviation decreased. Overall, the coefficient of variation (standard deviation divided by the mean) for all samples measured were small (0.01 to 0.09) and seem to be independent of the average resistivity.

In order to gain insight into the thermal behavior of boron doped diamond films and the results presented, it is necessary to examine the impurities introduced into the now electrically conducting diamond. Impurities in a semiconductor can scatter electrons and phonons in non-metallic crystals such as diamond. Impurities, which are brought about by the boron, can also introduce free electrons and holes, and these can reduce the phonon conductivity by increasing the scattering. If the concentration of holes or electrons is great enough, they can contribute an appreciable component to the total thermal conductivity (Berman, 1976). In order to simulate the measured thermal conductivity as a function of doping level (as measured by the resistivity), a comparison between the thermal conductivity of perfect single crystal diamond and boron doped polycrystalline diamond is investigated. The theoretical relation which governs thermal conductivity in single crystals is given by (Berman, 1976):

$$k = \frac{k_B}{2\pi^2 v} \left(\frac{k_B}{\hbar}\right)^3 T^3 \int_0^{\theta} \tau(x) \frac{x^4 e^x}{(e^x - 1)^2} dx \quad (6.1)$$

where $x = \hbar \omega / k_B T$

and

\hbar - Planck constant, k_B - Boltzman constant, Θ - Debye temperature (2230 K),
 T - Experimental temperature, ω - Phonon frequency, $\tau(x)$ - Total scattering rate,
 and v - average phonon velocity (speed of sound). Equation 6.1 is the Debye model for
 thermal conductivity. The Debye approximation works well because even pure crystals
 are usually just not perfect enough for N processes to be very important (Berman, 1976).
 Therefore, only resistive processes are considered in this analysis.

In the Graebner et al. work (1994), thermal conductivity of diamond was
 calculated using a combination of scattering processes. In Figure 6.8 below, the
 uppercurve is obtained using only boundary scattering and umklapp scattering. The
 curve labeled a+b is the same but with thickness, d , equal to $1.5\mu\text{m}$. The remaining
 curves are calculated with additional scattering by point defect (p), dislocation (s),
 extended defects (e), and microcracks (m). The graphs shows that thermal resistance is
 dominated by point defects, while extended defects, dislocations, and microcracks play a
 lesser role.

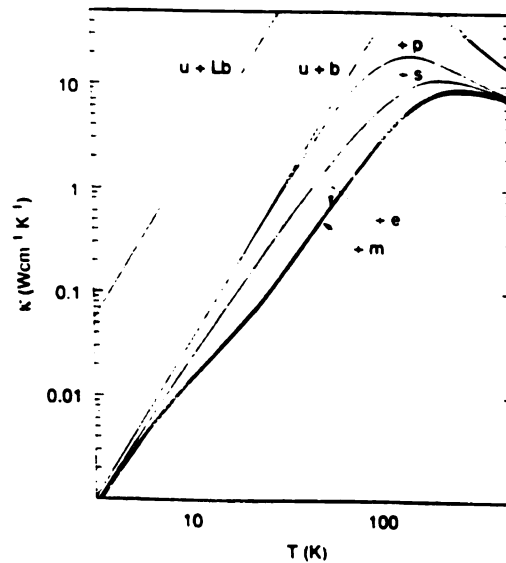


Figure 6.8 Graebner et al. results showing effect of each type of defect on thermal conductivity (Graebner, 1994)

Graebner et al. (1994) and Morelli et al. (1988) examined diamond film thermal conductivity over a range of temperatures using the theoretical relationship in order to quantify what effect scattering processes have on the measured thermal conductivity. While this approach cannot be used in the present study to analyze the measured values since all experiments were performed at about 10 °C above room temperature and the microstructural analysis necessary to measure grain size, etc. was not performed, the analysis can be carried out to verify whether the functional relationship given above (and used by Graebner and Morelli) is valid. Assuming that the total scattering rate is dominated by resistive processes, the governing equation can be simplified. With the governing theoretical equation a function of all scattering processes, it is now possible to simplify the model even further by assuming that point defects, brought about by boron addition, is responsible for the variation in measured thermal conductivity. Consider

scattering processes due to crystal boundaries, point defects, dislocations, and extended defects. A point defect is a defect which extends over a volume with linear dimensions much smaller than the phonon wavelength. At a given temperature the dominant phonon wavelengths for thermal conduction are on the order of a few interatomic distances (the exact value depends on the scattering law). The defect confined to a few atomic volumes will be small enough to appear as a point defect to the important phonons. A defect which fits this criteria may be another atom (such as Boron) on a lattice site substituting for the correct atom (carbon), a vacancy at a lattice site, an interstitial atom, or a combination of these. The scattering is then caused by the difference in mass and difference in bonding between the atoms (Berman, 1976). If a defect is larger than a few interatomic spacing, the scattering does not follow the same mathematical equation as a point defect and must be considered separately. Defects of this kind are referred to as larger or extended defects. A dislocation consists of a narrow region along its axis within which there is a drastically altered structure which may be represented by a change in density (Berman, 1976).

Taking into consideration that the films were created under similar conditions except for the variation in boron levels, its reasonable to assume that all resistive processes are constant for all films except for processes due to point defects. Total scattering is then given by

$$\tau(x)^{-1} = \tau_B(x)^{-1} + \tau_D(x)^{-1} + \tau_E(x)^{-1} + \tau_P(x)^{-1} \quad (6.2)$$

where $\tau_B(x)$ - scattering due to crystal boundaries, $\tau_D(x)$ - scattering due to dislocations, $\tau_E(x)$ - scattering due to extended defects, and $\tau_p(x)$ - scattering due to point defects,

$$\text{rewritten as } \tau(x) = \frac{\tau_B \tau_D \tau_E \tau_p}{(\tau_D \tau_E + \tau_B \tau_E + \tau_B \tau_D) \tau_p + \tau_B \tau_D \tau_E} \quad (6.3)$$

$$\text{this equation for total scattering rate can be simplified to } \tau(x) = \frac{C_1 \tau_p}{C_2 + C_3 \tau_p} \quad (6.4)$$

where $C_1 = \tau_B \tau_D \tau_E$, $C_2 = \tau_B \tau_D \tau_E$, and $C_3 = \tau_D \tau_E + \tau_B \tau_E + \tau_B \tau_D$

With these effects (scattering due to dislocation, extended defects, and grain boundary) considered constant for each film, the governing equation can be simplified even further to

$$k = \frac{C_4 \tau_p}{C_2 + C_3 \tau_p} \quad (6.5)$$

$$\text{where } C_4 = \frac{k_B}{2\pi^2 \nu} \left(\frac{k_B}{\hbar}\right)^3 T^3 \int_0^{\theta} \frac{C_1 x^4 e^x}{(e^x - 1)^2} dx$$

and τ_p is related to the concentration of point defects. This form was developed using the following assumptions:

- 1) All scattering mechanisms are independent of frequency (and therefore wavelength).
- 2) The films are imperfect and all modes are strongly scattered by resistive processes. Therefore in the Callaway expression for thermal conductivity $K_1 \gg K_2$.
- 3) N processes are neglected.

If the above analysis is correct then this is the functional form for thermal conductivity as a function of point defects due to boron substitution into diamond's lattice structure. A curve fit of experimental thermal conductivity as a function of local resistivity is shown in Figure 6.9.

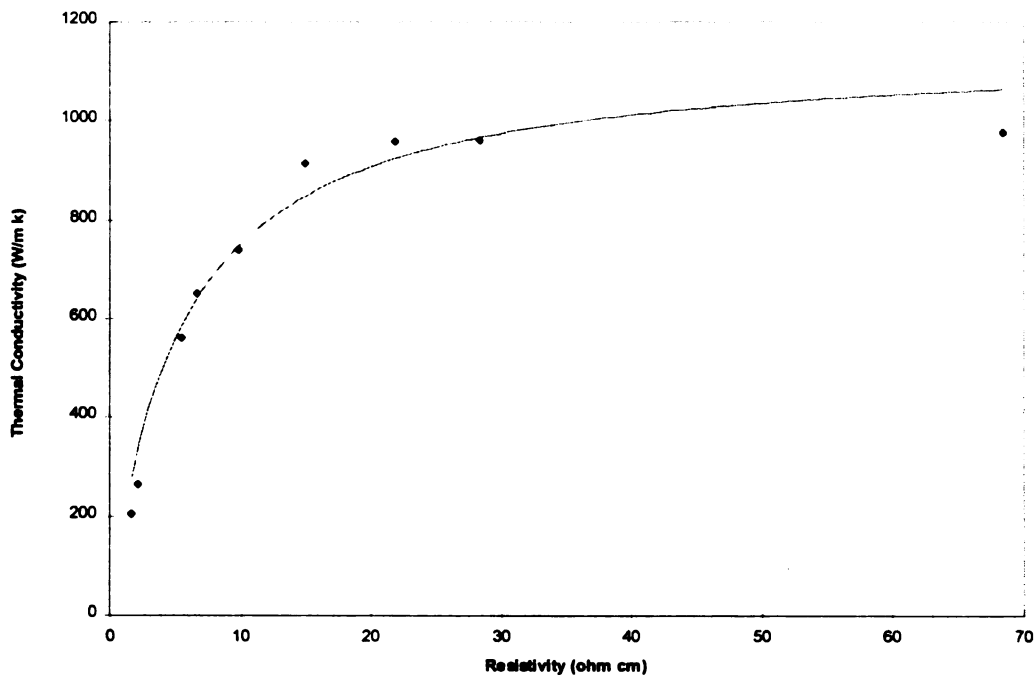


Figure 6.9 Curve fit of thermal conductivity as a function of middle resistivity

The software Tablecurve 2D by Jandel Scientific was used to analyze the data and produce functional equations. For the data, the equation

$$k^{-1} = a + \frac{b}{x}, \quad (6.6)$$

where a and b are constants, k is thermal conductivity, and x is concentration of boron (as measured by the resistivity), match the functional form given above with a correlation coefficient of 0.966. This is evidence that the functional relation given by the theoretical

equation (and used by Graebner and Morelli in their analysis of experimental thermal conductivity) governs the experimental work in this report. Since results are presented for local and average resistivities, it is useful to curve fit average data as well. The curve fit of thermal conductivity versus average resistivity is shown in Figure 6.10.

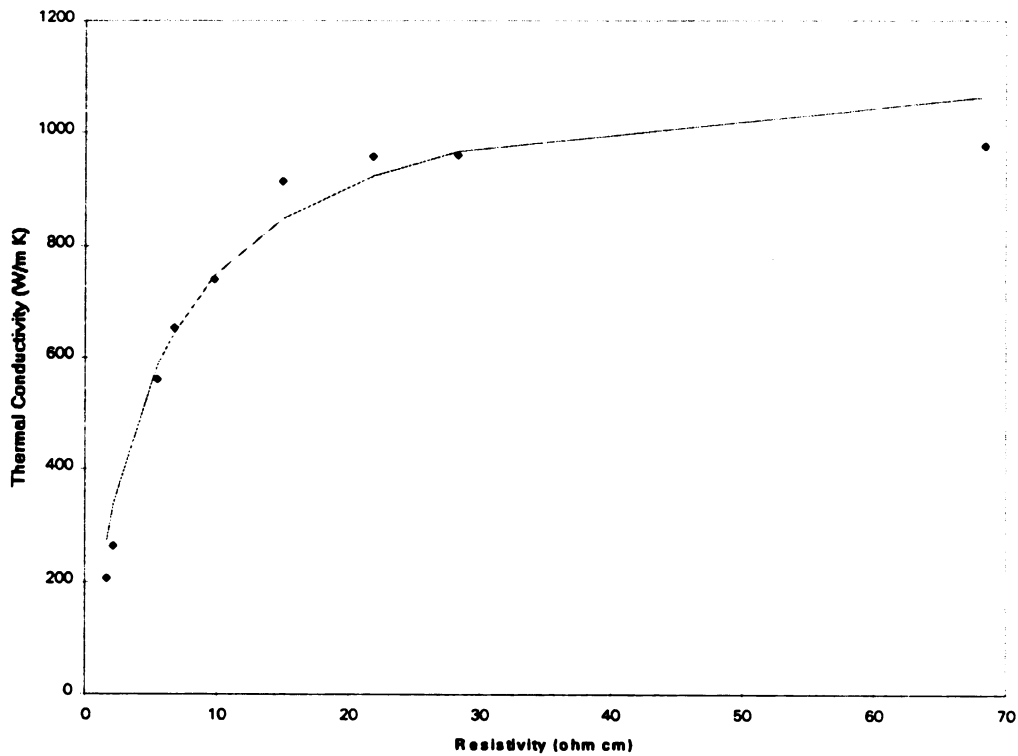


Figure 6.10 Curve fit of thermal conductivity as a function of average resistivity

For thermal conductivity as a function of average resistivity the correlation coefficient was 0.937. Once again the curve fit matches fairly well considering the microstructural analysis necessary for all scattering processes to be understood and quantified was not performed.

6.2 UNCERTAINTY ANALYSIS

Error may be defined as the difference between the measured result and the “true” value. Because the true value is never known, its difficult to know the error. However, it is possible to estimate an error. The process of assigning a value to an estimate of error is commonly referred to as an uncertainty (Beckwith, 1990). In determining the thermal conductivity of thin diamond films, many values were measured. Each of the measured values contain errors which must be accounted for. Since the measured values are subsequently used to determine the magnitude of the thermal conductivity, the uncertainty in the estimated thermal conductivity must be calculated.

The uncertainty in the thermal conductivity is determined using the estimated error for the measured parameters and the simplified governing equation written in terms of thermal conductivity as

$$K = \frac{V^2 b^2}{4RLW\theta(\delta_d + \delta_g)} \left(1 - \frac{r^2}{b^2}\right) \quad (6.7)$$

The uncertainty in K acts a global uncertainty which is driven by the precision with which all experimental unknowns can be measured (Herr, 1993). The uncertainty in the thermal conductivity is determined from the expression

$$\begin{aligned} \Delta K = & \left[\left(\frac{\partial K}{\partial V} \Delta V \right)^2 + \left(\frac{\partial K}{\partial R} \Delta R \right)^2 + \left(\frac{\partial K}{\partial L} \Delta L \right)^2 + \left(\frac{\partial K}{\partial W} \Delta W \right)^2 + \left(\frac{\partial K}{\partial \theta} \Delta \theta \right)^2 \right. \\ & \left. + \left(\frac{\partial K}{\partial b} \Delta b \right)^2 + \left(\frac{\partial K}{\partial \delta_g} \Delta \delta_g \right)^2 + \left(\frac{\partial K}{\partial \delta_d} \Delta \delta_d \right)^2 + \left(\frac{\partial K}{\partial r} \Delta r \right)^2 \right]^{1/2} \end{aligned} \quad (6.8)$$

where

$$\frac{\partial K}{\partial V} = -\frac{V^2 b^2}{2RLW\theta(\delta_d + \delta_g)} \left[1 - \left(\frac{r}{b} \right)^2 \right] \quad (6.9)$$

$$\frac{\partial K}{\partial R} = -\frac{V^2 b^2}{4R^2 LW\theta(\delta_d + \delta_g)} \left[1 - \left(\frac{r}{b} \right)^2 \right] \quad (6.10)$$

$$\frac{\partial K}{\partial L} = -\frac{V^2 b^2}{4RL^2 W\theta(\delta_d + \delta_g)} \left[1 - \left(\frac{r}{b} \right)^2 \right] \quad (6.11)$$

$$\frac{\partial K}{\partial \theta} = -\frac{V^2 b^2}{4RLW\theta^2(\delta_d + \delta_g)} \left[1 - \left(\frac{r}{b} \right)^2 \right] \quad (6.12)$$

$$\frac{\partial K}{\partial W} = -\frac{V^2 b^2}{4RLW^2\theta(\delta_d + \delta_g)} \left[1 - \left(\frac{r}{b} \right)^2 \right] \quad (6.13)$$

$$\frac{\partial K}{\partial b} = \frac{V^2 b}{2RLW\theta(\delta_d + \delta_g)} \quad (6.14)$$

$$\frac{\partial \mathcal{K}}{\partial \delta_d} = -\frac{V^2 b^2}{4RLW\theta(\delta_d + \delta_g)^2} \left[1 - \left(\frac{r}{b}\right)^2\right] \quad (6.15)$$

$$\frac{\partial \mathcal{K}}{\partial \delta_g} = -\frac{V^2 b^2}{4RLW\theta(\delta_d + \delta_g)^2} \left[1 - \left(\frac{r}{b}\right)^2\right] \quad (6.16)$$

$$\frac{\partial \mathcal{K}}{\partial r} = -\frac{V^2 r}{2RLW\theta(\delta_d + \delta_g)} \quad (6.17)$$

and $\Delta L=1 \times 10^{-5}$ m, $\Delta W=1 \times 10^{-5}$ m, $\Delta R=1 \times 10^{-3}$ Ω , $\Delta V=1 \times 10^{-3}$ V, $\Delta \theta=0.1$ °C, $\Delta \delta_d=1 \times 10^{-7}$ m, $\Delta \delta_g=1 \times 10^{-9}$ m, $\Delta b=1 \times 10^{-6}$ m, $\Delta r=1 \times 10^{-6}$ m. Since various power levels ($P=V^2/R$), lengths, widths, etc. were used to estimate the thermal conductivity, the uncertainty in thermal conductivity varies for each sample and for each experiment (due to various power settings). Because of the varying uncertainty, the analysis was performed for all conditions, however only worst case or highest value in the estimate of the errors are presented in this section.

The uncertainty in the measured parameters were estimated based on the precision of the instrument used. The uncertainty in the voltage was chosen as 0.001 volts because this is the precision to which the digital multimeter (DMM) can measure voltage. The same DMM was used to record sample resistance (not the diamond resistance as measured by the four probe method), and did so with a similar uncertainty of 0.001 Ω . The measurements of length, width, and radius were performed using a vernier caliper

which was capable of measuring to one hundredth of a millimeter. Therefore, the vernier caliper presented measurements with uncertainty of 0.00001 m. The uncertainty in temperature was chosen as 0.1 °C due to the sensitivity with which the infrared system measures temperature. The uncertainty in the thickness of the gold and diamond were conservative estimates based on the instruments used to sputter gold and measure thicknesses in each case. The uncertainty in the thickness of the gold was based on the manufacturer's calibration of sputtering rate. The uncertainty in the thickness of the diamond was chosen to be 0.1 microns based on the Dektak measurement precision used and the assumptions made. This is a very conservative estimate with a relative error of 5 percent. The estimate of each parameter uncertainty and the equation for uncertainty in thermal conductivity was then used to calculate worst case global uncertainty of thermal conductivity for all samples measured. Table 6.4 shows the uncertainty of each sample and the percent error associated with the measured value.

Sample #	Thermal Conductivity (W/m k)	Estimated Uncertainty (W/m k)	% uncertainty	Measured Standard Deviation (W/m K)
17	205	13.2	6.44	4.2
19	263	10.1	3.84	10.9
8	561	30.8	5.49	20
7	653	34.6	5.30	26.8
6	740	54.7	7.39	63.2
3	914	60.1	6.58	12
4	958	65.1	6.80	61.28
2	960	60.6	6.31	25.5

Table 6.4 Uncertainty in measured thermal conductivity

The % uncertainties are within the range reported by other researchers. In Herr's (1993) analysis of a doped diamond film, the thermal conductivity was found to be 249 ± 13 W/m

k. This analysis give a percent uncertainty of 5.22 which is close to the 6.0% average in the present work when all samples are considered. Comparing the measured standard deviation (Table 6.2) to the calculated uncertainty (Figure 6.11), it is easy to see that samples #1, #2, #3 and #17 have significantly different values for standard deviation and calculated uncertainty.

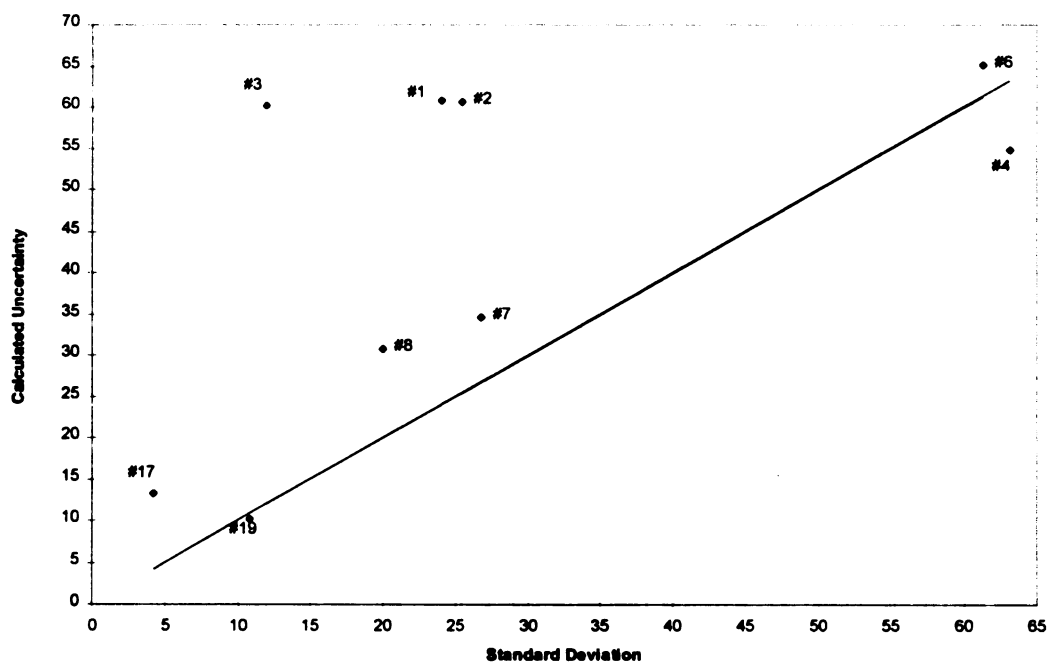


Figure 6.11 Comparison between calculated uncertainty and measured standard deviation

One possible explanation for the small standard deviation could be that these samples were estimated based on temperature data processed using IPPlus. Similar results showing small relative deviation for samples #1, #2, and #3 are shown in Figure 6.12, which is a plot of standard deviation versus thermal conductivity.

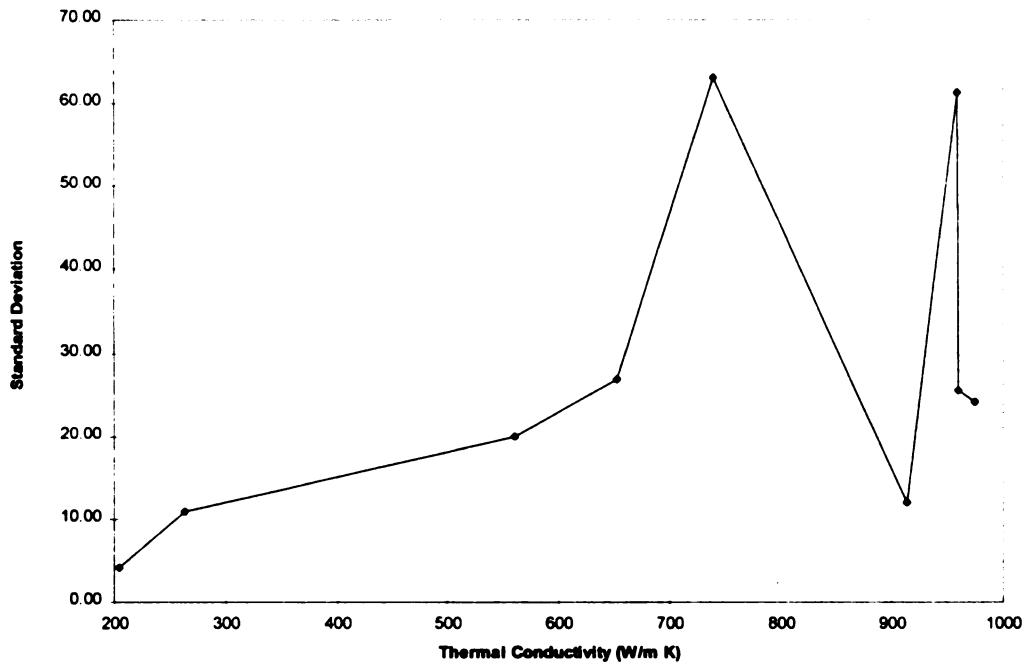


Figure 6.12 Measured uncertainty relative to mean thermal conductivity estimates

The complete uncertainty analysis has the advantage of revealing the contribution of each parameter to the overall uncertainty. Table 6.5 shows the magnitude to which each parameter contributes to the overall uncertainty in the estimate of thermal conductivity. Based on this information it can easily be seen that the thickness of the diamond and the sensitivity of the temperature difference are responsible for the error in the estimate of thermal conductivity. Therefore, in order to reduce the experimental uncertainty, accurate measurement of temperatures and diamond thickness' are crucial. While experimental limitation (such as sample size, etc.) require the use of an infrared system to record temperatures, there is certainly room for improvement in the

measurement of the diamond's thickness. One way to improve the uncertainty is to examine the sensitivity of thermal conductivity to thickness of diamond. Figure 6.13 shows the estimated thermal conductivity for a range of thicknesses for sample #2.

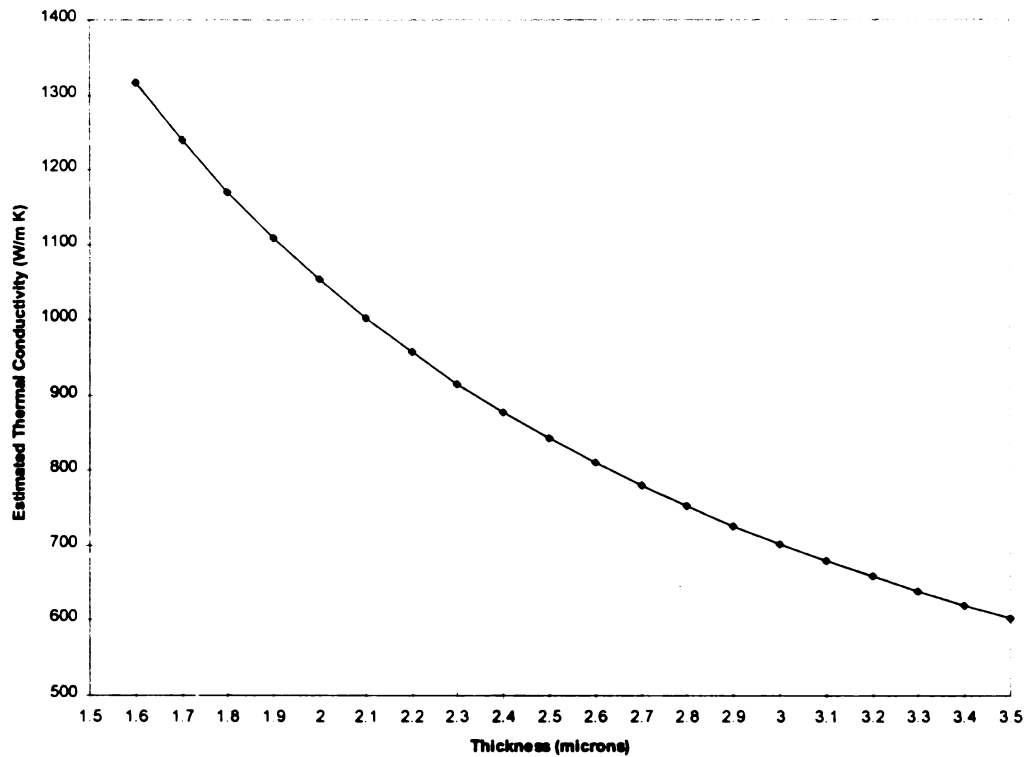


Figure 6.13 Sensitivity of thermal conductivity to thickness of diamond

It can easily be seen that thermal conductivity becomes less sensitive to thickness as the magnitude for thickness increase. For this reason, Herr (1993) and others measured thermal conductivity with thicker samples.

Parameter, x	Contribution $(\frac{dK}{dx} dx)^2$	% Contribution
Voltage, V	2.39	0.067
Resistance, R	0.38	0.011
Radius, b	38.09	1.054
Length, L	1.09	0.03
Width, W	0.46	0.013
Temperature Difference, θ	0.46	44.87
Gold Thickness, δ_g	1620.22	0.135
Diamond Thickness, δ_d	1943.58	53.823

Table 6.5 Parameter contribution to uncertainty in thermal conductivity

In order to quantify the results presented (thermal conductivity as a function of resistivity) earlier, the uncertainty in the measured resistivity must also be calculated.

Once again conservative estimates of the parameters were utilized so worst case uncertainty can be calculated. The uncertainty in resistivity is given by

$$\Delta\rho = [(\frac{\partial\rho}{\partial V} \Delta V)^2 + (\frac{\partial\rho}{\partial I} \Delta I)^2 + (\frac{\partial\rho}{\partial C} \Delta C)^2 + (\frac{\partial\rho}{\partial \delta} \Delta \delta)]^{\frac{1}{2}} \quad (6.17)$$

where

$$\frac{\partial\rho}{\partial V} = C \frac{\delta}{I} \quad (6.18)$$

$$\frac{\partial \rho}{\partial I} = -\delta C \frac{V}{I^2} \quad (6.19)$$

$$\frac{\partial \rho}{\partial C} = \delta \frac{V}{I} \quad (6.20)$$

$$\frac{\partial \rho}{\partial \delta} = C \frac{V}{I} \quad (6.21)$$

and $\Delta V = 1 \times 10^{-3}$ V, $\Delta I = 0.1$ A, $\Delta C = 0.1$, and $\Delta \delta = 1 \times 10^{-7}$ m.

The above equations were used to calculate the uncertainty in resistivity. The magnitudes of the uncertainty are shown in Table 6.6 and 6.7, along with percent error.

Sample #	Resistivity(middle) (ohm cm)	Uncertainty (ohm cm)	% error
17	1.63	0.094	5.77
19	2.2	0.101	4.59
8	5.5	0.166	3.02
7	6.73	0.194	2.88
6	9.82	0.268	2.73
3	14.96	0.397	2.65
4	21.86	0.574	2.63
2	28.38	0.742	2.61
1	68.4	1.946	2.85

Table 6.6 Middle resistivity, uncertainty, and percent uncertainty

Sample #	Resistivity (average) (ohm cm)	Uncertainty (ohm cm)	% error
17	1.621	0.093	5.74
19	3.987	0.133	3.34
8	6.76	0.194	2.87
7	8.06	0.225	2.79
6	11.68	0.315	2.70
3	18.39	0.485	2.64
4	28.5	0.746	2.62
2	31.68	0.827	2.61
1	80.14	2.279	2.84

Table 6.7 Average resistivity, uncertainty, and percent uncertainty

Parameter, x	Contribution	% Contribution
Voltage, V	0.007	68.62
Constant, C	0.003	29.41
Current, I	0.0004828	4.73
Thickness, δ	0.000001207	0.01

Table 6.8 Parameter contribution to uncertainty in resistivity

Table 6.8 shows the significance of each parameter on the overall uncertainty.

Another way of presenting the uncertainty is with the use of error bars. Error bars has the added advantage of showing the range of error relative to the scale of all estimates graphically. Figures 6.14 and 6.15 shows a graph of thermal conductivity versus resistivity with error bars.

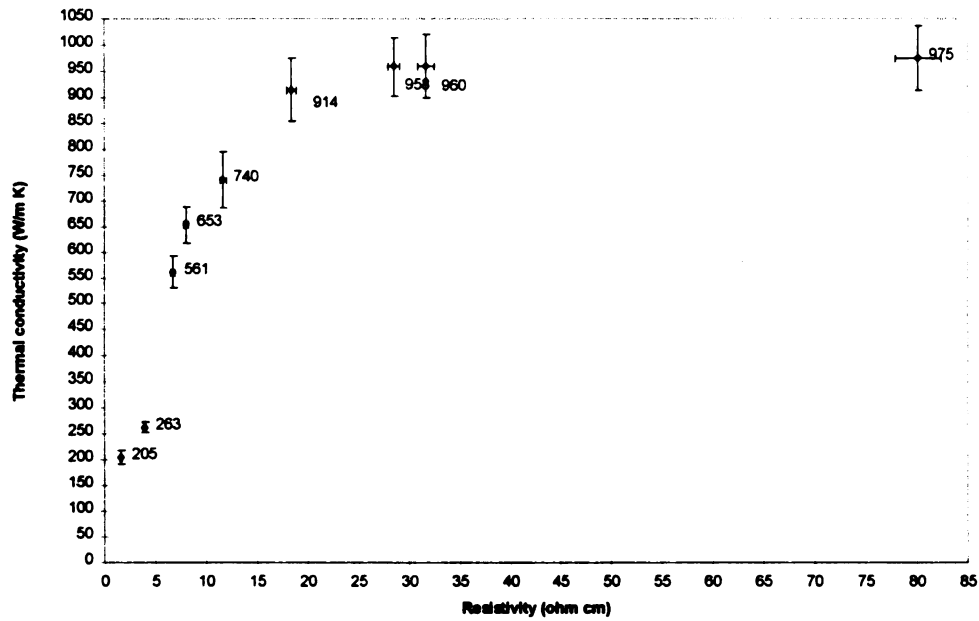


Figure 6.14 Thermal conductivity as a function of average resistivity with error bars

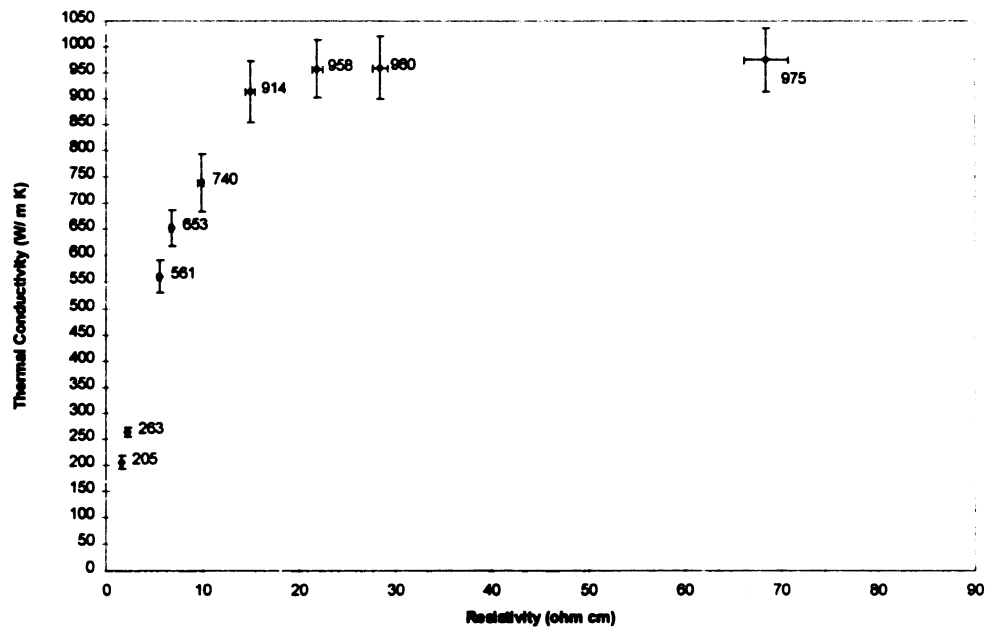


Figure 6.15 Thermal conductivity as a function of middle resistivity with error bars

It can easily be seen that the magnitude of the error increased as the magnitude of the measured quantity increased. However, the percentage or relative error did not change significantly.

CHAPTER 7

SUMMARY AND CONCLUSIONS

The goal of this research was to determine the effects of boron doping on the thermal conductivity of diamond films. In pursuit of such a goal, an experimental technique was used which allowed for electrical resistance heating for a range of doping levels. The preceding chapters present a comprehensive method for the fabrication and thermal analysis of boron doped CVD diamond films. The basic techniques and procedures necessary for the growth of diamond using the hot filament CVD method is described, along with the required sample design for the radial heat flow model, and then the thermal activation and capture of the temperature distribution for the estimation of thermal conductivity using the methods of parameter estimation.

In accomplishing the goals of the project, thin diamond films were deposited on silicon wafer using the hot filament chemical vapor deposition method. Doping was made possible by placing boron powder in a honeycomb shape holder on the silicon wafer. A mask was used in order to have many diamond films with various doping levels on a single 4 inch silicon wafer. The HFCVD system deposited diamond for 10 hours at

a rate of approximately 0.2 microns per hour. The silicon wafer was then cut along the mask regions in order to separate each film from the bulk wafer. The doping level, as measured by the film's resistivity, was then measured using the four probe method. Thickness measurements were then made using the Sloan Dektak IIA profilometer before a 3mm diameter of free standing diamond was created by chemically etching the silicon. The etched sample is prepared by forming an electric circuit with the diamond. In order for the infrared thermograph system to measure accurate temperatures, a thin layer of gold is added to one surface of the diamond. The experiment is carried out by passing an electric current through the diamond. The internal heat generated by the current causes temperature gradient within the 3mm free standing diamond. The radial heat flow model and the measured temperatures are then used to estimate the thermal conductivity. Each sample was fabricated in a similar manner, and the estimated thermal conductivities were averaged for several experimental runs.

The results of the investigation revealed that boron doping decrease the thermal conductivity (when compared to undoped diamond). This result is predicted by theory since the addition of boron to the diamond structure brings in defects in an otherwise pure material. The defects in the diamond is responsible for the reduced thermal conductivity measurements, and the relative amount of defects present is responsible for the magnitude of the thermal conductivity. Because of the complex nature of the theoretical equation governing thermal conductivity and the molecular structure responsible for heat conduction in diamond crystals, it was not possible to compare calculated theoretical

thermal conductivity to measured values. However, the functional form of theoretical thermal conductivity was compared to the functional form of the experimentally determined thermal conductivities. This analysis revealed that resistive processes is responsible for the measured conductivities. However, its important to note that the dominant process is point defects. Since all samples were fabricated under similar conditions, its reasonable to assume that extended defects, boundary scattering, and dislocations would be constant for all samples. Point defects is not constant however, since the boron source contributed varying amounts of boron atoms to substitute into the diamond lattice.

While the thermal conductivity is given as a function of average and local resistivity, it should be noted that local resistivity gives a better indication of the amount of boron present in the region of interest. It is within the etched region where experiments are performed and temperature distribution are extracted for use in estimating the thermal conductivity. For this reason, the local resistivity versus thermal conductivity gives a better fit to the theoretical equation as a function of point defects.

Lastly, since little information was found in the literature related to thermal analysis of boron doped diamond film, it was not possible to compare the results to other experimental studies. For this reason, this work is an initial study and will aid future studies on the thermal properties of boron doped diamond films and all related applications.

CHAPTER 8

RECOMMENDATIONS FOR FUTURE WORK

The present work describes an experimental technique and results for thermal conductivity of boron doped diamond films. As in most experimental work there is always room for further study in order to minimize the uncertainty and improve the overall wealth of knowledge in the field of study. In this section, some of the necessary procedures which can be used by future research in the study of semiconducting diamond films will be addressed. The recommendations will include the following:

- ◆ Development of a technique which can control the level of doping. This technique might include depositing diamond samples one at a time using a solid or gas form of boron. The mass of boron could then be adjusted in order to acquire the desired resistivity. While a solid source can still lead to varying resistivities over small regions, a gaseous source might not. However it should be noted that little is known about boron distribution when boron powder is used as the doping source.

- ◆ Development of an accurate and non-destructive method to measure film thickness and thickness profile.

- ◆ Check the accuracy of the technique using a known material or a different technique with the same samples.

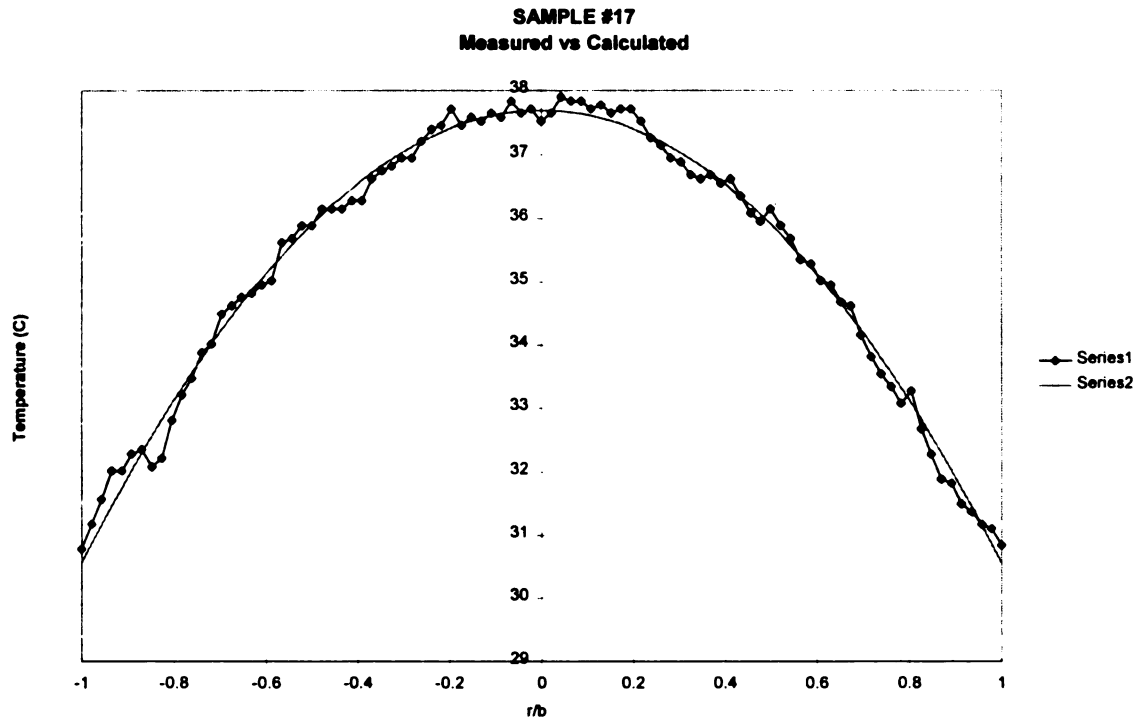
- ◆ Expand the range of resistivities and include more samples.

- ◆ Examine samples on the microscopic level in order to investigate defects. This could include using Raman spectroscopy, Scanning electron microscope, or other instruments which can quantify the presence and abundance of defects.

- ◆ Use a Secondary Ion Mass Spectroscopy (SIMS) to quantify the amount of boron present. This will permit determining the thermal conductivity as a function of the amount of boron atoms present which can be related to measured resistivity.

APPENDIX A

EXPERIMENTAL DATA FOR EACH SAMPLE

SAMPLE#17**FIGURE A.1**

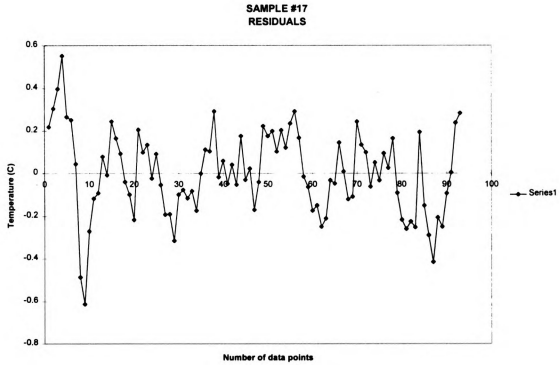


FIGURE A.2

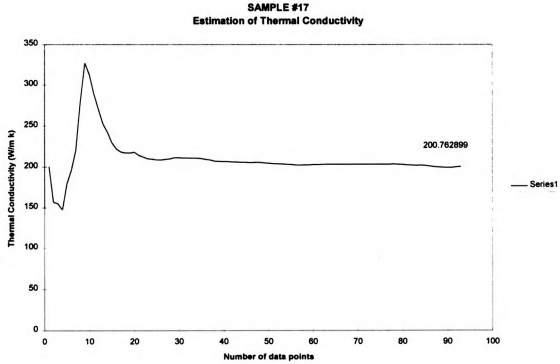


FIGURE A.3

SAMPLE #8

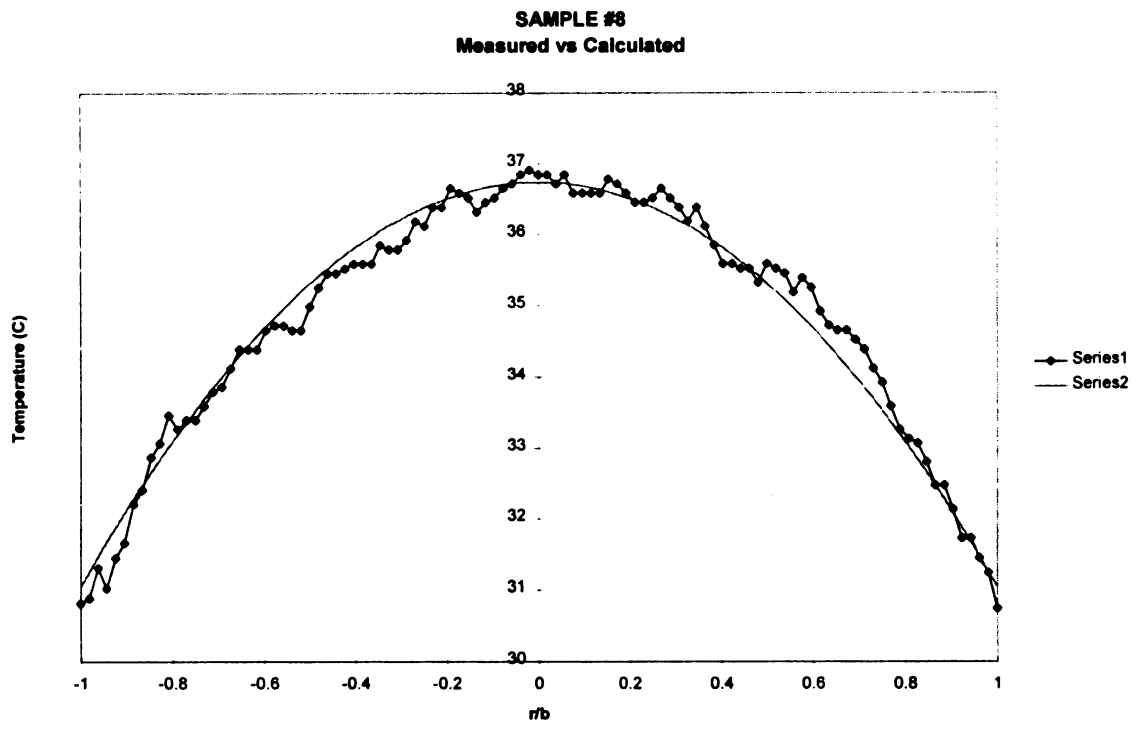


FIGURE A.4

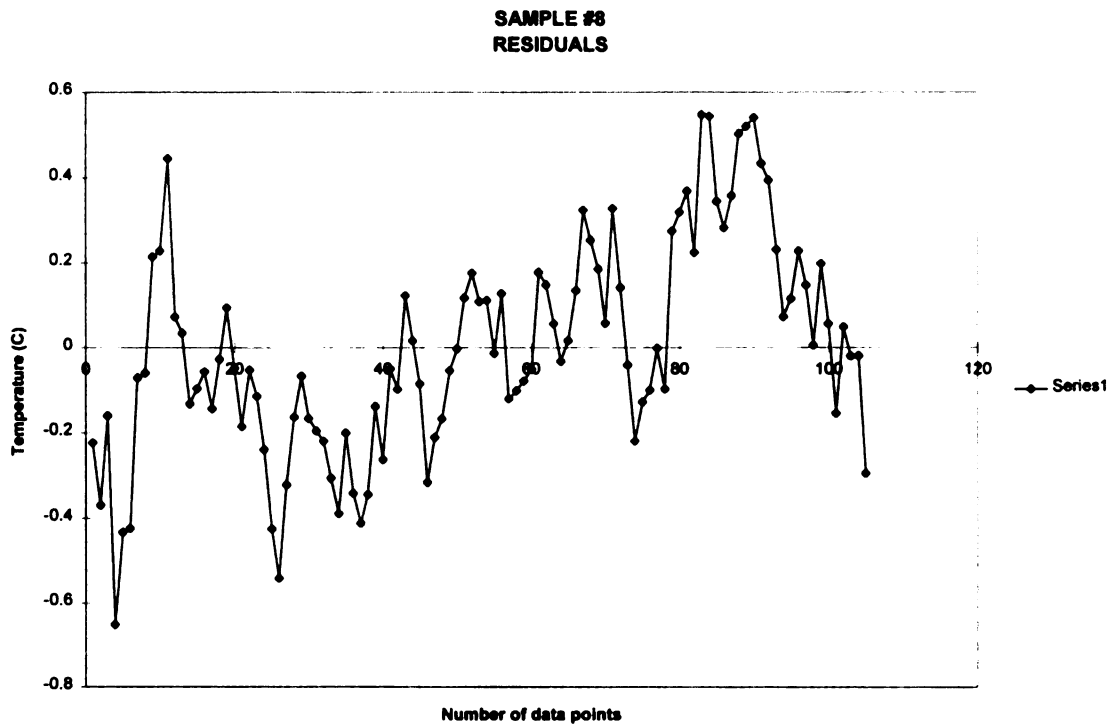


FIGURE A.5

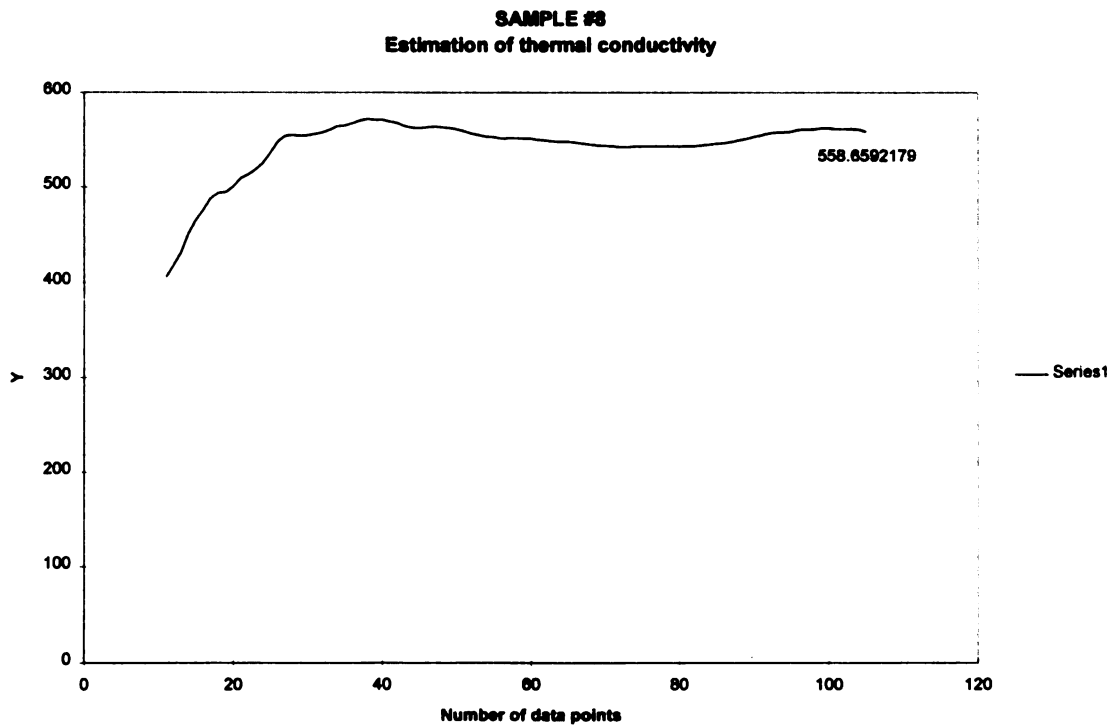
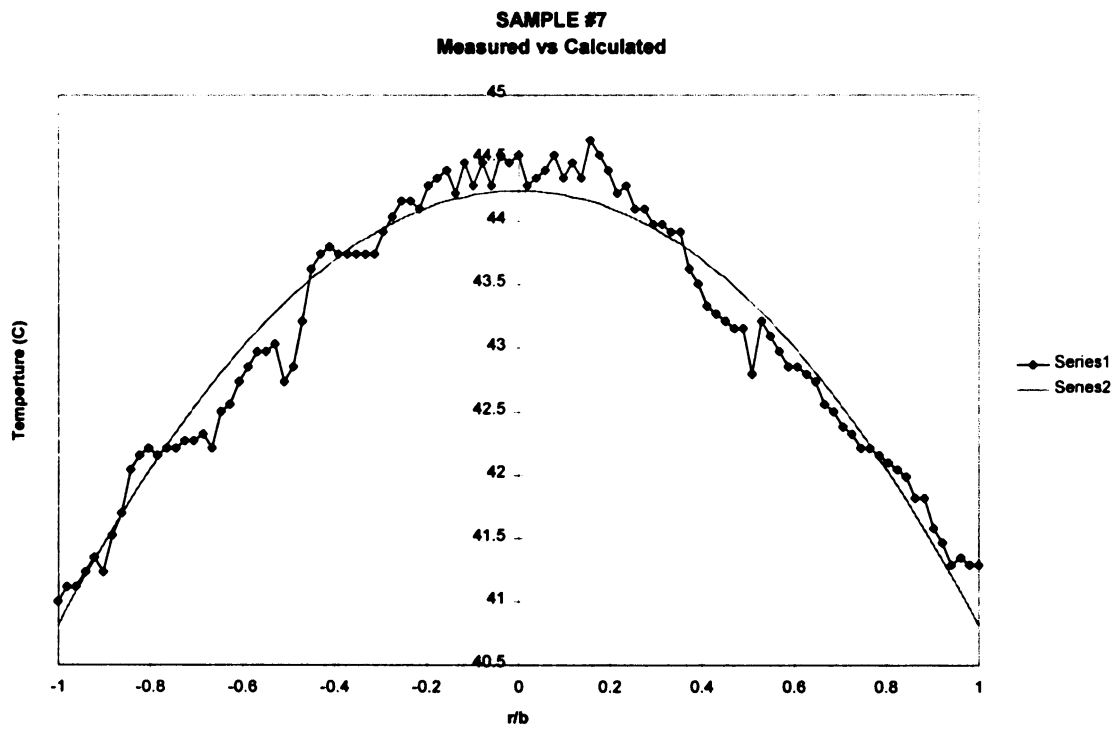


FIGURE A.6

SAMPLE #7**FIGURE A.7**

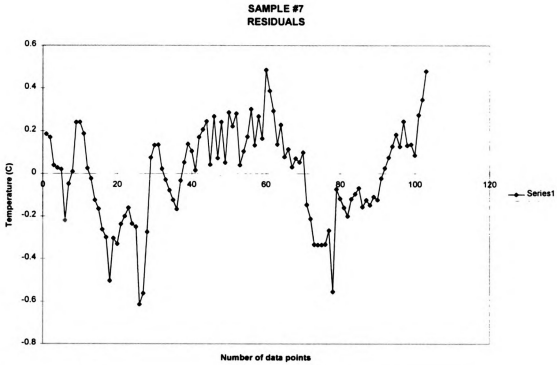


FIGURE A.8

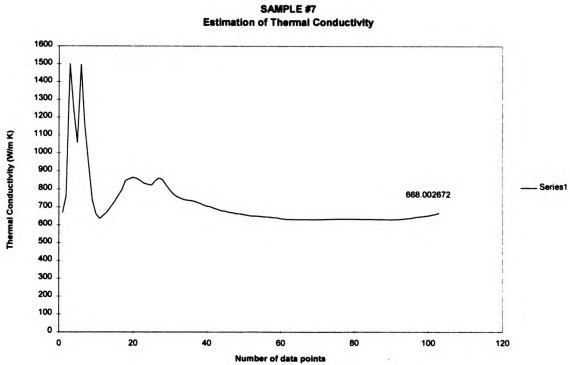
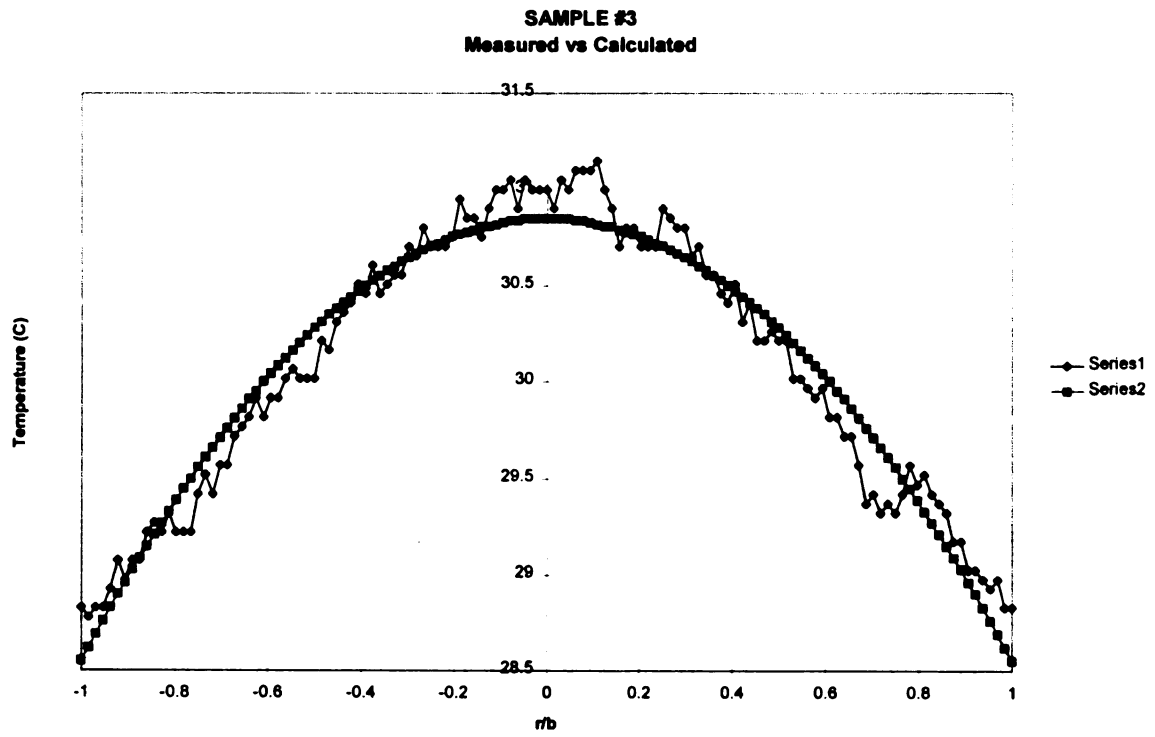


FIGURE A.9

SAMPLE #3**FIGURE A.10**

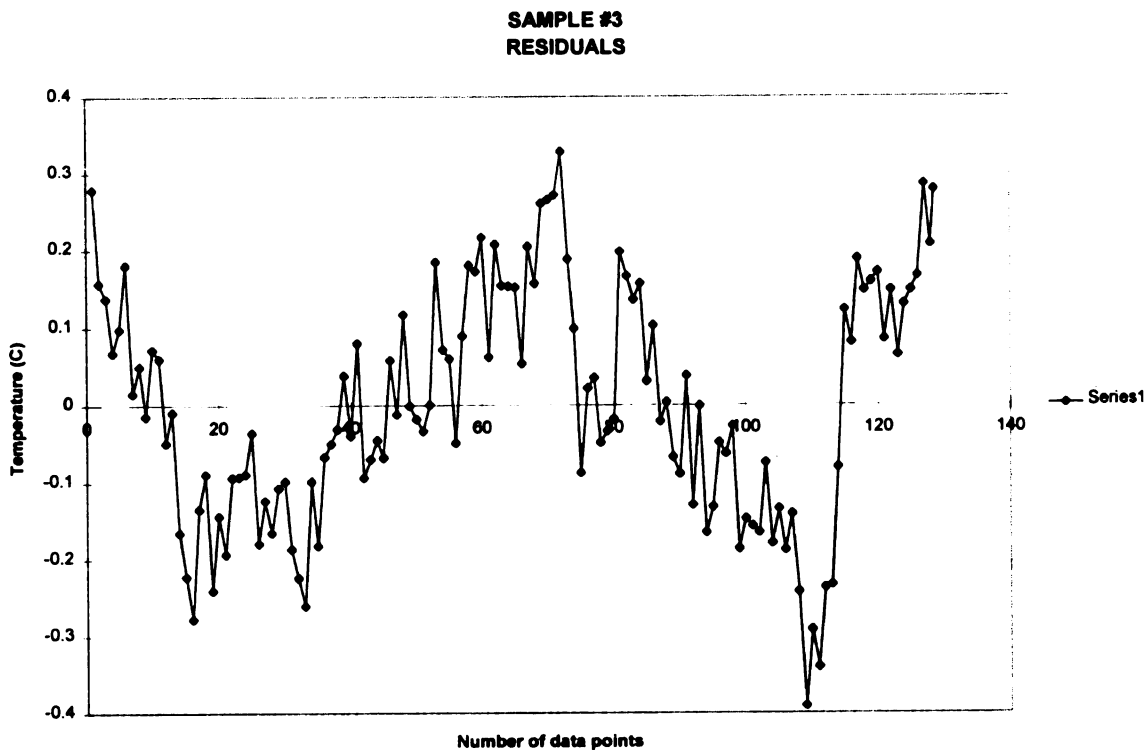


FIGURE A.11

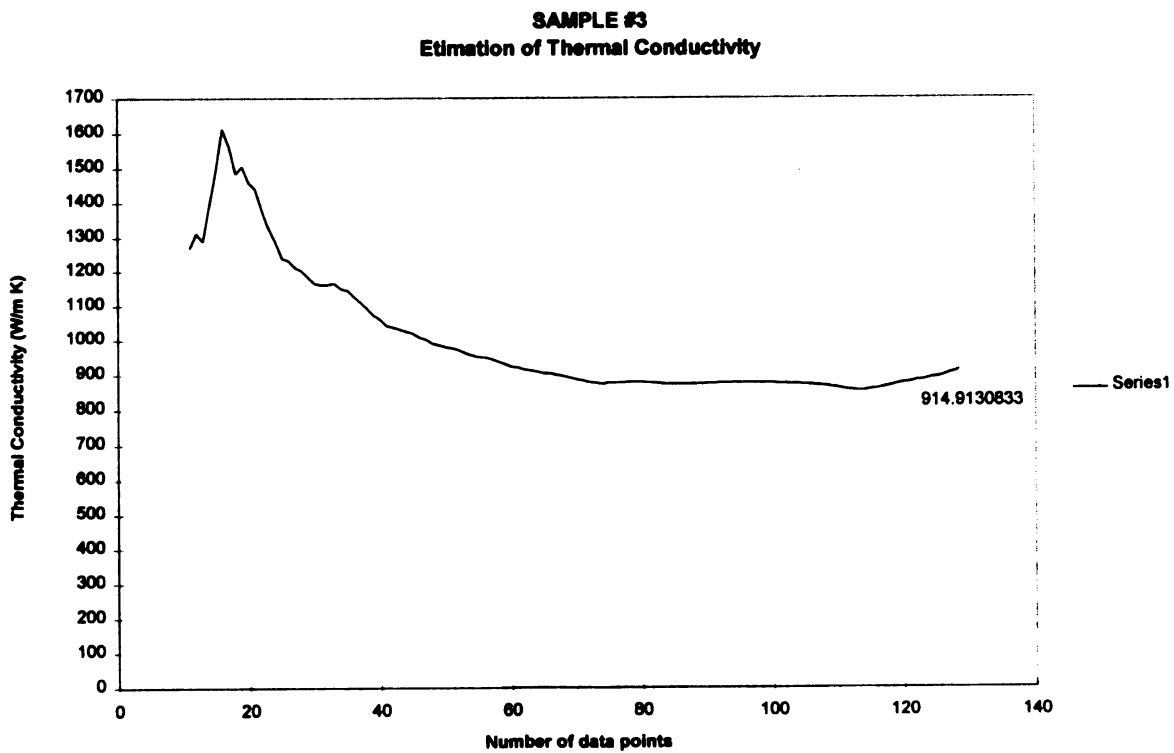


FIGURE A.12

SAMPLE #2

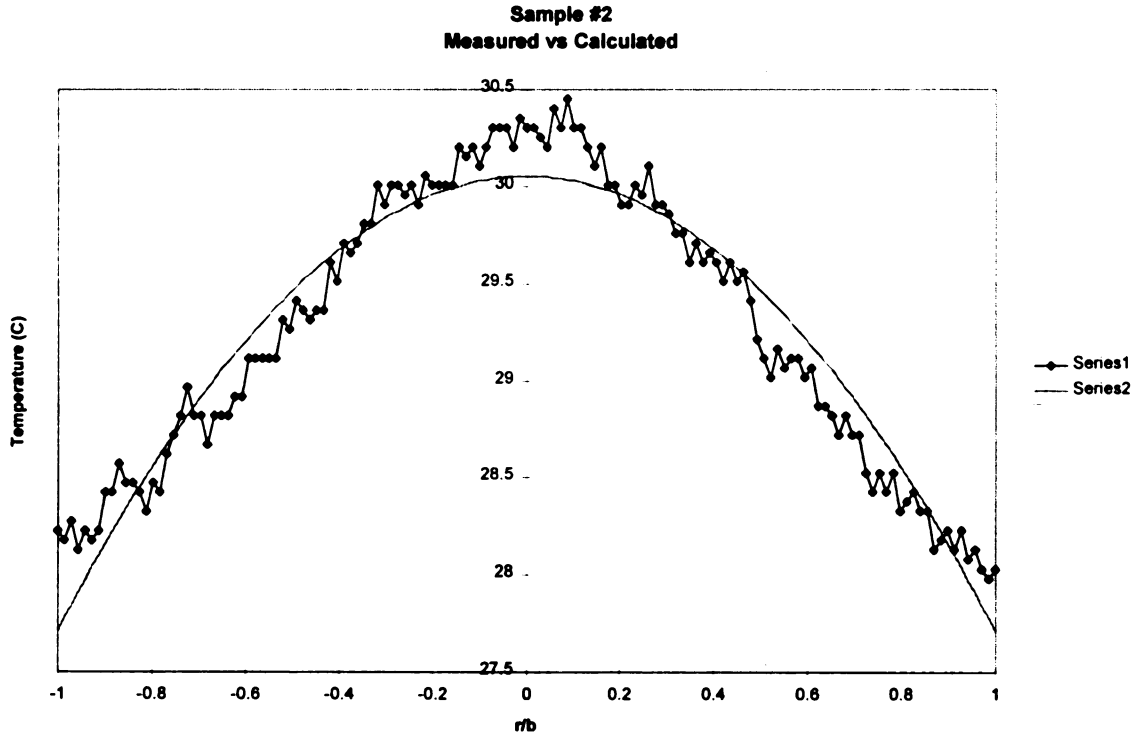


FIGURE A.13

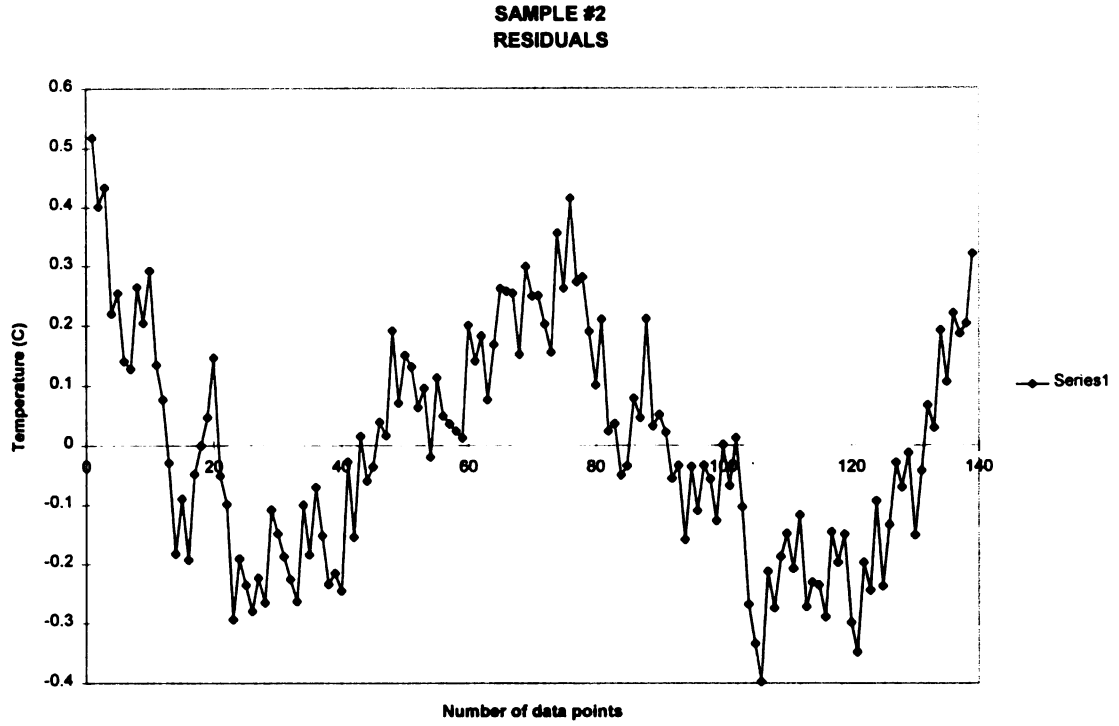


FIGURE A.14

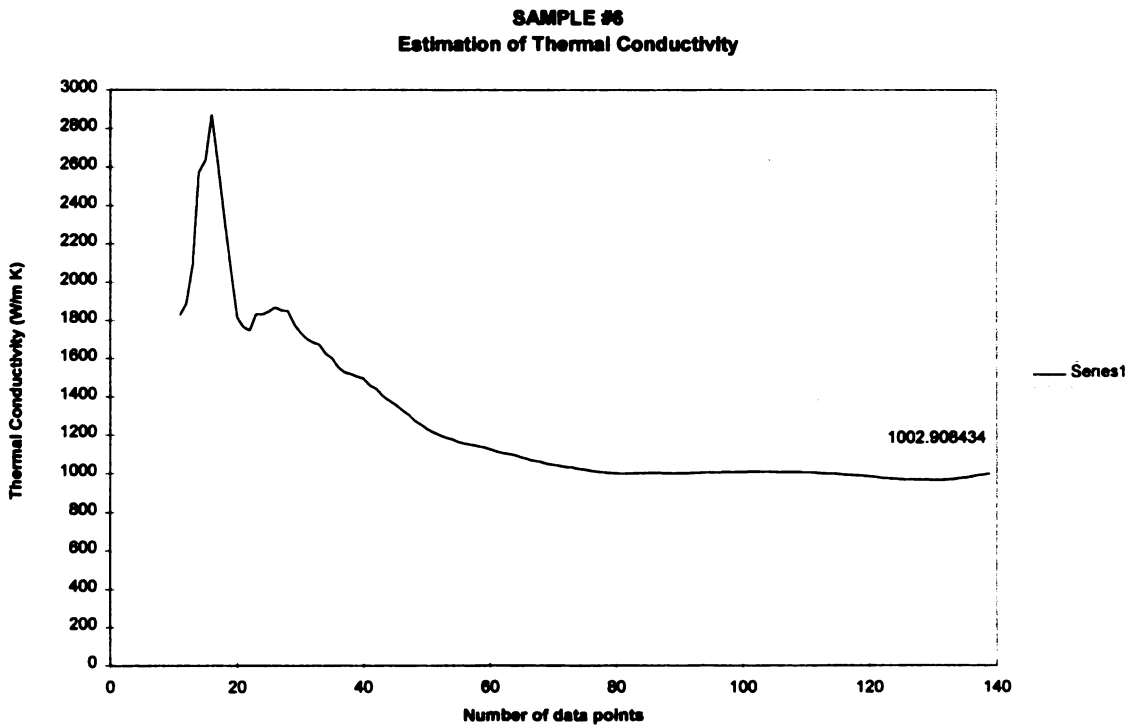


FIGURE A.15

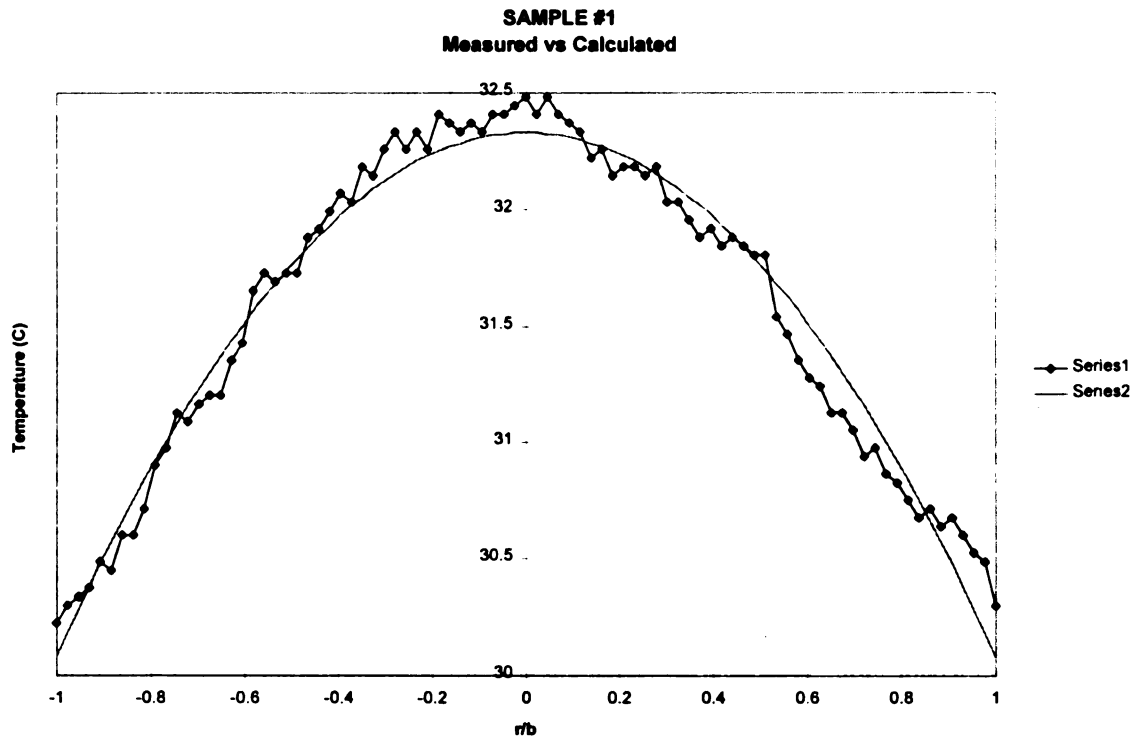
SAMPLE #1

FIGURE A.16

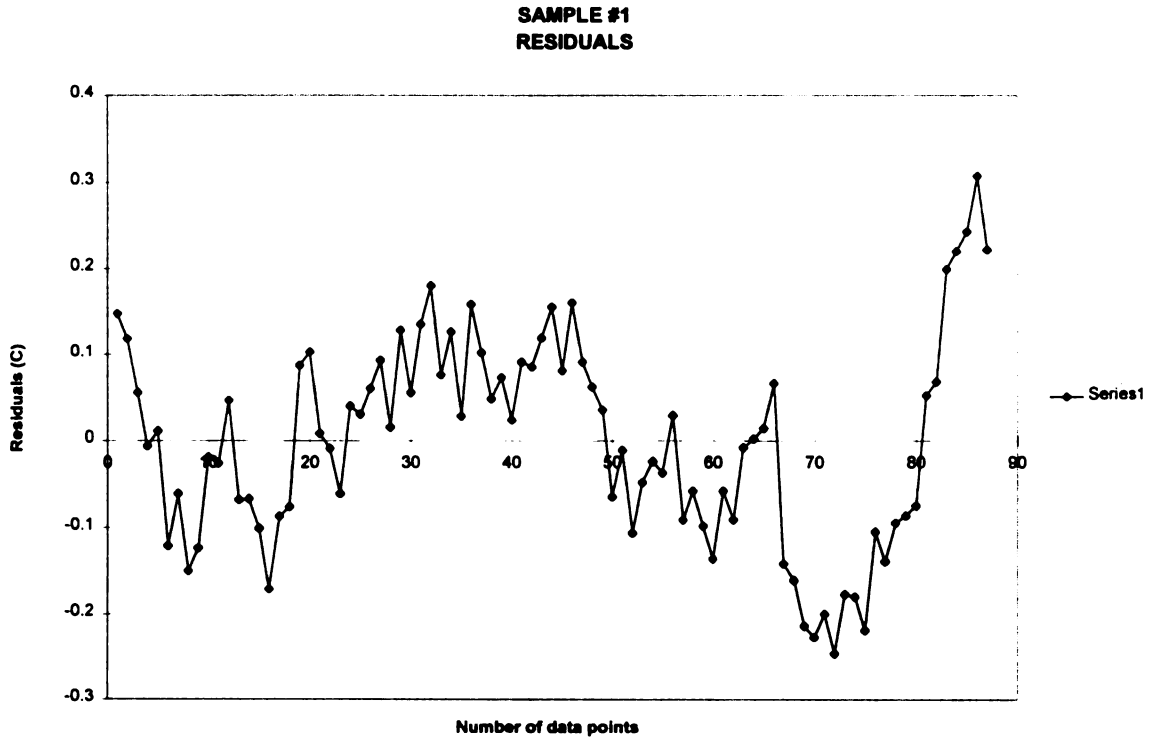


FIGURE A.17

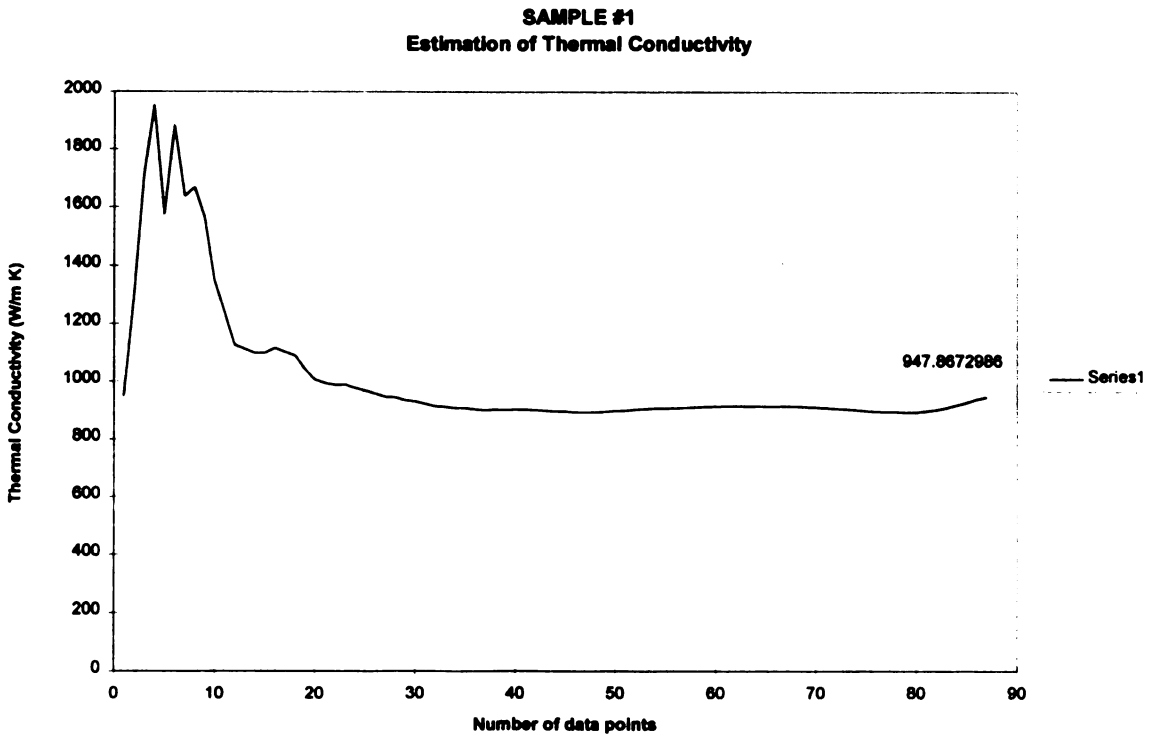


FIGURE A.18

SAMPLE #19

**SAMPLE #19
Measured vs Calculated**

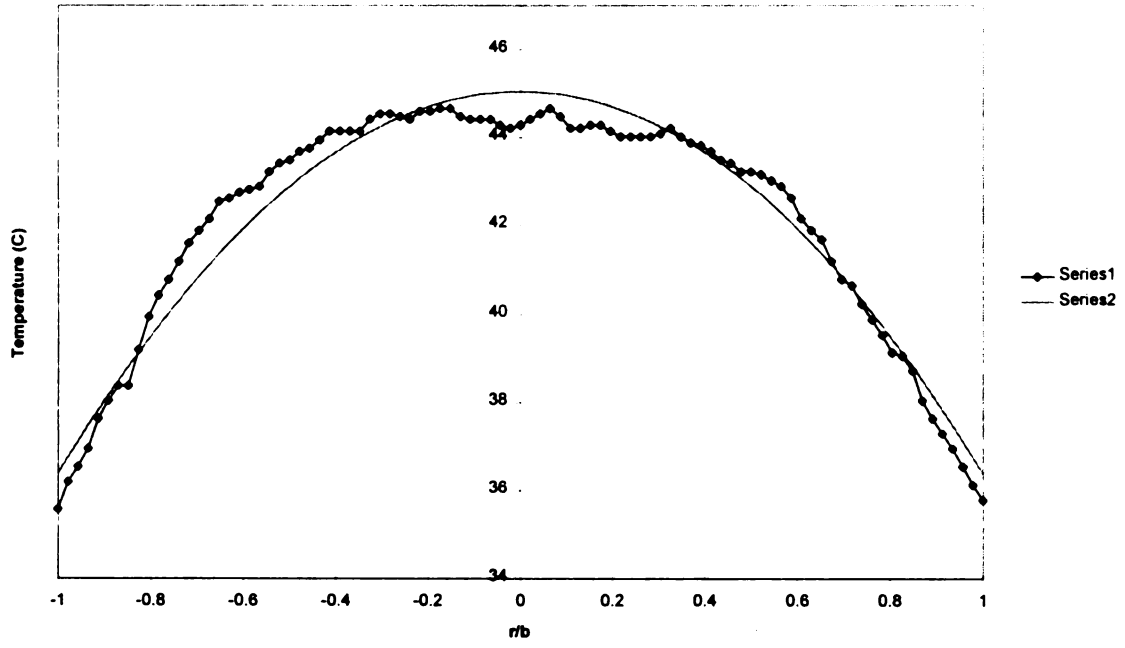


FIGURE A.19

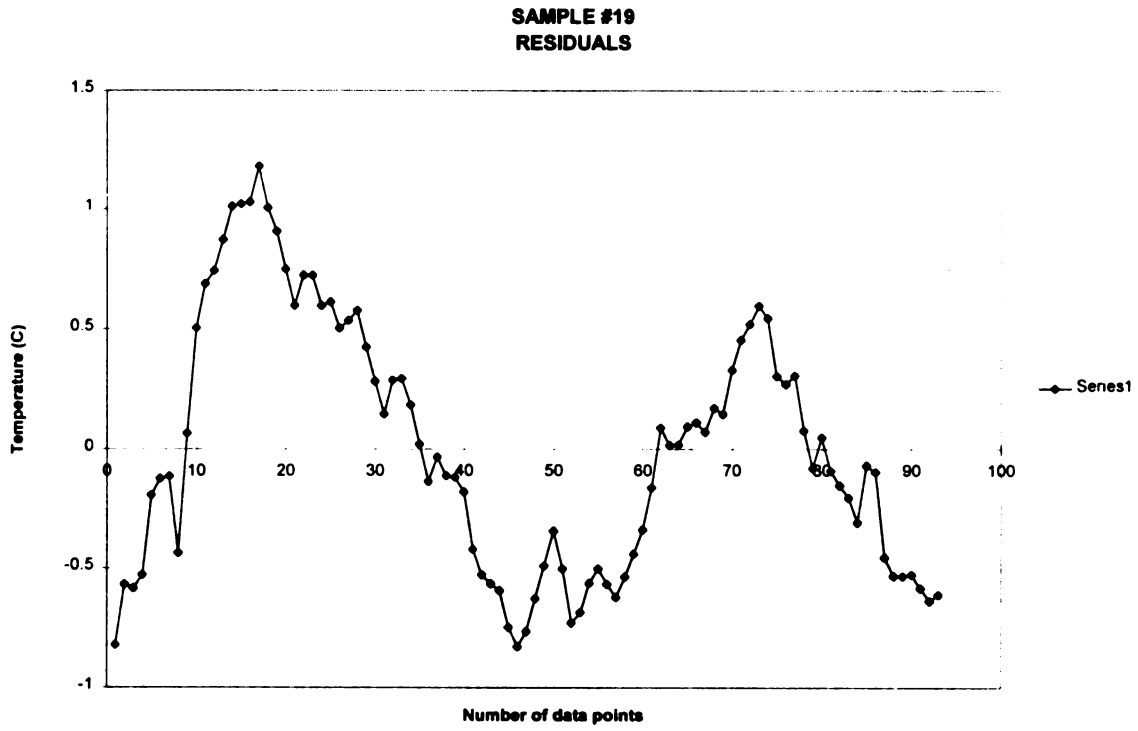


FIGURE A.20

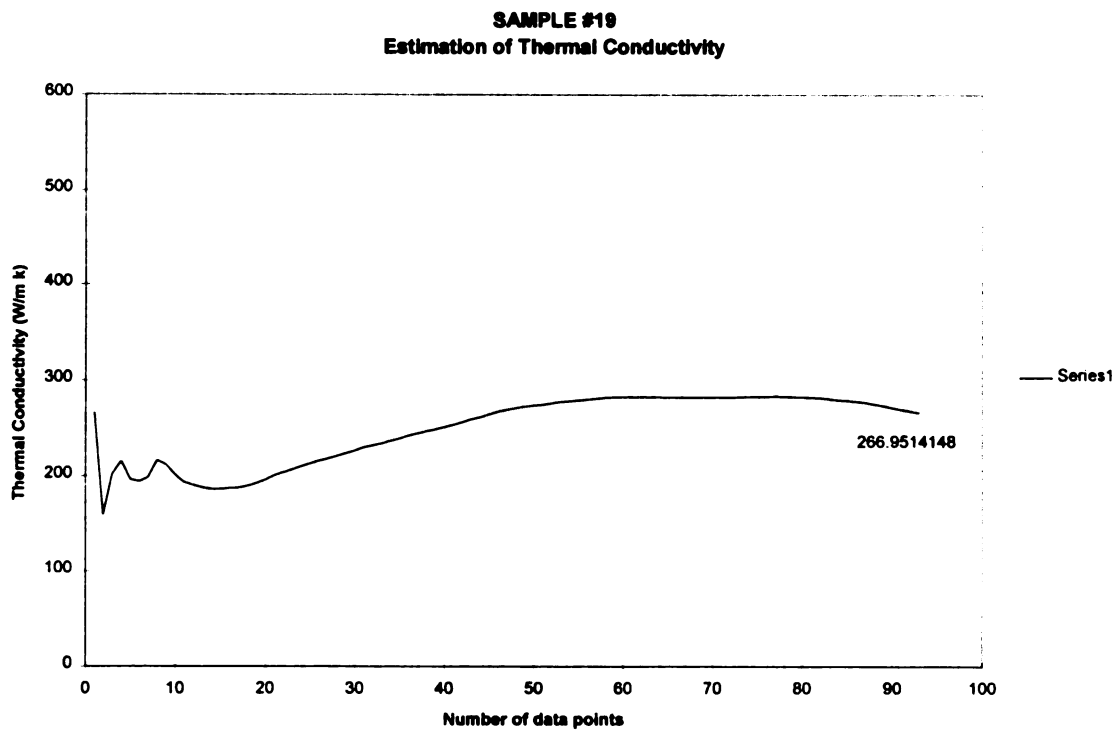


FIGURE A.21

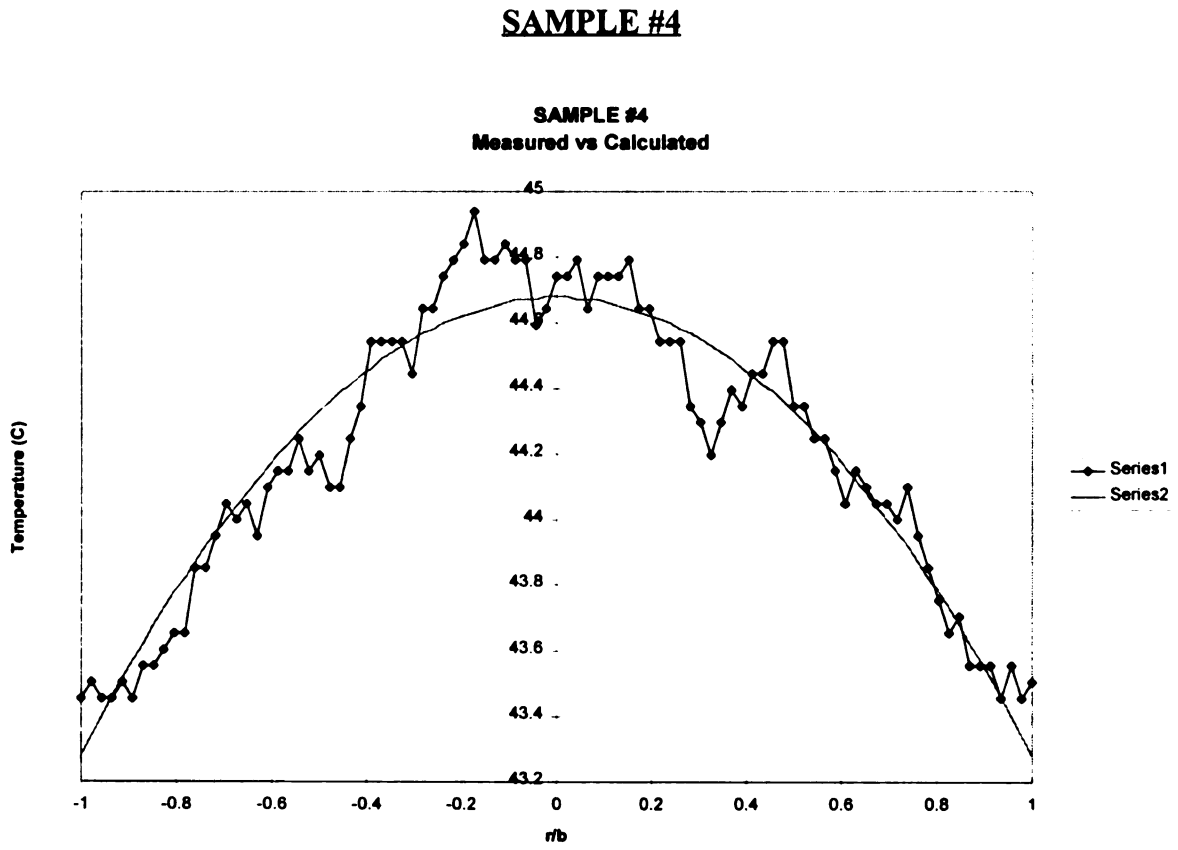


FIGURE A.22

**SAMPLE #4
RESIDUALS**

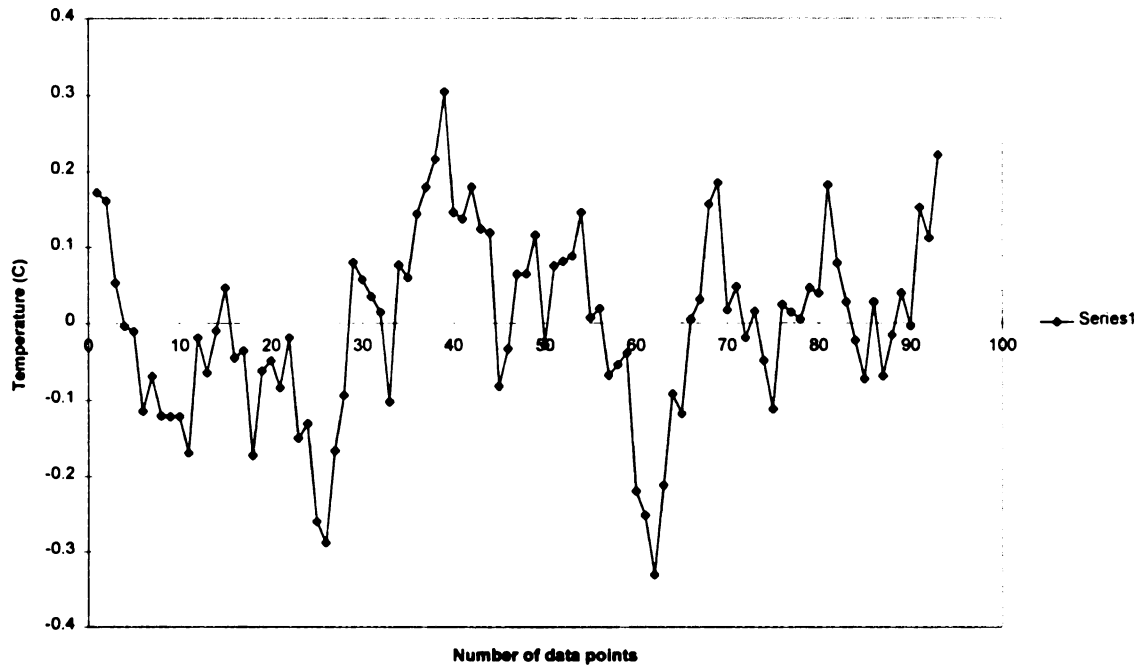


FIGURE A.23

**SAMPLE #4
Estimation of Thermal Conductivity**

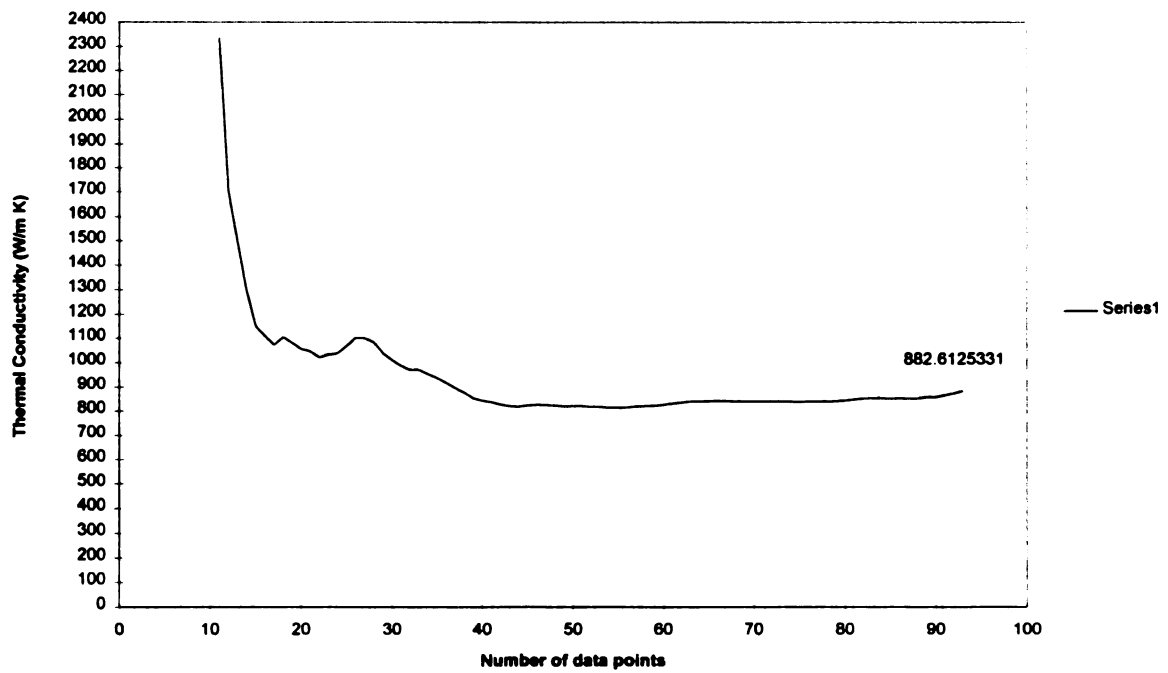


FIGURE A.24

SAMPLE #6

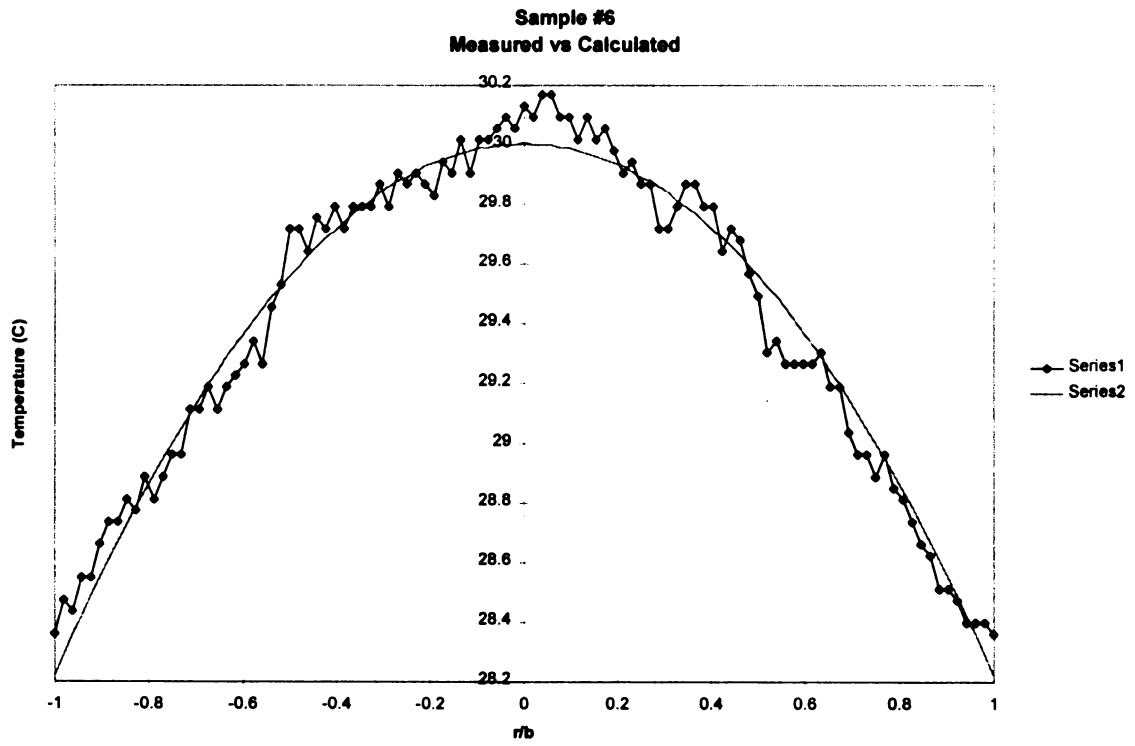


FIGURE A.25

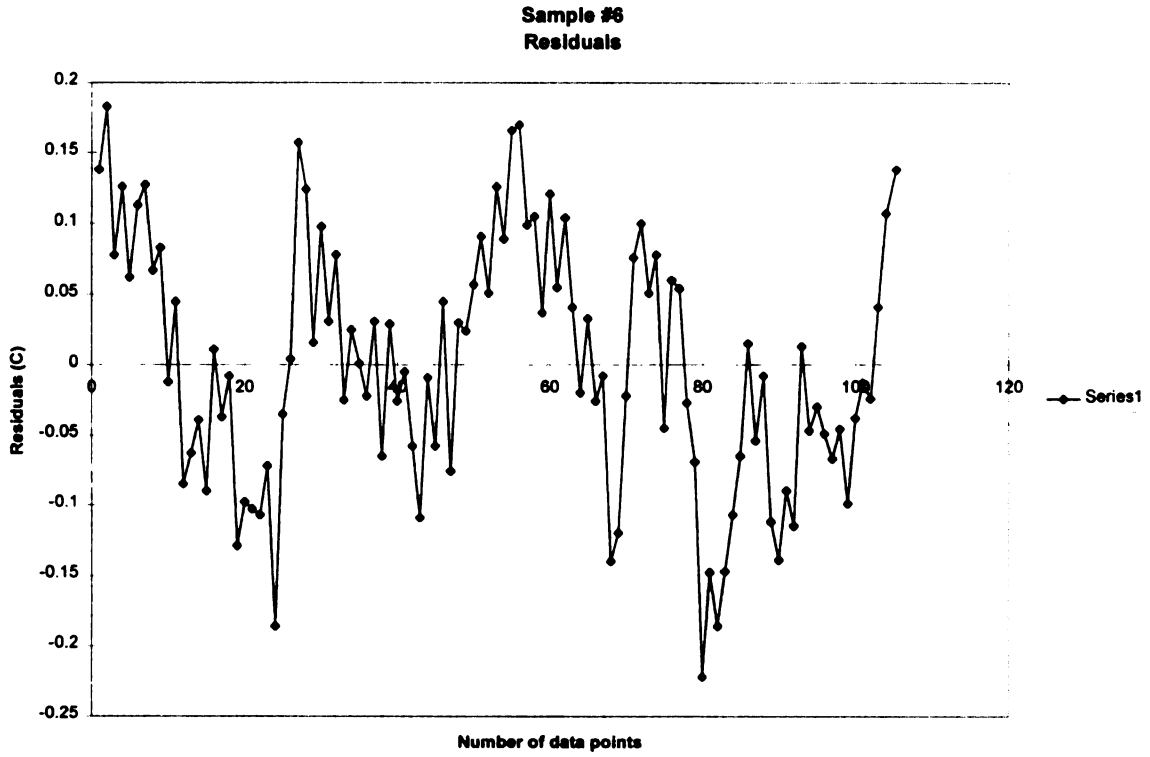


FIGURE A.26

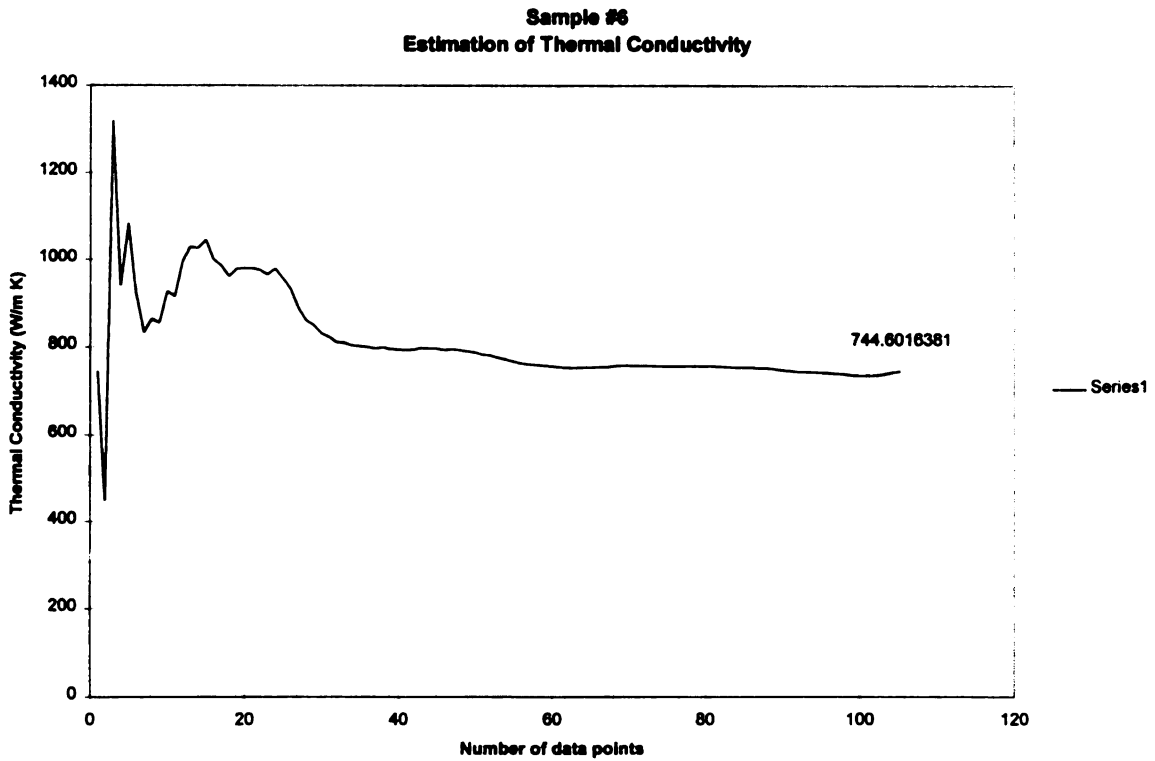


FIGURE A.27

APPENDIX B

FORTRAN PROGRAM NLIN

```

PROGRAM NLINA
CCCCCCCC      PROGRAM DESCRIPTION      CCCCC
C
C          C
C    PROGRAM NLINC
C  WRITTEN BY JAMES V. BECK              C
C  LAST REVISED JUL. 27, 1994 FOR ANDREW SAYERS
C*****C
C          C
CVCCCCCCCC    VARIABLE IDENTIFICATION    CCCCCCCC
C          C
C          C
C*****C
C          C
CDCCCCCCCC    DIMENSION BLOCK            BLOCK 0000
C          C
C          C
  IMPLICIT REAL*8 (A-H,O-Z)
  DIMENSION T(1000,5),Y(1000),SIG2(1000),B(5),Z(5),A(5),BS(5),
  1 VINV(5,5),BSS(5),CG(5),BSV(5),R(5,5),EXTRA(20),ERR(1000)
  1, PS(5,5),P(5,5),PSV(5,5),
  1 XTX(5,5),XTY(5),SUM(5),BET(50,2)
  CHARACTER*40 DFILE,OUTFIL
C          C
C*****C
C          C
COCCCCCCCC    COMMON BLOCK              BLOCK 0100
C          C
  COMMON T,N,Z,BS,I,ETA,PS,P,B,A,Y,SIG2,MODL,VINV,NP,EXTRA
  COMMON/ERROR/ERR
  COMMON/MOD/AA,TL,SUM,BET,IH,CONST
C          C
C          C
C*****C
C          C
CACCCCCCCCC    DATA BLOCK              BLOCK 0200
C          C
  DATA EPS,EPSS,IIN,IOUT/1.0D-30,0.0001D+0,5,7/
C          C
C*****C
C          C
CICCCCCCCCC    INITIALIZATION BLOCK      BLOCK 0400
C          C
  WRITE(*,*)'ENTER THE NAME OF THE DATA FILE'
  READ(*,'(A40)') DFILE
  OPEN(8,FILE=DFILE)
  WRITE(*,*)'ENTER THE NAME OF THE OUTPUT FILE'
  READ(*,'(A40)') OUTFIL
  OPEN(7,FILE=OUTFIL)

```

```

C                                     C
C*****C
C                                     C
CPCCCCCCCC      PROCESS BLOCK          BLOCK 0500
C                                     C
C --- START INPUT
C  BLOCK 1
  WRITE(7,*)'BEGIN LISTING INPUT QUANTITIES'
200 READ(8,*) N,NP,NT,ITMAX,MODL,IPRINT
  WRITE(7,*)
  WRITE(7,*)'BLOCK 1'
  WRITE(7,*)'N = NO. DATA POINTS, NP = NO. PARAMETERS'
  WRITE(7,*)'NT = NO. OF INDEPENDENT VARIABLES'
  WRITE(7,*)'ITMAX = MAXIMUM NO. OF ITERATIONS'
  WRITE(7,*)'MODEL = MODEL NUMBER, IF SEVERAL MODELS IN SUBROUTINES:
1 MODEL AND SENS'
  WRITE(7,*)'IPRINT = 1 FOR USUAL PRINTOUTS, 0 FOR LESS'
  WRITE(7,*)
  IF(N.LE.0) THEN
    STOP
  END IF
  WRITE(*,(/,9X,"N",8X,"NP",8X,"NT",5X,"ITMAX",5X,
+"MODEL",4X,"IPRINT"))
  WRITE(*,(7I10)) N,NP,NT,ITMAX,MODL,IPRINT
  WRITE(7,(/,9X,"N",8X,"NP",8X,"NT",5X,"ITMAX",5X,
+"MODEL",4X,"IPRINT"))
  WRITE(7,(7I10)) N,NP,NT,ITMAX,MODL,IPRINT
  IOPT=0
C --- IF IOPT=0 THEN ON THE 2ND AND SUCCEEDING STACKED CASES, THE DATA IS
C --- NOT REPRINTED.
C --- IF IPRINT=1, EXTRA PRINT OUT OF ETA, RESIDUALS B(1),... ARE GIVEN.
C  BLOCK 2
  WRITE(7,*)
  WRITE(7,*)'BLOCK 2'
  WRITE(7,*)'B(1),B(2),...,B(NP) ARE INITIAL PARAMETER ESTIMATES'
  WRITE(7,*)
  READ(8,*)(B(I),I=1,NP)
  WRITE(7,(10X,"B(",I1,") = ",E16.5)) (I,B(I),I=1,NP)
C
  DO 150 J1=2,5
    BS(J1) = 0
150 CONTINUE
C
  IF(IOPT.LE.0) THEN
C  BLOCK 3
  WRITE(7,*)
  WRITE(7,*)'BLOCK 3'
  WRITE(7,*)'J = DATA POINT INDEX, Y(J) = MEASURED VALUE'
  WRITE(7,*)'SIGMA(J) = STANDARD DEVIATION OF Y(J)'
  WRITE(7,*)'T(J,1) = FIRST INDEPENDENT VARIABLE'
  WRITE(7,*)
  WRITE(7,(/,9X,"J",6X,"Y(J)",3X,"SIGMA(J)",6X,"T(J,1)"
+6X,"T(J,2)"))
  DO 10 I2=1,N

```

```

      READ(8,*)J,Y(J),SIG2(J),(T(J,KT),KT=1,NT)
      WRITE(7,'(I10,7F10.5)') J,Y(J),SIG2(J),(T(J,KT),KT=1,NT)
      SIG2(J) = SIG2(J)*SIG2(J)
10  CONTINUE
    END IF
  C
313 DO 2 IP=1,NP
      DO 2 KP=1,NP
          PS(KP,IP) = 0
          P(KP,IP) = 0
  2  CONTINUE
  C  WRITE(7,'(/,5X,"P(1,KP)",9X,"P(2,KP)",9X,"P(3,KP)",9X,
  C  +"P(4,KP)",9X,"P(5,KP)")')
  C  DO 6 IP=1,NP
  C
  C  READ(8,*)(PS(IP,KP),KP=1,NP)
  C  WRITE(7,'(5D16.5)') (PS(IP,KP),KP=1,NP)
  6  CONTINUE
  C  BLOCK 4
      DO 88 IP=1,NP
88  PS(IP,IP)=B(IP)*B(IP)
      READ(8,*)IEXTRA
  C  IEXTRA=0 FOR NO EXTRA INPUT WHICH COULD BE FOR CONSTANTS
  C  IN MODELS
  C  =1 FOR ONE INPUT, NAMELY: EXTRA(1), ETC.
      WRITE(7,*)
      WRITE(7,*)'BLOCK 4'
      WRITE(7,*)'IEXTRA = NO. OF EXTRA(I) PARAMETERS, 0 IF NONE'
      WRITE(7,*)
      WRITE(7,'(10X,"IEXTRA = ",I10)')IEXTRA
      IF(IEXTRA .LT. 1) GOTO 21
      WRITE(7,*)
      WRITE(7,*)'BLOCK 5'
      WRITE(7,*)'EXTRA(1),... ARE EXTRA CONSTANTS USED AS DESIRED'
      WRITE(7,*)
      READ(8,*)(EXTRA(IE),IE=1,IEXTRA)
      WRITE(7,'("EXTRA(",I2,") = ",F16.5)') (IE,EXTRA(IE),IE=1
      1,IEXTRA)
  21 CONTINUE
  C
  C --- ADD BLANK CARD AFTER LAST INPUT CARD
  C ---END INPUT
      WRITE(7,*)'END INPUT QUANTITIES - - BEGIN OUTPUT CALCULATIONS'
      WRITE(7,*)
      WRITE(7,*)'SY = SUM OF SQUARES FOR PRESENT PARAMETER VALUES'
      WRITE(7,*)'SYP = SUM OF SQUARES FOR GAUSS PARAMETER VALUES, SHOULD
  1 BE SMALLER THAN SY'
      WRITE(7,*)' SYP DECREASES TOWARD A POSITIVE CONSTANT'
      WRITE(7,*)'G = MEASURE OF THE SLOPE, SHOULD BECOME SMALLER AS
  1 ITERATIONS PROCEED'
      WRITE(7,*)' G SHOULD APPROACH ZERO AT CONVERGENCE'
      WRITE(7,*)'H = FRACTION OF THE GAUSS STEP, AS GIVEN BY THE
  1 BOX-KANEMASU METHOD'
      WRITE(7,*)

```

```

WRITE(7,*)
DO 18 IL=1,NP
  BS(IL)=B(IL)
  CG(IL) = 0
18 CONTINUE
DO 19 IP=1,NP
  XTY(IP)=0.0D+0
  DO 19 KP=1,NP
    P(KP,IP) = PS(KP,IP)
    XTX(IP,KP)=0.0D+0
19 CONTINUE
  I = 0
  MAX = 0
C
99  MAX = MAX + 1
C --- START BASIC LOOP GIVES B(I) AND SY
C
  SY = 0.0D+0
  DO 100 I3=1,N
    I = I3
    CALL MODEL
    CALL SENS
CCCC  CALL MODEL
    RISD = Y(I)-ETA
    SY = SY + RISD*RISD/SIG2(I)
    SUMX= 0.0D+0
    DO 20 K=1,NP
      XTY(K)=XTY(K)+Z(K)*RISD/SIG2(I)
      DO 20 L=1,NP
        SUMX= SUMX+ Z(L)*P(K,L)*Z(K)
        XTX(K,L)= XTX(K,L) + Z(L)*Z(K)/SIG2(I)
20  CONTINUE
    DELTA = SIG2(I) + SUMX
    DO 29 JJ=1,NP
      A(JJ) = 0.0D+0
29  CONTINUE
    DO 30 JA=1,NP
      DO 30 KA=1,NP
        A(JA) = A(JA) + Z(KA)*P(JA,KA)
30  CONTINUE
    CS = 0.0D+0
    DO 40 JC=1,NP
      CS = CS + Z(JC)*(B(JC)-BS(JC))
      CG(JC) = CG(JC) + Z(JC)*RISD/SIG2(I)
40  CONTINUE
    C = Y(I) - CS - ETA
    DO 50 IB=1,NP
      B(IB) = B(IB) + (A(IB)*C)/DELTA
50  CONTINUE
    DO 41 ISV=1,NP
      DO 41 JSV=1,NP
        PSV(JSV,ISV) = P(JSV,ISV)
41  CONTINUE
    DO 52 IV=1,NP

```

```

DO 52 IU=IV,NP
  SUMP = 0.0D+0
  DO 51 KP=1,NP
    DO 51 JP=1,NP
      IF(KP-IV.EQ.0.OR.JP-IU.EQ.0) GOTO 51
      PSQ1 = PSV(KP,JP)*PSV(IU,IV)
      PSQ2 = PSV(IU,KP)*PSV(IV,JP)
      PSQ = PSQ1 - PSQ2
      IF(DABS(PSQ1)+DABS(PSQ2).LT.1.D-15) THEN
        RP = PSQ * 1.D15
      ELSE
        RP = PSQ / (DABS(PSQ1)+DABS(PSQ2))
      END IF
      RP = ABS(RP)
      RPP = RP - 1.0D-12
      IF(RPP.LE.0.0D+0) THEN
        PSQ = 0.0D+0
      END IF
      SUMP = SUMP + Z(JP)*Z(KP)*PSQ
51  CONTINUE
    P(IU,IV) = (PSV(IU,IV)*SIG2(I)+SUMP)/DELTA
52  CONTINUE
  DO 53 IV=2,NP
    IVM = IV - 1
    DO 53 IU = 1,IVM
      P(IU,IV)= P(IV,IU)
53  CONTINUE
    IF(IPRINT.GT.0) THEN
      IF(I.EQ.1) THEN
        WRITE(7,*)
        WRITE(7,*)'SEQUENTIAL ESTIMATES OF THE PARAMETERS GIVEN BELOW'
        WRITE(7,('(//,3X,"I",6X,"ETA",3X,"RES.",2X,
1"B(1)",7X,"B(2)",7X,"B(3)",7X,"B(4)"))
        END IF
      C   WRITE(7,('(14,6E12.5)')I,ETA,RISD,(B(JC),JC=1,NP)
        WRITE(7,('(13,F10.2,F8.3,5E11.4)')I,ETA,RISD,(B(JC),JC=1,NP)
      END IF
100 CONTINUE
C --- END BASIC LOOP, GIVES B(I) AND SY
C --- START BOX-KANEMASU MODIFICATION
C
C   START BOX-KANEMASU MODIFICATION
    IF(MAX-1)104,104,103
103  SS=SY/2.0D+0
    IF(SS-SYP)104,104,105
105  DO 210 IBS=1,NP
      B(IBS)= BSV(IBS)
210  CONTINUE
    WRITE(IOUT,212)
212  FORMAT(7X,'USE BSV(IBS)')
    GOTO 211
104  CONTINUE
    DO 102 IBS=1,NP
      BSS(IBS)= BS(IBS)

```

```

102 CONTINUE
  ALPHA= 2.0D+0
  AA= 1.1D+0
110 ALPHA= ALPHA/2.0D+0
  DO 116 IBS=1,NP
    BS(IBS)= BSS(IBS) + ALPHA*( B(IBS)-BSS(IBS) )
    BSV(IBS)= BS(IBS)
116 CONTINUE
  INDEX=0
  G= 0.0D+0
  DO 115 IP=1,NP
    DELB= BS(IP)-BSS(IP)
    G= G + DELB*CG(IP)
    RATIO= DELB/( BSS(IP)+EPS )
    RATIO= ABS(RATIO)
    IF(RATIO-EPSS)113,113,114
113  INDEX= INDEX+1
    WRITE(IOUT,314)
314  FORMAT(7X,'MAX',8X,'NP',5X,'INDEX',8X,'IP')
    WRITE(7,'(7I10)') MAX,NP,INDEX,IP
114 CONTINUE
C  WRITE(7,122) I,Y(I),ETA,RISD,Z(IP),XYP,DELB,SIG2(I)
115 CONTINUE
  SYP= 0.0D+0
  DO 117 I3=1,N
    I=I3
    CALL MODEL
    RISD= Y(I)-ETA
    SYP= SYP + RISD*RISD/SIG2(I)
117 CONTINUE
  IF(NP-INDEX)106,106,107
106 H=1.0D+0
  GOTO 132
107 CONTINUE
  SYN= SYP*0.999D+0
  IF(SYN-SY)112,112,111
111 IF(ALPHA-0.01D+0)109,109,110
109 WRITE(7,108) ALPHA,SYP,SY
108 FORMAT(3X,'ALPHA TOO SMALL,ALPHA=',F12.6,2X,'SYP=',E15.6,2X,
  1'SY',E15.6)
  WRITE(7,1001)
1001 FORMAT(8X,'Z(1)',10X,'Z(2)',10X,'Z(3)',10X,'Z(4)',10X,'Z(5)')
1002 FORMAT(6E13.4)
  DO 1003 I=1,N
    CALL SENS
    WRITE(7,1002) (Z(IBB),IBB=1,NP)
1003 CONTINUE
  GOTO 1000
112 CONTINUE
  SKSUM= SY - ALPHA*G*( 2.0D+0-1.0D+0/AA )
  IF(SYP-SKSUM)131,131,130
130 H= ALPHA * ALPHA*G/( SYP-SY+2.0D+0*ALPHA*G )
  GOTO 132
131 CONTINUE

```

```

H= ALPHA*AA
132 CONTINUE
DO 118 IBN= 1,NP
  B(IBN)= BSS(IBN) + H * ( B(IBN)-BSS(IBN) )
118 CONTINUE
211 CONTINUE
  WRITE(IOUT,121)
  WRITE(*,121)
121 FORMAT(5X,'MAX',10X,'H',13X,'G',12X,
  1'SY',11X,'SYP')
  WRITE(7,122) MAX,H,G,SY,SYP
  WRITE(*,122) MAX,H,G,SY,SYP
122 FORMAT(I8,1F13.6,4E14.6)
  WRITE(7,'(10X,"B(",I1,") = ",E16.6)') (I,B(I),I=1,NP)
  WRITE(*,'(10X,"B(",I1,") = ",E16.6)') (I,B(I),I=1,NP)
C END BOX-KANEMASU MODIFICATION
  WRITE(7,'(/,5X,"P(1,KP)",9X,"P(2,KP)",9X,"P(3,KP)",9X,
  1"P(4,KP)",9X,"P(5,KP)")')
  DO 206 IP=1,NP
    WRITE(7,207) (P(IP,KP),KP=1,NP)
206 CONTINUE
207 FORMAT(5D15.7)
  WRITE(7,135)
135 FORMAT(5X,'CORRELATION MATRIX')
  DO 136 IR=1,NP
    DO 136 IR2=1,IR
      AR= P(IR,IR) * P(IR2,IR2)
      R(IR,IR2)= P(IR,IR2)/SQRT(AR)
136 CONTINUE
  DO 137 IR=1,NP
    WRITE(7,'(5E15.7)') (R(IR,III),III=1,IR)
137 CONTINUE
  DO 126 IPS=1,NP
    PS(IPS,IPS)= (1.0E+7) * P(IPS,IPS)
126 CONTINUE
  WRITE(7,*)'XTX(I,K),K=1,NP'
  DO 220 K=1,NP
220 WRITE(7,'(5E15.7)')(XTX(K,III),III=1,NP)
  WRITE(7,*)'XTY(I),I=1,NP, WHERE Y IS RESID'
  WRITE(7,'(5E15.7)')(XTY(I),I=1,NP)
127 FORMAT(3X,'IPS=',I4,3X,'PS(IPS,IPS)=',D15.8)
  WRITE(7,*)'XTY(I),I=1,NP, Y IS Y, NOT RESID'
  WRITE(7,'(5E15.7)')(SUM(I),I=1,NP)
  DO 119 IP=1,NP
    XTY(IP)=0.0D+0
    DO 119 KP=1,NP
      P(IP,KP)= PS(IP,KP)
      XTX(IP,KP)=0.0D+0
119 CONTINUE
  DO 120 IP=1,NP
    BS(IP)= B(IP)
    CG(IP)= 0.0D+0
120 CONTINUE
  WRITE(7,314)

```

```

WRITE(7,'(7I10,4F10.4)') MAX,NP,INDEX,IP
IF(NP-INDEX)101,101,123
123 CONTINUE
M=ITMAX
IF(MAX-M)99,99,101
101 CONTINUE
IF(IPRINT)133,133,134
133 IPRINT=IPRINT+1
GOTO 99
134 CONTINUE
C
1000 CONTINUE
CLOSE(IIN)
CLOSE(IOUT)
C
C*****C
C
CECCCCCCC      ERROR MESSAGES      BLOCK 0900
C
C*****C
C
CFCCCCCCC      FORMAT STATEMENTS    BLOCK 9000
C
C*****C
C
STOP
END
SUBROUTINE MODEL
C THIS SUBROUTINE IS FOR CALCULATING ETA, THE MODEL VALUE
IMPLICIT REAL*8 (A-H,O-Z)
DIMENSION T(1000,5),Y(1000),SIG2(1000),B(5),Z(5),BET(50,2),
+A(5),BS(5),VINV(5,5),EXTRA(20)
DIMENSION P(5,5),PS(5,5),SUM(5)
COMMON T,N,Z,BS,I,ETA,PS,P,B,A,Y,SIG2,MODL,VINV,NP,EXTRA
COMMON/MOD/AA,TL,SUM,BET,IH,CONST
C WRITTEN BY JAMES V. BECK
PI=4.0D+0*DATAN(1.0D+0)
C IF(MODL .EQ. 1) GOTO 800
800 CONTINUE

TR=T(I,1)/EXTRA(2)
ETA=BS(1)+BS(2)*EXTRA(1)*(1.0D+0-TR*TR)

1000 CONTINUE
C WRITE(*,*)I,T(I,1),ETA,Z(1),I,T(I,1),ETA,Z(1)
RETURN
END
SUBROUTINE SENS
C THIS SUBROUTINE IS FOR CALCULATING THE SENSITIVITY COEFFICIENTS
IMPLICIT REAL*8 (A-H,O-Z)
DIMENSION T(1000,5),Y(1000),SIG2(1000),B(5),BET(50,2),
+Z(5),A(5),BS(5),VINV(5,5),EXTRA(20)

```

```
DIMENSION P(5,5),PS(5,5),SUM(5)
COMMON T,N,Z,BS,I,ETA,PS,P,B,A,Y,SIG2,MODL,VINV,NP,EXTRA
COMMON/MOD/AA,TL,SUM,BET,IH,CONST
PI=4.0D+0*DATAN(1.0D+0)

Z(1)=1.0D+0
TR=T(1,1)/EXTRA(2)
Z(2)=EXTRA(1)*(1.0D+0-TR*TR)

DO 312 IPP=1,NP
312  SUM(IPP)=0.0D+0
313  CONTINUE
800  CONTINUE
C   IF(I.LT.N)GOTO 2000
    DO 1001 JPP=1,NP
C   TZ=? TRY ETA FOR NOW
    TZ=ETA
1001 SUM(JPP)=SUM(JPP)+Z(JPP)*(Y(I)-TZ)/SIG2(I)
2000 CONTINUE
    RETURN
    END
```

APPENDIX C
NLIN OUTPUT AND INPUT FILES

Sample #4
Output file

BEGIN LISTING INPUT QUANTITIES

BLOCK 1

N = NO. DATA POINTS, NP = NO. PARAMETERS

NT = NO. OF INDEPENDENT VARIABLES

ITMAX = MAXIMUM NO. OF ITERATIONS

MODEL = MODEL NUMBER, IF SEVERAL MODELS IN SUBROUTINES: MODEL AND SENS

IPRINT = 1 FOR USUAL PRINTOUTS, 0 FOR LESS

N	NP	NT	ITMAX	MODEL	IPRINT
93	2	1	100	1	1

BLOCK 2

B(1),B(2),...,B(NP) ARE INITIAL PARAMETER ESTIMATES

B(1) = .43500E+02

B(2) = .25000E-02

BLOCK 3

J = DATA POINT INDEX, Y(J) = MEASURED VALUE

SIGMA(J) = STANDARD DEVIATION OF Y(J)

T(J,1) = FIRST INDEPENDENT VARIABLE

J	Y(J)	SIGMA(J)	T(J,1)	T(J,2)
1	43.65344	1.00000	-1.00000	
2	43.55461	1.00000	-.97826	
3	43.65344	1.00000	-.95652	
4	43.60403	1.00000	-.93478	
5	43.65344	1.00000	-.91304	
6	43.75226	1.00000	-.89130	
7	43.75226	1.00000	-.86957	
8	43.90050	1.00000	-.84783	
9	43.85109	1.00000	-.82609	
10	43.94992	1.00000	-.80435	
11	43.99933	1.00000	-.78261	
12	43.94992	1.00000	-.76087	
13	44.09816	1.00000	-.73913	
14	44.04874	1.00000	-.71739	
15	44.09816	1.00000	-.69565	
16	44.04874	1.00000	-.67391	
17	44.04874	1.00000	-.65217	
18	44.14757	1.00000	-.63043	
19	44.09816	1.00000	-.60870	

20	44.34522	1.00000	-.58696
21	44.39464	1.00000	-.56522
22	44.44405	1.00000	-.54348
23	44.49346	1.00000	-.52174
24	44.44405	1.00000	-.50000
25	44.59229	1.00000	-.47826
26	44.64170	1.00000	-.45652
27	44.74053	1.00000	-.43478
28	44.74053	1.00000	-.41304
29	44.59229	1.00000	-.39130
30	44.64170	1.00000	-.36957
31	44.64170	1.00000	-.34783
32	44.69111	1.00000	-.32609
33	44.74053	1.00000	-.30435
34	44.69111	1.00000	-.28261
35	44.83935	1.00000	-.26087
36	44.74053	1.00000	-.23913
37	44.83935	1.00000	-.21739
38	44.83935	1.00000	-.19565
39	44.83935	1.00000	-.17391
40	44.93818	1.00000	-.15217
41	44.83935	1.00000	-.13043
42	44.83935	1.00000	-.10870
43	44.78994	1.00000	-.08696
44	44.83935	1.00000	-.06522
45	44.93818	1.00000	-.04348
46	44.83935	1.00000	-.02174
47	44.83935	1.00000	.00000
48	44.74053	1.00000	.02174
49	44.83935	1.00000	.04348
50	44.83935	1.00000	.06522
51	44.69111	1.00000	.08696
52	44.74053	1.00000	.10870
53	44.64170	1.00000	.13044
54	44.74053	1.00000	.15217
55	44.74053	1.00000	.17391
56	44.74053	1.00000	.19565
57	44.83935	1.00000	.21739
58	44.74053	1.00000	.23913
59	44.78994	1.00000	.26087
60	44.74053	1.00000	.28261
61	44.74053	1.00000	.30435
62	44.78994	1.00000	.32609
63	44.64170	1.00000	.34783
64	44.69111	1.00000	.36957
65	44.64170	1.00000	.39130
66	44.59229	1.00000	.41304
67	44.59229	1.00000	.43478
68	44.44405	1.00000	.45652
69	44.49346	1.00000	.47826
70	44.44405	1.00000	.50000
71	44.44405	1.00000	.52174
72	44.49346	1.00000	.54348
73	44.34522	1.00000	.56522

74	44.39464	1.00000	.58696
75	44.24640	1.00000	.60870
76	44.14757	1.00000	.63044
77	44.24640	1.00000	.65217
78	44.19698	1.00000	.67391
79	44.29581	1.00000	.69565
80	44.24640	1.00000	.71739
81	44.24640	1.00000	.73913
82	44.24640	1.00000	.76087
83	44.19698	1.00000	.78261
84	44.24640	1.00000	.80435
85	44.09816	1.00000	.82609
86	43.99933	1.00000	.84783
87	43.94992	1.00000	.86957
88	43.80168	1.00000	.89130
89	43.85109	1.00000	.91304
90	43.75226	1.00000	.93478
91	43.70285	1.00000	.95652
92	43.70285	1.00000	.97826
93	43.55461	1.00000	1.00000

BLOCK 4

IEXTRA = NO. OF EXTRA(I) PARAMETERS, 0 IF NONE

IEXTRA = 2

BLOCK 5

EXTRA(1),... ARE EXTRA CONSTANTS USED AS DESIRED

EXTRA(1) = 1228.90000

EXTRA(2) = 1.00000

END INPUT QUANTITIES - - BEGIN OUTPUT CALCULATIONS

SY = SUM OF SQUARES FOR PRESENT PARAMETER VALUES

SYP = SUM OF SQUARES FOR GAUSS PARAMETER VALUES, SHOULD BE SMALLER THAN SY

SYP DECREASES TOWARD A POSITIVE CONSTANT

G = MEASURE OF THE SLOPE, SHOULD BECOME SMALLER AS ITERATIONS PROCEED

G SHOULD APPROACH ZERO AT CONVERGENCE

H = FRACTION OF THE GAUSS STEP, AS GIVEN BY THE BOX-KANEMASU METHOD

SEQUENTIAL ESTIMATES OF THE PARAMETERS GIVEN BELOW

I	ETA	RES.	B(1)	B(2)	B(3)	B(4)
1	43.50	.153	.4365E+02	.2500E-02		
2	43.63	-.078	.4354E+02	.2462E-02		
3	43.76	-.108	.4349E+02	.2417E-02		
4	43.89	-.284	.4344E+02	.2300E-02		
5	44.01	-.358	.4340E+02	.2162E-02		
6	44.13	-.379	.4338E+02	.2044E-02		
7	44.25	-.497	.4337E+02	.1889E-02		

8	44.36	-.463	.4337E+02	.1809E-02
9	44.48	-.625	.4337E+02	.1668E-02
10	44.58	-.635	.4338E+02	.1580E-02
11	44.69	-.691	.4339E+02	.1506E-02
12	44.79	-.844	.4340E+02	.1394E-02
13	44.89	-.796	.4340E+02	.1358E-02
14	44.99	-.942	.4341E+02	.1285E-02
15	45.09	-.987	.4342E+02	.1232E-02
16	45.18	-1.128	.4344E+02	.1158E-02
17	45.27	-1.217	.4345E+02	.1087E-02
18	45.35	-1.204	.4346E+02	.1053E-02
19	45.43	-1.336	.4347E+02	.1001E-02
20	45.51	-1.169	.4347E+02	.1020E-02
21	45.59	-1.196	.4346E+02	.1039E-02
22	45.66	-1.221	.4346E+02	.1059E-02
23	45.74	-1.242	.4345E+02	.1079E-02
24	45.80	-1.360	.4345E+02	.1079E-02
25	45.87	-1.277	.4344E+02	.1102E-02
26	45.93	-1.290	.4343E+02	.1124E-02
27	45.99	-1.251	.4342E+02	.1156E-02
28	46.05	-1.308	.4342E+02	.1178E-02
29	46.10	-1.510	.4342E+02	.1170E-02
30	46.15	-1.511	.4342E+02	.1167E-02
31	46.20	-1.559	.4342E+02	.1162E-02
32	46.25	-1.554	.4342E+02	.1161E-02
33	46.29	-1.547	.4342E+02	.1164E-02
34	46.33	-1.636	.4342E+02	.1159E-02
35	46.36	-1.524	.4342E+02	.1168E-02
36	46.40	-1.656	.4342E+02	.1165E-02
37	46.43	-1.588	.4342E+02	.1170E-02
38	46.45	-1.615	.4342E+02	.1174E-02
39	46.48	-1.640	.4342E+02	.1176E-02
40	46.50	-1.563	.4341E+02	.1185E-02
41	46.52	-1.681	.4341E+02	.1185E-02
42	46.54	-1.697	.4341E+02	.1184E-02
43	46.55	-1.759	.4341E+02	.1179E-02
44	46.56	-1.720	.4342E+02	.1178E-02
45	46.57	-1.628	.4341E+02	.1183E-02
46	46.57	-1.731	.4341E+02	.1181E-02
47	46.57	-1.733	.4341E+02	.1180E-02
48	46.57	-1.830	.4342E+02	.1173E-02
49	46.57	-1.727	.4342E+02	.1172E-02
50	46.56	-1.720	.4342E+02	.1171E-02
51	46.55	-1.858	.4342E+02	.1163E-02
52	46.54	-1.795	.4342E+02	.1159E-02
53	46.52	-1.878	.4343E+02	.1150E-02
54	46.50	-1.761	.4343E+02	.1147E-02
55	46.48	-1.739	.4343E+02	.1145E-02
56	46.45	-1.714	.4343E+02	.1144E-02
57	46.43	-1.588	.4343E+02	.1146E-02
58	46.40	-1.656	.4343E+02	.1145E-02
59	46.36	-1.573	.4343E+02	.1147E-02
60	46.33	-1.586	.4343E+02	.1147E-02
61	46.29	-1.547	.4343E+02	.1148E-02

62 46.25 -1.456 .4343E+02 .1151E-02
63 46.20 -1.559 .4343E+02 .1150E-02
64 46.15 -1.462 .4343E+02 .1151E-02
65 46.10 -1.460 .4343E+02 .1151E-02
66 46.05 -1.456 .4343E+02 .1151E-02
67 45.99 -1.399 .4343E+02 .1151E-02
68 45.93 -1.488 .4343E+02 .1150E-02
69 45.87 -1.376 .4343E+02 .1150E-02
70 45.80 -1.360 .4343E+02 .1150E-02
71 45.74 -1.292 .4343E+02 .1150E-02
72 45.66 -1.171 .4343E+02 .1150E-02
73 45.59 -1.246 .4343E+02 .1150E-02
74 45.51 -1.119 .4343E+02 .1150E-02
75 45.43 -1.188 .4343E+02 .1151E-02
76 45.35 -1.204 .4342E+02 .1153E-02
77 45.27 -1.019 .4342E+02 .1153E-02
78 45.18 -.980 .4342E+02 .1153E-02
79 45.09 -.790 .4343E+02 .1149E-02
80 44.99 -.745 .4343E+02 .1144E-02
81 44.89 -.647 .4344E+02 .1138E-02
82 44.79 -.547 .4345E+02 .1129E-02
83 44.69 -.494 .4346E+02 .1120E-02
84 44.58 -.338 .4348E+02 .1106E-02
85 44.48 -.378 .4349E+02 .1096E-02
86 44.36 -.365 .4350E+02 .1089E-02
87 44.25 -.299 .4350E+02 .1082E-02
88 44.13 -.330 .4351E+02 .1081E-02
89 44.01 -.160 .4351E+02 .1074E-02
90 43.89 -.135 .4352E+02 .1069E-02
91 43.76 -.058 .4352E+02 .1065E-02
92 43.63 .071 .4353E+02 .1057E-02
93 43.50 .055 .4353E+02 .1056E-02

MAX H G SY SYP
1 1.002257 .148214E+03 .149325E+03 .776581E+00
B(1) = .435313E+02
B(2) = .105239E-02

P(1,KP) P(2,KP) P(3,KP) P(4,KP) P(5,KP)
.6054330D-01 -.6144288D-04
-.6144288D-04 .7582198D-07
CORRELATION MATRIX
.1000000E+01
-.9068615E+00 .1000000E+01
XTX(I,K),K=1,NP
.9300000E+02 .7536364E+05
.7536364E+05 .7410024E+08
XTY(I),I=1,NP, WHERE Y IS RESID
-.1059492E+03 -.1049059E+06
XTY(I),I=1,NP, Y IS Y, NOT RESID
.5461000E-01 .0000000E+00
MAX NP INDEX IP
1 2 0 3

SEQUENTIAL ESTIMATES OF THE PARAMETERS GIVEN BELOW

I	ETA	RES.	B(1)	B(2)	B(3)	B(4)
1	43.53	.122	.4365E+02	.1052E-02		
2	43.59	-.032	.4365E+02	-.1867E-02		
3	43.64	.012	.4362E+02	-.6746E-05		
4	43.69	-.090	.4362E+02	-.9759E-04		
5	43.75	-.093	.4361E+02	.9343E-04		
6	43.80	-.045	.4359E+02	.4122E-03		
7	43.85	-.094	.4359E+02	.4887E-03		
8	43.89	.006	.4356E+02	.7289E-03		
9	43.94	-.091	.4356E+02	.7356E-03		
10	43.99	-.038	.4355E+02	.8121E-03		
11	44.03	-.033	.4354E+02	.8690E-03		
12	44.08	-.126	.4355E+02	.8361E-03		
13	44.12	-.020	.4354E+02	.8931E-03		
14	44.16	-.110	.4354E+02	.8805E-03		
15	44.20	-.101	.4354E+02	.8804E-03		
16	44.24	-.188	.4355E+02	.8426E-03		
17	44.27	-.226	.4356E+02	.8035E-03		
18	44.31	-.163	.4356E+02	.8017E-03		
19	44.35	-.247	.4356E+02	.7747E-03		
20	44.38	-.034	.4355E+02	.8228E-03		
21	44.41	-.017	.4354E+02	.8664E-03		
22	44.44	.001	.4353E+02	.9064E-03		
23	44.47	.021	.4352E+02	.9435E-03		
24	44.50	-.057	.4351E+02	.9565E-03		
25	44.53	.064	.4350E+02	.9923E-03		
26	44.56	.087	.4349E+02	.1026E-02		
27	44.58	.160	.4347E+02	.1067E-02		
28	44.60	.137	.4346E+02	.1097E-02		
29	44.63	-.034	.4346E+02	.1095E-02		
30	44.65	-.006	.4346E+02	.1098E-02		
31	44.67	-.026	.4346E+02	.1097E-02		
32	44.69	.004	.4346E+02	.1100E-02		
33	44.70	.036	.4346E+02	.1106E-02		
34	44.72	-.030	.4346E+02	.1104E-02		
35	44.74	.103	.4345E+02	.1117E-02		
36	44.75	-.010	.4345E+02	.1116E-02		
37	44.76	.076	.4345E+02	.1124E-02		
38	44.78	.064	.4345E+02	.1130E-02		
39	44.79	.054	.4345E+02	.1134E-02		
40	44.79	.144	.4344E+02	.1145E-02		
41	44.80	.037	.4344E+02	.1146E-02		
42	44.81	.030	.4344E+02	.1147E-02		
43	44.81	-.025	.4344E+02	.1143E-02		
44	44.82	.020	.4344E+02	.1143E-02		
45	44.82	.116	.4344E+02	.1149E-02		
46	44.82	.015	.4344E+02	.1149E-02		
47	44.82	.015	.4344E+02	.1148E-02		
48	44.82	-.083	.4344E+02	.1141E-02		
49	44.82	.017	.4344E+02	.1141E-02		
50	44.82	.020	.4344E+02	.1141E-02		
51	44.81	-.124	.4345E+02	.1134E-02		

```

52 44.81 -.069 .4345E+02 .1129E-02
53 44.80 -.161 .4345E+02 .1121E-02
54 44.79 -.054 .4345E+02 .1119E-02
55 44.79 -.045 .4345E+02 .1117E-02
56 44.78 -.035 .4346E+02 .1116E-02
57 44.76 .076 .4345E+02 .1118E-02
58 44.75 -.010 .4345E+02 .1118E-02
59 44.74 .053 .4345E+02 .1120E-02
60 44.72 .019 .4345E+02 .1120E-02
61 44.70 .036 .4345E+02 .1121E-02
62 44.69 .103 .4345E+02 .1124E-02
63 44.67 -.026 .4345E+02 .1123E-02
64 44.65 .043 .4345E+02 .1124E-02
65 44.63 .015 .4345E+02 .1125E-02
66 44.60 -.012 .4345E+02 .1125E-02
67 44.58 .012 .4345E+02 .1125E-02
68 44.56 -.111 .4345E+02 .1124E-02
69 44.53 -.035 .4345E+02 .1124E-02
70 44.50 -.057 .4345E+02 .1124E-02
71 44.47 -.028 .4345E+02 .1124E-02
72 44.44 .051 .4345E+02 .1124E-02
73 44.41 -.066 .4345E+02 .1124E-02
74 44.38 .016 .4345E+02 .1123E-02
75 44.35 -.099 .4345E+02 .1125E-02
76 44.31 -.163 .4345E+02 .1127E-02
77 44.27 -.028 .4345E+02 .1127E-02
78 44.24 -.040 .4345E+02 .1127E-02
79 44.20 .097 .4345E+02 .1123E-02
80 44.16 .087 .4346E+02 .1119E-02
81 44.12 .128 .4346E+02 .1112E-02
82 44.08 .171 .4347E+02 .1104E-02
83 44.03 .165 .4348E+02 .1095E-02
84 43.99 .259 .4350E+02 .1081E-02
85 43.94 .156 .4351E+02 .1072E-02
86 43.89 .104 .4352E+02 .1066E-02
87 43.85 .103 .4352E+02 .1060E-02
88 43.80 .005 .4352E+02 .1059E-02
89 43.75 .105 .4353E+02 .1052E-02
90 43.69 .058 .4353E+02 .1049E-02
91 43.64 .062 .4354E+02 .1045E-02
92 43.59 .116 .4354E+02 .1039E-02
93 43.53 .023 .4355E+02 .1038E-02
MAX      H      G      SY      SYP
2 1.000000 .334621E-02 .775828E+00 .772482E+00
B(1) = .435456E+02
B(2) = .103792E-02

P(1,KP)  P(2,KP)  P(3,KP)  P(4,KP)  P(5,KP)
.6115672D-01 -.6219943D-04
-.6219943D-04 .7675514D-07
CORRELATION MATRIX
.1000000E+01
-.9078426E+00 .1000000E+01
XTX(I,K),K=1,NP

```

```

.9300000E+02 .7536364E+05
.7536364E+05 .7410024E+08
XTY(I),I=1,NP, WHERE Y IS RESID
.2391551E+00 .5166700E+01
XTY(I),I=1,NP, Y IS Y, NOT RESID
.2333597E-01 .0000000E+00
  MAX    NP  INDEX    IP
    2     2     0     3

```

SEQUENTIAL ESTIMATES OF THE PARAMETERS GIVEN BELOW

I	ETA	RES.	B(1)	B(2)	B(3)	B(4)
1	43.55	.108	.4365E+02	.1038E-02		
2	43.60	-.046	.4365E+02	-.1867E-02		
3	43.65	-.001	.4362E+02	-.6752E-05		
4	43.71	-.102	.4362E+02	-.9760E-04		
5	43.76	-.104	.4361E+02	.9343E-04		
6	43.81	-.056	.4359E+02	.4122E-03		
7	43.86	-.104	.4359E+02	.4887E-03		
8	43.90	-.004	.4356E+02	.7289E-03		
9	43.95	-.100	.4356E+02	.7356E-03		
10	44.00	-.046	.4355E+02	.8121E-03		
11	44.04	-.041	.4354E+02	.8690E-03		
12	44.08	-.133	.4355E+02	.8361E-03		
13	44.12	-.026	.4354E+02	.8931E-03		
14	44.16	-.116	.4354E+02	.8805E-03		
15	44.20	-.106	.4354E+02	.8804E-03		
16	44.24	-.193	.4355E+02	.8426E-03		
17	44.28	-.230	.4356E+02	.8035E-03		
18	44.31	-.167	.4356E+02	.8017E-03		
19	44.35	-.250	.4356E+02	.7747E-03		
20	44.38	-.036	.4355E+02	.8228E-03		
21	44.41	-.019	.4354E+02	.8664E-03		
22	44.44	.000	.4353E+02	.9064E-03		
23	44.47	.020	.4352E+02	.9435E-03		
24	44.50	-.058	.4351E+02	.9565E-03		
25	44.53	.063	.4350E+02	.9923E-03		
26	44.56	.086	.4349E+02	.1026E-02		
27	44.58	.161	.4347E+02	.1067E-02		
28	44.60	.137	.4346E+02	.1097E-02		
29	44.63	-.033	.4346E+02	.1095E-02		
30	44.65	-.005	.4346E+02	.1098E-02		
31	44.67	-.025	.4346E+02	.1097E-02		
32	44.69	.006	.4346E+02	.1100E-02		
33	44.70	.038	.4346E+02	.1106E-02		
34	44.72	-.028	.4346E+02	.1104E-02		
35	44.73	.105	.4345E+02	.1117E-02		
36	44.75	-.008	.4345E+02	.1116E-02		
37	44.76	.079	.4345E+02	.1124E-02		
38	44.77	.067	.4345E+02	.1130E-02		
39	44.78	.057	.4345E+02	.1134E-02		
40	44.79	.147	.4344E+02	.1145E-02		
41	44.80	.040	.4344E+02	.1146E-02		

42	44.81	.033	.4344E+02	.1147E-02
43	44.81	-.021	.4344E+02	.1143E-02
44	44.82	.024	.4344E+02	.1143E-02
45	44.82	.120	.4344E+02	.1149E-02
46	44.82	.019	.4344E+02	.1149E-02
47	44.82	.018	.4344E+02	.1148E-02
48	44.82	-.080	.4344E+02	.1141E-02
49	44.82	.021	.4344E+02	.1141E-02
50	44.82	.024	.4344E+02	.1141E-02
51	44.81	-.120	.4345E+02	.1134E-02
52	44.81	-.065	.4345E+02	.1129E-02
53	44.80	-.158	.4345E+02	.1121E-02
54	44.79	-.051	.4345E+02	.1119E-02
55	44.78	-.042	.4345E+02	.1117E-02
56	44.77	-.032	.4346E+02	.1116E-02
57	44.76	.079	.4345E+02	.1118E-02
58	44.75	-.008	.4345E+02	.1118E-02
59	44.73	.056	.4345E+02	.1120E-02
60	44.72	.021	.4345E+02	.1120E-02
61	44.70	.038	.4345E+02	.1121E-02
62	44.69	.104	.4345E+02	.1124E-02
63	44.67	-.025	.4345E+02	.1123E-02
64	44.65	.044	.4345E+02	.1124E-02
65	44.63	.016	.4345E+02	.1125E-02
66	44.60	-.011	.4345E+02	.1125E-02
67	44.58	.012	.4345E+02	.1125E-02
68	44.56	-.111	.4345E+02	.1124E-02
69	44.53	-.036	.4345E+02	.1124E-02
70	44.50	-.058	.4345E+02	.1124E-02
71	44.47	-.030	.4345E+02	.1124E-02
72	44.44	.049	.4345E+02	.1124E-02
73	44.41	-.068	.4345E+02	.1124E-02
74	44.38	.013	.4345E+02	.1123E-02
75	44.35	-.102	.4345E+02	.1125E-02
76	44.31	-.167	.4345E+02	.1127E-02
77	44.28	-.032	.4345E+02	.1127E-02
78	44.24	-.045	.4345E+02	.1127E-02
79	44.20	.092	.4345E+02	.1123E-02
80	44.16	.082	.4346E+02	.1119E-02
81	44.12	.122	.4346E+02	.1112E-02
82	44.08	.164	.4347E+02	.1104E-02
83	44.04	.157	.4348E+02	.1095E-02
84	44.00	.251	.4350E+02	.1081E-02
85	43.95	.148	.4351E+02	.1072E-02
86	43.90	.095	.4352E+02	.1066E-02
87	43.86	.093	.4352E+02	.1060E-02
88	43.81	-.006	.4352E+02	.1059E-02
89	43.76	.093	.4353E+02	.1052E-02
90	43.71	.046	.4353E+02	.1049E-02
91	43.65	.049	.4354E+02	.1045E-02
92	43.60	.102	.4354E+02	.1039E-02
93	43.55	.009	.4355E+02	.1038E-02
	MAX	NP	INDEX	IP
	3	2	1	1

```

MAX   NP  INDEX  IP
  3    2    2    2
MAX   H    G    SY    SYP
  3  1.000000 .542254E-17 .772482E+00 .772482E+00
    B(1) = .435456E+02
    B(2) = .103792E-02

P(1,KP)  P(2,KP)  P(3,KP)  P(4,KP)  P(5,KP)
.6115672D-01 -.6219943D-04
-.6219943D-04 .7675514D-07
CORRELATION MATRIX
.1000000E+01
-.9078426E+00 .1000000E+01
XTX(I,K),K=1,NP
.9300000E+02 .7536364E+05
.7536364E+05 .7410024E+08
XTY(I),I=1,NP, WHERE Y IS RESID
-.2028688E-07 -.2004377E-04
XTY(I),I=1,NP, Y IS Y, NOT RESID
.9031387E-02 .0000000E+00
MAX   NP  INDEX  IP
  3    2    2    3

```

Input file

```

105  2  1  100  1  1
26  0.0025
1  27.77786  1  -1
2  28.05399  1  -0.98077
3  28.19208  1  -0.96154
4  28.39914  1  -0.94231
5  28.67529  1  -0.92308
6  28.95142  1  -0.90385
7  29.0882  1  -0.88462
8  29.22266  1  -0.86538
9  29.28989  1  -0.84615
10  29.42438  1  -0.82692
11  29.35712  1  -0.80769
12  29.62604  1  -0.78846
13  29.55881  1  -0.76923
14  29.62604  1  -0.75
15  29.76053  1  -0.73077
16  29.62604  1  -0.71154
17  29.55881  1  -0.69231
18  29.89496  1  -0.67308
19  30.29837  1  -0.65385
20  30.70175  1  -0.63462
21  30.90347  1  -0.61538
22  30.83621  1  -0.59615
23  30.63452  1  -0.57692
24  30.50006  1  -0.55769
25  30.50006  1  -0.53846
26  30.70175  1  -0.51923

```

27	30.83621	1	-0.5
28	30.9707	1	-0.48077
29	31.10516	1	-0.46154
30	31.23963	1	-0.44231
31	31.23963	1	-0.42308
32	31.37409	1	-0.40385
33	31.37409	1	-0.38462
34	31.10516	1	-0.36538
35	31.37409	1	-0.34615
36	31.50852	1	-0.32692
37	31.57578	1	-0.30769
38	31.64191	1	-0.28846
39	31.64191	1	-0.26923
40	31.83847	1	-0.25
41	31.70743	1	-0.23077
42	31.57578	1	-0.21154
43	31.90399	1	-0.19231
44	31.83847	1	-0.17308
45	31.96951	1	-0.15385
46	31.90399	1	-0.13462
47	32.03504	1	-0.11538
48	31.90399	1	-0.09615
49	31.83847	1	-0.07692
50	31.90399	1	-0.05769
51	32.03504	1	-0.03846
52	32.23163	1	-0.01923
53	32.43912	1	0
54	32.16608	1	0.019231
55	32.29715	1	0.038462
56	32.03504	1	0.057692
57	32.03504	1	0.076923
58	31.90399	1	0.096154
59	31.96951	1	0.115385
60	32.03504	1	0.134615
61	32.29715	1	0.153846
62	32.23163	1	0.173077
63	32.03504	1	0.192308
64	31.90399	1	0.211538
65	32.03504	1	0.230769
66	32.03504	1	0.25
67	31.96951	1	0.269231
68	31.83847	1	0.288462
69	31.77295	1	0.307692
70	31.77295	1	0.326923
71	31.50852	1	0.346154
72	31.44129	1	0.365385
73	31.17236	1	0.384615
74	31.30686	1	0.403846
75	31.30686	1	0.423077
76	31.23963	1	0.442308
77	31.17236	1	0.461538
78	31.10516	1	0.480769
79	31.03793	1	0.5
80	31.10516	1	0.519231

81	31.03793	1	0.538462
82	31.10516	1	0.557692
83	31.03793	1	0.576923
84	30.83621	1	0.596154
85	30.90347	1	0.615385
86	30.83621	1	0.634615
87	30.90347	1	0.653846
88	30.83621	1	0.673077
89	30.83621	1	0.692308
90	30.76898	1	0.711538
91	30.50006	1	0.730769
92	30.23114	1	0.75
93	30.3656	1	0.769231
94	30.16391	1	0.788462
95	30.3656	1	0.807692
96	30.02945	1	0.826923
97	29.82776	1	0.846154
98	29.62604	1	0.865385
99	29.49158	1	0.884615
100	29.22266	1	0.903846
101	29.02045	1	0.923077
102	28.74432	1	0.942308
103	28.53723	1	0.961538
104	28.19208	1	0.980769
105	28.4682	1	
2			
2142.477	1		

Appendix D

Calibration of IPPLUS for Infrared Temperature Measurements (White, 1996)

This appendix discusses the steps involved in obtaining a calibration between the IPPLUS image processing system and the Inframetrics thermal imaging system.

EXPERIMENTAL EQUIPMENT

1. A thin (1/8") Aluminum disc 2 inches in diameter
2. Minco disc heater 2" inches in diameter
3. Omega-High Thermal Conductivity Paste
4. Radiometer and Control Unit
5. Video Recorder
6. DC Power Supply
7. IPPLUS image processing system

EXPERIMENTAL PREPARATION

1. Aluminum disc is painted with black paint to improve emissive properties.
2. Minco heater is attached to disc using paste.

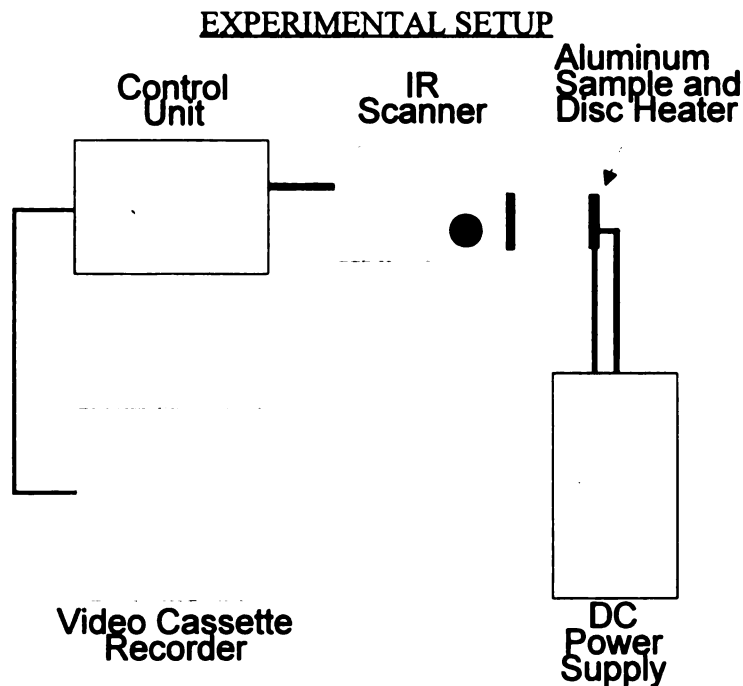


Figure D1. Experimental Setup

EXPERIMENTAL PROCEDURE

1. In calibrating the system the radiometer was operated in the point mode. As shown in Figure B2, the crosshairs were placed near the center of the disk and the cursor temperature in the text line was used in the calibration.

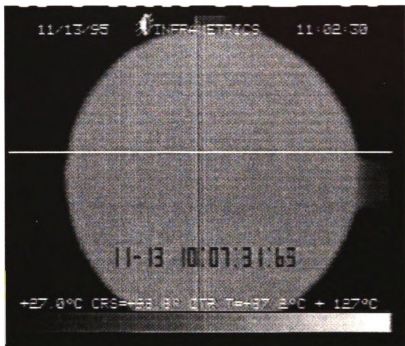


Figure D2. Camera operated in the point mode. The temperature at the location of the “cross hairs” is indicated in the text line along the bottom of the image.

2. In the first calibration test the temperature span was set to five degrees and the range was adjusted so the entire field of view was dark. Therefore, initially the temperature of the disk was below the range of the radiometer.
3. Then as the voltage supplied to the heater was slowly increased the output of the radiometer was stored on video cassette. The test continued until the disk temperature exceeded the radiometer's temperature range.
4. The recorded data was then analyzed using the IPPLUS image processing system. As the temperature of the disk slowly increased, thermal fields as shown in Figure D2 were randomly captured.
5. Using the line profile or bit map analysis function of IPPLUS the gray scale intensities of four regions, indicated in Figure D2 with red rectangles, were average and compared with the cursor temperature. If this is done several times throughout the temperature range, a plot of temperature versus gray scale can be developed. Since the output of the radiometer is a standard 8 bit video format, the gray scale intensities will range between 0 and 255. Therefore, regardless of the temperature setting the output of the radiometer is divided into 256 discrete levels. This being the

case, the slope of a gray scale to temperature calibration curve with radiometer in the 20 temperature range is different than the slope of the of a gray scale to temperature calibration curve with the radiometer temperature range at 5 degrees. These differences in slope can be eliminated if the gray scale is plotted as a function of non-dimensional temperature.

6. A non-dimensional temperature was determined based on the minimum and maximum temperature for the particular temperature span setting. For example, in Figure D2

the minimum temperature $T_L=27.0^\circ\text{C}$

the maximum temperature $T_H=127^\circ\text{C}$

and the temperature at the location of the cursor is $T = 98^\circ\text{C}$.

$$\theta = \frac{T - T_L}{T_H - T_L} = .71 \quad (\text{B.1})$$

7. This non-dimensional temperature is then plotted as a function of the gray scale intensity and a linear regression can be performed on the data to find a relationship between gray scale and temperature. This plot is illustrated in Figure B3.
8. Steps 1 through 7 are repeated with the temperature span set at 10°C , 20°C , 50°C , and 100°C .

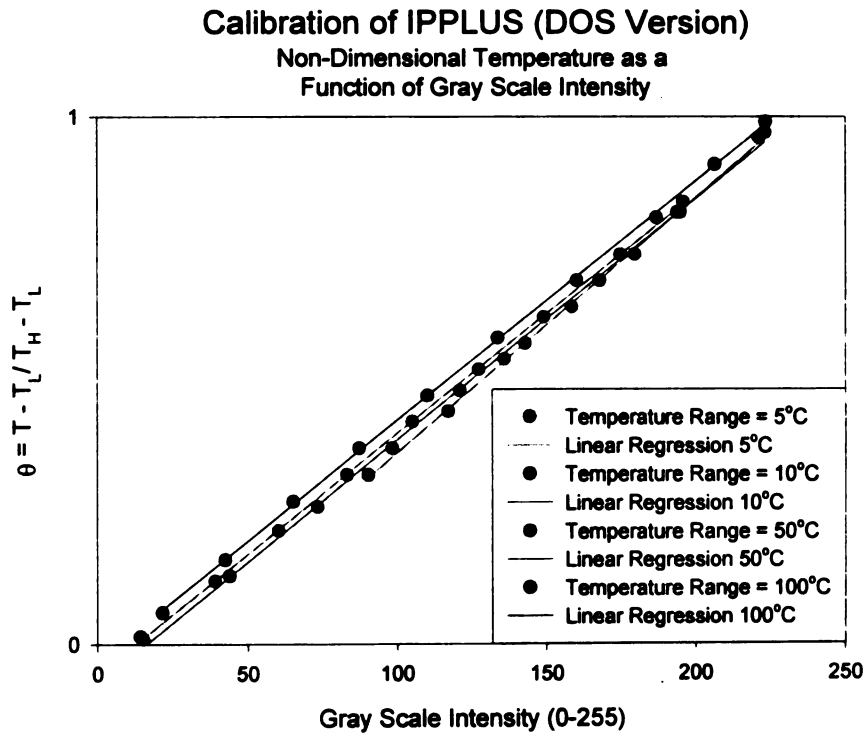


Figure D3. Non-dimensional temperature as function of gray scale intensity.

DISCUSSION OF RESULTS

Calibrations such as those in Figure D3 illustrate that the gray scale output of the radiometer is linearly related to temperature. It is interesting that the calibration curve does not cross through the origin and causes an offset in the relationship between gray scale and temperature. This offset is a characteristic of the radiometer's output.

Normally, a black image will have a gray scale intensity of 0, while a white image will have a gray scale value of 255. Although the output of the radiometer varies between "black or cold" and "white or hot", these images do not produce typical gray scale values. For example, pixels which are below the temperature range of the radiometer appear "black". Normally, the gray intensity of these pixels would be zero. However, the "black" pixels produced by the radiometer are digitized to values higher than zero. Therefore, since the "black" values produced by the radiometer are not truly black an offset exist.

The linear scale used corresponds to : y-intercept = -0.011879
slope = 3.96652×10^{-3}

Appendix E

Sample Number	Distance (cm)
18	1.5
17	2.5
13	3.5
8	4.5
3	7.5
16	4
14	4
7	6
4	7.5
5	8
6	6.5
15	5.5
2	7.5
1	8
9	6
10	6.5
11	5.5
12	4
19	2.5
20	4

Table E.1 Measured distance from the boron source

The distances were measured from the middle of the boron source to the middle of the sample.

Sample Data

Sample Number	Length (mm)	Width (mm)	Resistance (ohm)
1	5.7	9.3	1.5
6	9.3	14	1.6
2	8.85	13.95	1.5
3	8.95	13.6	1.15
4	13	14	1.5
17	7.6	13.4	1.4
8	7.8	13.5	1.5
7	8	13.1	1
19	8	14	1.6

Table E.2 Measured data used for NLIN

Voltage (volts)	Calculated Temperature Difference (θ)	Error in Thermal Conductivity (δ)	Sample Number	Estimated Thermal Conductivity
1.275	2.45	60.61	2	960
1.375	2.86	56.927		
1.048	4.33	34.657	7	653
1.213	5.8	33.174		
1.359	7.28	32.494		
1.124	3.82	30.764	8	561
1.263	4.822	29.435		
1.37	5.67	28.808		
1.016	1.79	54.713	6	740
1.203	2.51	46.356		
1.203	4.63	55.633	1	975
0.995	3.167	60.708		
2.3	1.198	60.092	3	914
1.396	13.9	12.835	17	205
1.285	11.4	12.865		
1.021	7.45	13.156		
1.151	9.65	10.117	19	263
1.312	12.55	10.014		
1.214	10.75	10.059		
1.254	2.089	65.088	4	958

Table E.3 Complete uncertainty analysis

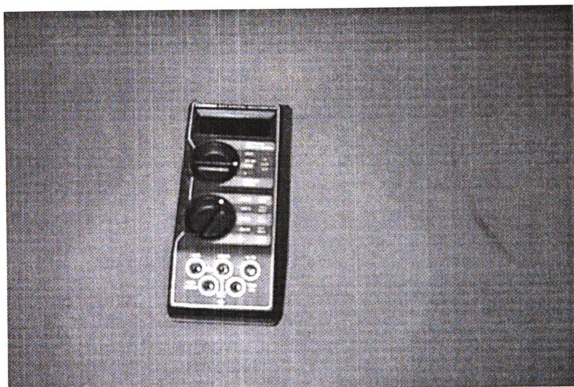


Figure E.1 Photograph of DMM

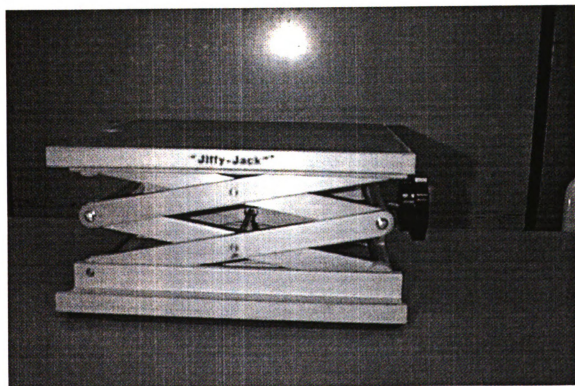


Figure E.2 Photograph of the jiffy jack

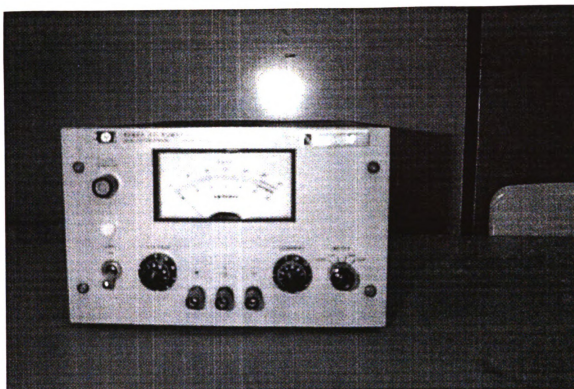


Figure E.3 Photograph of the power supply

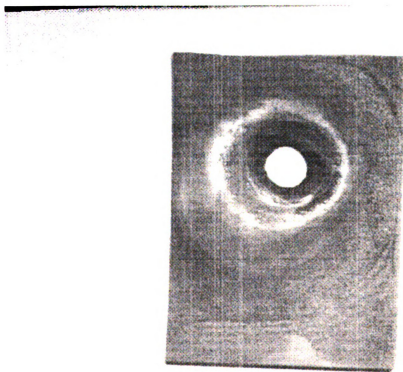


Figure E.4 Diamond Sample (silicon side)

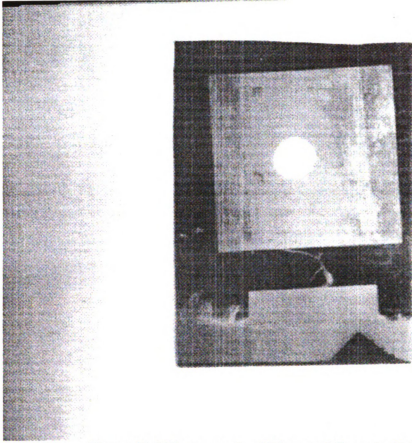


Figure E.5 Photograph of Diamond Sample (Diamond Side)

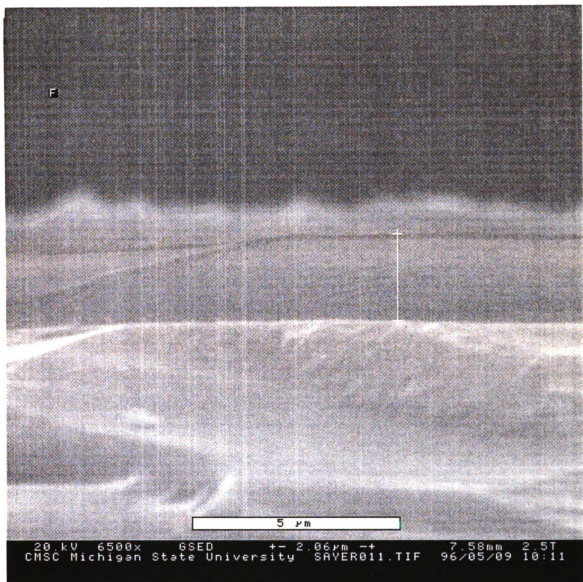


Figure ESEM results showing a thickness of 2.06 μm

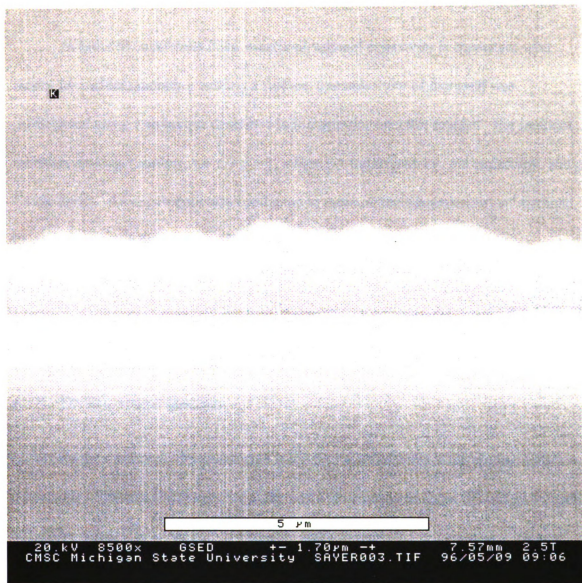


Figure E. ESEM results showing thickness of 1.70 μm

In order to understand if the measured value of emissivity is consistent with theory for incident radiation striking a surface, transmissivity of diamond was investigated using a technique described in inframetrix operator manual. For incident radiation striking a surface, $\tau + \varepsilon + \rho = 1$, where τ = transmissivity, ε = emissivity, and ρ = reflectivity. An experiment was conducted to measure the transmissivity of diamond by considering two heat source. The experimental setup consist of:

- 2 Power supplies
- 4 Electrical lead wires
- The data acquisition system
- The heat source specimen

A heat source specimen was constructed using four electric wires, each approximately 4 inches long. The insulating material at the end was removed to about 0.5 inches on each end of the wires. The outer pair of wires are approximately 2.5 cm apart, and the two inner wires are about 1 cm apart. The two fine wires are about 2.5 mm apart. Two fine wires (approximately 500 microns in diameter), with known resistivity, are connected to each pair of wires at one end of the stripped electrical wires as shown in Figure E.1 below

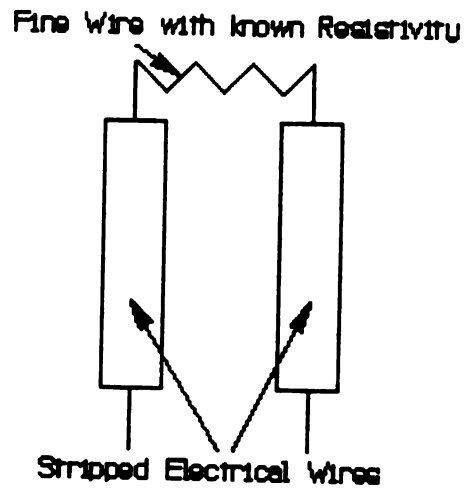


Figure E.1 Fine wire connection to the electrical wires

The pair of resistors created are bonded to a 0.5 inches by 2.0 inches using Duro super glue. The heat source specimen is shown in Figure E.2

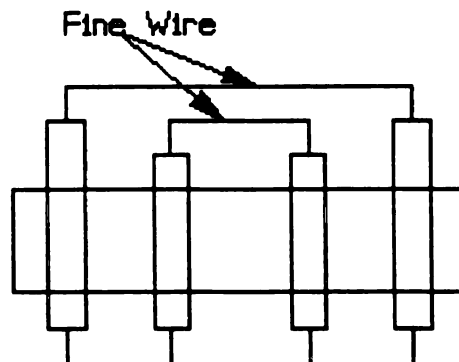


Figure E.2 Heat source specimen

The electrical lead wires are then connected to the stripped wires in order to create an electric circuit with each of the fine wires. The setup used is shown in Figure E.3

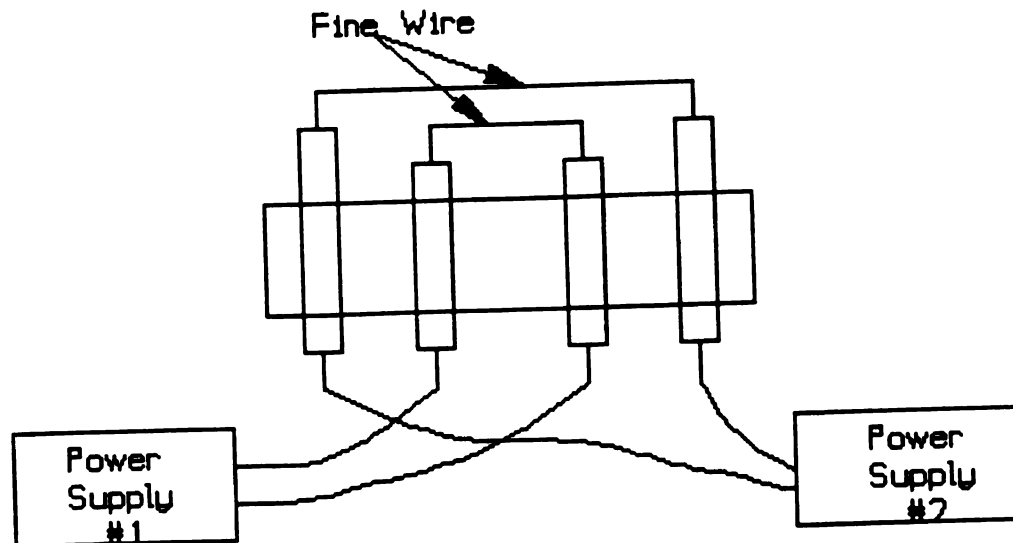


Figure E.3 The experimental setup

The heat source specimen is then placed in front of the scanner and known voltages are applied (PS1=11, PS2=6.5) to each of the wires, resulting in a temperature difference between the two wires. The radiometer settings is then adjusted to the correct inputs using the control panel. The radiometer settings are:

Temperature Span = 10 °C

Units = LVL

Emittance = 1.0

Center Temperature = Auto

The experiment is then conducted by recording the LVL output for each fine wire using the point mode function on the radiometer. The level output from each fine wire with the diamond sample present and without the diamond sample are recorded. The transmissivity is then calculated from

$$\tau = (LVL A - LVL B)_{\text{with diamond}} / (LVL A - LVL B)_{\text{without diamond}}$$

Data from three experimental runs are shown in Table E.1 below

	LVL without Diamond	LVL Without Diamond	LVL with Diamond	LVL With Diamond	Transmissivity
Test Number	Wire #1	Wire #2	Wire #1	Wire #2	
1	4100	5780	3543	4070	0.314
2	4055	5830	3533	3976	0.250
3	4148	5720	3543	4020	0.303
Average	4101	5777	3540	4022	0.29
Standard Deviation	38.0	45.0	4.71	38.4	0.03

Table E.1 Results of transmissivity test

The average value of emissivity is consistent with the measured result of .62.

Since reflectivity, ρ , is $1 - \tau + \epsilon$, it is safe to assume that the reflectivity of diamond is about 0.09.

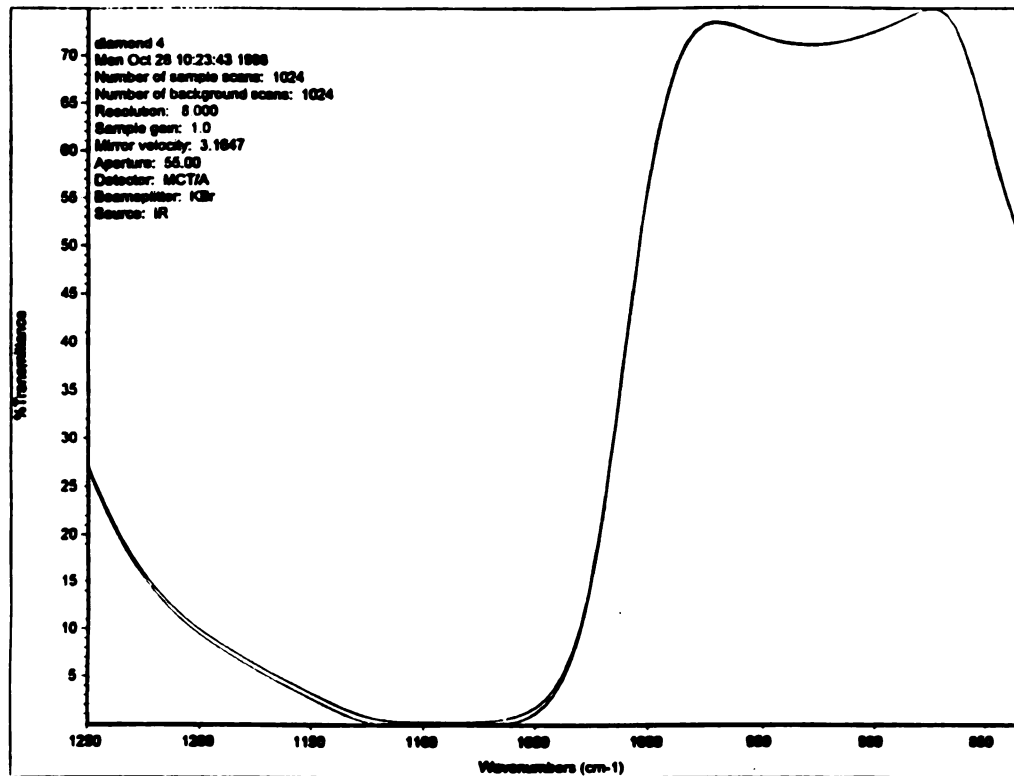


Figure E.4 Measurement of transmissivity using FTIR

Figure E.4 shows the transmissivity measurement from an FTIR. The result from the FTIR indicates that the measured average value of 0.29 is in the range given by the technique used.

BIBLIOGRAPHY

- 1) Baba, K., Aikawa, Y., and Shohata, N. "Thermal Conductivity of Diamond Film". J. Appl. Phys. 69, 7313-7315. 1991
- 2) Beck, James V., et al. Heat Conduction Using Green's Functions. Washington, DC: Hemisphere Publishing Corporation, 1992
- 3) Beck J.V., and Arnold, K.J. Parameter Estimation in Engineering and Science. John Wiley and Sons, 1977
- 4) Beckwith, Thomas G., and Marangoni, Roy D. Mechanical Measurements 4th Ed. New York: Addison-Wesley Publishing Company, 1990
- 5) Berman, R. Thermal Conduction in Solids. Oxford: Clarendon Press, 1976
- 6) Caber, Paul J., Martinek, Stephen J, and Niemann, Robert J. "A New Interferometric Profiler for Smooth and Rough Surfaces." Wyko Corporation. Tucson, AZ. 1996
- 7) Das, Kalyan K., "Electronic Application of Diamond Films and Coatings." Diamond Films and Coatings. Ed Robert Davis. Park Ridge, NJ: Noyes Publications. 1993
- 8) Graebner, J E. et al. "Thermal Conductivity in Chemical Vapor Deposited Diamond." J. Appl. Phys. 71. 5353-5356 April 1992
- 9) Graebner J E., et al. "Phonon Scattering in Chemical-Vapor-Deposited Diamond." The American Physical Society. Vol 50 No. 6. Aug 1994
- 10) Graebner, J. E., Hartnett, T. M., and Miller R. P. "Improved Thermal Conductivity in Isotopically Chemical Vapor Deposited Diamond." Appl. Phys. Lett. 64. May 1994
- 11) Herr, S A. "Experimental Design and Technique for Measurement of CVD Diamond Film Thermal Conductivity using Infrared Thermography." M.S. Thesis, Dept. of Mechanical Engineering. Michigan State University, 1993
- 12) Holman, P.J. Heat Transfer. 2nd ed New York: McGraw Hill Publishing Company, 1990

- 13) Inframetrics 600 Operator Manual, Document # 05250-200 Rev C. Billerico, MA. Unpublished, 1988
- 14) Khatami, Saeid. "Microwave Cavity Plasma Reactor Field Map Development and CVD Diamond Film Characterizations." Ph. D Proposal. Dept of Electrical Engineering. Michigan State University. 1995
- 15) Kittel, Charles. Introduction to Solid State Physics. 7th ed. New York: John Wiley & Sons, 1996
- 16) Maissel, L I, and Francombe, M H. An Introduction to Thin Films. New York: Gordon and Breach Science Publishers. 1973
- 17) Malta, D M. et al. "Comparison of the electrical properties of simultaneously deposited homoepitaxial and polycrystalline diamond films." J. Appl. Phys. 77 (4). 1995
- 18) May, Paul W. "CVD Diamond: A New Technology for the Future." Endeavour. Vol. 19 no. 3. 1995
- 19) Morelli, D T., Beetz, C D., and Perry, T A. "Thermal Conductivity of Synthetic Diamond Film" J. Appl. Phys. 64, 3063-3066. 1988
- 20) Nassau, Kurt. "Synthesis of Bulk Diamond: History and Present Status." Diamond Films and Coatings. Ed Robert Davis. Park Ridge, NJ: Noyes Publications. 1993
- 21) Ono, A., et al. "Thermal Conductivity of Diamond Films Synthesized by Microwave Plasma CVD." Japanese J. Appl. Phys., 25, L808-L810. 1986
- 22) Pehrsson, Pehr, et al. "Chemical Mechanisms of Diamond CVD." Diamond Films and Coatings. Ed Robert Davis. Park Ridge, NJ: Noyes Publications. 1993
- 23) Peterson, K E. "Silicon as a Mechanical Material" Proceedings of the IEEE. 70, 420-429. 1982
- 24) Reinhard, D. K. Introduction to Integrated Circuit Engineering. Boston: Houghton Mifflin Co. 1987
- 25) Van Zant, Peter. Microchip Fabrication: A Practical Guide to Semiconductor Processing 2nd Ed. New York: McGraw Hill Publishing Company. 1990
- 26) Werner, M. et al. "The Relationship between Resistivity and Boron Doping Concentration of Single and Polycrystalline Diamond." Physica Status Solidi. (a) 154, 385. 1996

- 27) Whallon, Joanne. "The laser Scanning Microscope Laboratory." Michigan State University. East Lansing, Michigan. Unpublished. 1996
- 28) White, Matthew. "Development of non-Contact and Non-Destructive Experimental Techniques Capable of Measuring the Thermal Diffusivity of CVD Diamond Film". M.S. Thesis. Dept. of Mechanical Engineering. Michigan State University. 1996
- 29) Wilks, John, and Wilks, Eileen. Properties and Applications of Diamond. Oxford: Butterworth-Heinemann. 1991
- 30) Yang, Gwo-shii. Dissertation Proposal. Dept of Electrical Engineering. Michigan State University. Unpublished. 1996
- 31) Zygo Corporation. "3D Imaging Surface Structure Analyzer." Middlefield, Connecticut. Unpublished. 1996

MICHIGAN STATE UNIV. LIBRARIES



31293015654407